Tampere University

Lackson Kashobwe

ANTIGEN-ANTIBODY AFFINITY MAPPING
Characterization of monoclonal antibodies reactivity to viral proteins

Faculty of Medicine and Health Technology
Master's Thesis
November 1, 2021

ABSTRACT

LACKSON KASHOBWE: ANTIGEN-ANTIBODY AFFINITY MAPPING
Subtitle: Characterization of monoclonal antibody reactivity to viral proteins
Pages: 84
Primary Supervisor: MSc Niila Saarinen
Co-Supervisor: Professor Vesa Hytönen
Reviewers: Professor Heli Skottman, MSc Niila Saarinen
Master's Thesis
Tampere University
MSc degree program in Biotechnology and Biomedical Engineering,
Specialization in Molecular Biology
November 2021

Enteroviruses (EVs) belong to the Picornaviridae family, and their genomes are made up of single-stranded, positive-sense RNA. Infections from EVs can be asymptomatic or have a wide variety of symptoms, including paralysis, rash, poliomyelitis, hand-foot, mouth disease, encephalitis, and myocarditis. Also, human rhinoviruses (HRV) are widespread picornaviruses that cause the common cold and cost billions of dollars due to many missed work hours. Several monoclonal antibodies have been developed against EVs for the past decades. Some are specific to a single species or serotype, and others are group-specific. However, due to the vast array of enteroviruses circulating, better molecular tools would be needed to establish virus diagnostics. This thesis evaluated the diagnostic potential of five novel monoclonal antibodies against the eight viral proteins.

Eight recombinant Enterovirus structural proteins VP1s (CVA4, CVB1, PV1, EV-D68, RV-A89, RV-B14, RV-C3) were produced in *E. coli* and purified using glutathione and immobilized metal affinity chromatography. Also, two monoclonal antibodies (mAb) (4D12 and 9B9) were produced in rat hybridoma cells and purified in addition to three purified mAb (7C1, 12A4, 3A6) using affinity chromatography. The cross-reactivity of mAb to different VP1-proteins was mapped to generate the binding profile of each mAb using Western blot (WB), ELISA, and Biolayer interferometry (BLI).

It was discovered that the binding response of 3A6 mAb to eight VP1 in BLI and ELISA was superior to 9B9, 4D12, 7C1, 12A4, and Dako mAb. In ELISA and BLI measurements, 3A6mAb showed broad specificity and high affinity to CVB1 and E30. 12A4 and Dako mAb were found to react to CVA4, CVB1, PV1, and E30 in ELISA. Also, Dako mAb showed specificity and high affinity to CVB1 in BLI and Polio in ELISA. In contrast, 9B9, 4D12, and 7C1 had less affinity to the VP1 antigens in BLI, WB, and ELISA. Moreover, with further optimization, 3A6, 12A4, and Dako mAb can be used as a panel of antibodies to diagnose and distinguish EV infecting species based on the binding response kinetics and specificity.

Keywords: VP1, BLI, mAb, EVs, IgG, IMAC, cross-reactivity, ELISA, WB, HRV

PREFACE

The work reported in this master's thesis has been carried out at the University of Tampere in the faculty of Medicine and Health Technology between June 2020 and December 2020.

I want to thank my thesis supervisor Niila Saarinen for his support and guidance during my course project, internship, thesis practical, and writing. I greatly appreciate the time and sacrifices he made throughout my project and period of thesis writing. Our discussions were fruitful, and I learned a lot. Blessings to you Niila Saarinen.

I want to express my gratitude to Professor Vesa Hytönen as my thesis supervisor and for allowing me to do my course project, internship, and thesis practical at his research group (Protein dynamics). I greatly value his unconditional support during the project, providing me with valuable feedback on my work. Thank you, Professor Hytonen, and blessings to you too.

I thank Niklas Kähkönen for his unwavering dedication to helping and guiding every student, including me. Thank you, Juha Määttä, for teaching me how to perform Biolayer interferometry measurements and our fruitful discussion. To all the protein dynamics group members, I thank you so much for the direct or indirect help I got from you. I don't forget Minna Hankaniemi for her advice and the positive energy she brings to the group. What a wonderful and diverse group you are.

Finally, I want to thank God for my thesis journey and his blessings on my family and me. My thesis journey was not easy, but thanks to my family for supporting and encouraging me, I am forever indebted for their love and care.

Tampere, 20 November 2021

Lackson Kashobwe

CONTENTS

1. INTRODUCTION 1
    1.1 Why enteroviruses? 2
    1.2 Enteroviruses life cycle 3
        1.2.1 Cell entry and uncoating 3
        1.2.2 Translation 3
        1.2.3 RNA replication 4
        1.2.4 Assembly and release 5
        1.2.5 Enteroviruses persistence 6
        1.2.6 Enteroviruses in a host cell 6
        1.2.7 Enteroviruses pathogenesis 7
    1.3 Innate and adaptive immunity 8
        1.3.1 Innate immunity 8
        1.3.2 Adaptive immunity 10
    1.4 Antibody structure and function 11
    1.5 Monoclonal antibodies 13
    1.6 Binding parameters 15
        1.6.1 Affinity 16
        1.6.2 Avidity 16
    1.7 Antibody and viral protein purification methods 18
        1.7.1 Chromatography techniques 18
        1.7.2 Use of protein G in antibody purification 21
    1.8 SDS-PAGE and Western blotting 22
    1.9 Principle of ELISA 23
        1.9.1 Direct ELISA 24
        1.9.2 Indirect ELISA 24
        1.9.3 Sandwich ELISA 24
        1.9.4 Competitive ELISA 25
    1.10 Principle of biolayer interferometry 25
2. MATERIALS AND METHODS 28
    2.1 VP1 protein production and purification 28
    2.2 Production and purification of monoclonal antibodies 32
        2.2.1 mAb production 32
        2.2.2 mAb purification 33
    2.3 ELISA: Mapping of mAb-VP1 antigen interactions 35
    2.4 Biolayer interferometry (BLI) 36
3. THE MAIN SCOPE OF THE THESIS 39
4. RESULTS 40
    4.1 Quality assessment of purified proteins 40
    4.2 VP1 antigens detected in SDS-PAGE and Western blotting 41
        4.2.1 All viral protein antigens were successfully purified 42
    4.3 Determination of Antibody-Antigen interaction by ELISA 43
    4.4 Determination of 3A6mAb Dako and 12A4mAb affinity 46
    4.5 Biolayer interferometry BLI 48
        4.5.1 Regeneration condition 48
        4.5.2 3A6mAb reacts broadly with enterovirus antigens 49

4.5.3 12A4, 9B9, 4D12, and 7C1 did not recognize VP1 in BLI 50
5. DISCUSSION 53
5.1 Good quality purified VP1 antigens and mAb 54
5.2 Binding profile of 3A6 mAb, Dako mAb, and 12A4 mAb in ELISA 55
5.3 3A6mAb had a better binding profile to VP1 than other mAbs in BLI 56
5.4 Generated KD values from ELISA and BLI experiment 59
5.5 Future studies 61
5.5.1 Recommended optimization steps 61
5.5.2 Challenges in diagnosing HEV and RV infection 62
5.5.3 Application of 3A6 and 12A4mAb 63
6. CONCLUSIONS 67
7. REFERENCES 68

LIST OF SYMBOLS AND ABBREVIATIONS

AC	affinity chromatography
APC	antigen-presenting cells
BLI	Biolayer interferometry
CDRs	complimentary determining regions
CVA	coxsackievirus A
CVB	coxsackievirus B
DAMPs	damage associated molecular patterns
DCs	dendritic cells
DNA	deoxyribonucleic acid
ds	double stranded
eIF	eukaryotic initiation factors
EV	enterovirus
Fab	fragment antigen-binding
Fc	fragment crystallizable
GST	Glutathione S-Transferase
HIC	hydrophobic interaction chromatography
IFN	Interferon
IFNAR	IFN-α receptor
IMAC	Immobilized metal affinity chromatography
IRES	Internal ribosomal entry site
ISRE	Interferon –stimulated response
ISGF3	IFN-stimulated gene factor 3
IEX	ion exchange chromatography
Kd	dissociation constant
LC	liquid chromatography
mAb	monoclonal antibodies

pAb	Polyclonal antibody
PAMPs	pathogen-associated molecular patterns
PCR	polymerase chain reaction
PEG	polyethylene glycol
PRRs	pattern-recognition receptors
RNA	ribonucleic acid
RLR	RIG-I-like receptors
RT	room temperature
SDS-PAGE	sodium dodecyl sulfate-polyacrylamide gel
SEC	size-exclusion chromatography
TBP	TATA box-binding protein
T1D	type 1 diabetes
TF	Transcription factor
TLR	Toll-like receptor
UTR	untranslated region
VP	viral protein
VPg	virus encoded protein
WB	Western blotting

1. INTRODUCTION

Enteroviruses (EVs) belong to the Picornavirdae family and commonly infect humans. Infections from EVs can be asymptomatic or have symptoms such as paralysis, rash, poliomyelitis, hand-foot, mouth disease, encephalitis, and myocarditis. The human infecting EVs are divided into seven species: enteroviruses A, B, C, and D and rhinoviruses A, B, C, based on their genome and sequences for the capsid viral protein 1 (VP1). Often a distinction is drawn between polioviruses (EV-C) and the other non-polio enteroviruses due to the significant impact on human health caused by polioviruses. EVs have an icosahedral capsid structure that protects the viral genome and facilitates host cell entry (Pallansch et al., 2013; Tracy et al., 1991). The capsid is formed from 60 copies of each of the four structural viral protein1-4 (VP1-VP4). The VP1-VP3 is located on the outer capsid surface, and VP4 is found on the inner capsid (Saarinen et al., 2018; Samuelson et al., 1994). The EVs' VP1 exhibits the highest sequence variation between serotypes and has a conserved immunodominant epitope of PALTAVETG except for some echoviruses. (Fan et al., 2015 ; Saarinen et al., 2018 ; Shin et al., 2003).

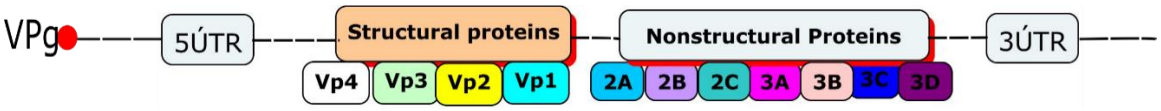

Figure 1. *EV genome structure represents the locations for structural and nonstructural proteins.*

The EV's genome consists of approximately 7.5kb long-stranded positive-sense single-stranded RNA, an open reading frame flanked by untranslated regions (UTRs) at the N and C terminal (**Figure 1**). The UTR regions play a critical role in replicating viral RNA and translation. The N terminal (5'UTR) consists of an internal ribosomal entry site (IRES), facilitating the cap-independent translation initiation. The EVs protein genome-linked (VPg) binds to the 5' end of the RNA and functions as a primer for the positive and negative-strand synthesis during RNA replication. A poly-A tail acts as a template for the VPg protein's uridylation by binding to the 3' end. The EVs genome's coding region includes the P1 encoding

for the structural proteins VP1 to VP4, while P2 and P3 encode for the nonstructural proteins (**Figure 1**). These proteins are responsible for polyprotein processing, RNA replication, cleavage of the host cell proteins, and modification of the host cell to promote the EVs lifecycle (see **Figure 2**) (Howley & Knipe, 2020; Pallansch et al., 2013; Tracy et al., 1991).

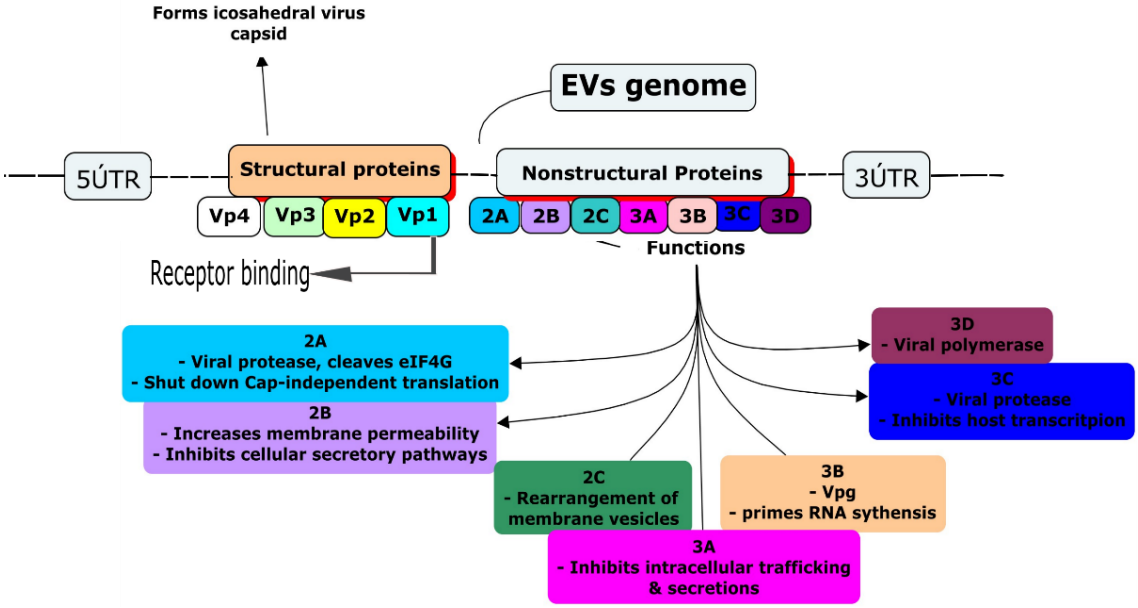

***Figure 2**. The functions of EV nonstructural and structural proteins. The specific role of nonstructural proteins that are crucial in viral replication and viral genome assembly.*

1.1 Why enteroviruses?

EVs cause infections that affect public health. For example, Polioviruses cause fatal diseases such as poliomyelitis, and Coxsackieviruses cause hand, foot, and mouth disease in children (Jacobs et al., 2013). Moreover, human rhinoviruses (HRV) are also a public concern because they cause the common cold (Österback, 2015). Even though the common cold symptoms are not particularly serious for most people, they cost billions of dollars due to many missed work hours (Leotte et al., 2017). Furthermore, the common cold can be much more severe for people with respiratory diseases such as asthma and bronchitis (Cathcart et al., 2015). Therefore, the diagnostic and management of EV and HRV infections are essential.

1.2 Enteroviruses life cycle

Enteroviruses can be characterized by specific tissue tropism and differences in virulence. Factors such as the host immune system, genetics of the infecting virus, and internal ribosome entry site (IRES) play a role in EV life cycle and pathogenesis.

1.2.1 Cell entry and uncoating

When an EV virion attaches to the viral receptor (host) **Figure 3**, the viral structural protein undergoes a conformational change into an A-particle. An A-particle has the internalized hydrophobic N terminus of the VP1 on the virion's outer surface and lacks the VP4 protein (Howley & Knipe, 2020; Pallansch et al., 2013). A-particle has an increased affinity to the cell membranes compared to immature virion, and they are involved in cell membranes' pore formation to free the viral genome (Howley & Knipe, 2020; Pallansch et al., 2013). Different EVs use different pathways and mechanisms to facilitate cell entry. However, the type of host receptor is critical in freeing the viral genome (Coyne & Bergelson, 2006; Patel et al., 2009). For example, CVB3 utilizes caveolin dependent and dynamin independent pathways in polarized CaCo2 cells, whereas, in Hela cells, they use the dynamin lipid raft dependent and clathrin caveolin independent pathway (Coyne & Bergelson, 2006; Patel et al., 2009).

1.2.2 Translation

When the viral genome is released into the host cell, VPg is cleaved by the cellular unlinkase enzyme. The viral RNA is translated into a single polyprotein through IRES's cap-independent mechanism (Howley & Knipe, 2020; Pallansch et al., 2013). Subsequently, the newly produced polyprotein is broken down into precursor proteins P1, later cleaved into structural proteins VP0, VP1, and VP3. In contrast, P2 and P3 undergo series of cleavage to generate non-structural proteins (2A, 2B, 2C, 3A, 3B, 3C, 3CD, and 3Dpol) (**Figure 2** &**Figure *3***) (Cathcart et al., 2015; Howley & Knipe, 2020; Pallansch et al., 2013; Tracy et al., 1991).

1.2.3 RNA replication

RNA replication of the EVs occurs in the cytoplasm of the infected cell on the membranous vesicles, formed by 2B and 2C viral proteins through rearranging the cellular membranes. 2B and 2C proteins function as a scaffold for RNA stability, facilitate positioning and concentration of viral replicating proteins in the right place, to ensure efficient catalyzation of RNA synthesis (Howley & Knipe, 2020; Pallansch et al., 2013). During RNA replication, genomic RNA is used as a template to synthesize a negative RNA strand. A 3D polymerase initiates the negative-strand synthesis at the 3' poly-A tail using uridinylated VPg as a primer. Then, the newly produced negative-strand acts as a template for synthesizing the positive-strand RNA multiple times. The dsRNA is an intermediate molecule during RNA replication. Furthermore, the newly synthesized positive RNA strands can be loaded into virions or undergo translation to generate viral proteins (**Figure 3**) (Howley & Knipe, 2020; Pallansch et al., 2013; Tracy et al., 1991).

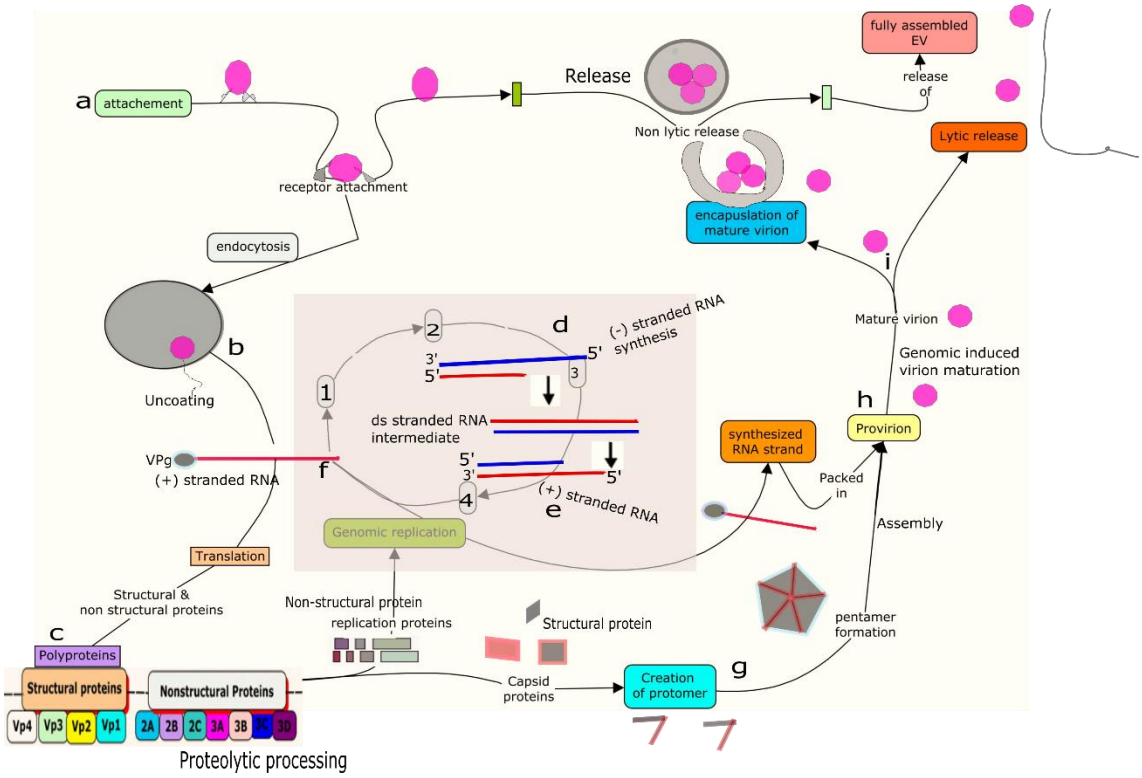

Figure 3. *Overview of the enterovirus life cycle. a) Virion binds to the host cell receptor and enters the cells via endocytosis. b) virion releases its positive-stranded RNA genome into the cytoplasm, and the viral genome binds to the VPg, which acts as a primer during replication. c) The translation of (+) RNA produces a polyprotein cleaved into replication structural and nonstructural proteins. d) RNA polymerase (3Dpol) uses (+) RNA-strand to synthesize (-) RNA-strand. e) The newly produced (-) RNA-strand serves as a template for the synthesis of the new (+) RNA-strand. f) Newly synthesized (+) RNA-strand either used as a template during replication or packaged into progeny virions. g) structural proteins forms protomers, and then pentamers formation. h) Assembly of provirions and mature virions are genomically induced and cleavage of VP0 into VP4 and VP2. i) The mature virions are released from the cell by either nonlytic release of extracellular vesicles or through cell lysis in a late infection stage. The dsRNA serves as an intermediate between (+) RNA and (-) RNA. Figure adapted from (Baggen et al., 2018).*

1.2.4 Assembly and release

The VP0, VP1, and VP3 precursor proteins assemble newly produced virions by forming a protomer. Then, five protomers create a 5S pentamer, and subsequently, the twelve pentamers form a procapsid that envelops the viral genome. Finally, the late stage of the virion assembly involves breaking down VP0 protein to generate VP2 and VP4, resulting in mature virion. **Figure 3** shows the newly assembled and fully matured virion released in a lytic or non-lytic infection through vesicles budding (Howley & Knipe, 2020; Pallansch et al., 2013).

1.2.5 Enteroviruses persistence

EVs have been shown to cause persistent infections in cultured cells in vitro and in vivo organs such as the heart and skeletal muscle (Feuer et al., 2002; Frisk, 2001; Pavio et al., 2000; Pelletier et al., 1991). EV infection persistence may be associated with viral, cellular components, and the immune response, leading to infectious or non-infectious EVs (Frisk, 2001). A mutation in the viral receptor, genome, or capsid coding region may lead to EV infection persistence. Cells such as neuroblastoma and Hep-2c-cells having capsid mutation showed persistent EV infection in-vitro (Duncan & Colbère-Garapin, 1999; Pelletier et al., 1991). The mechanism of EV persistence may vary. However, a mutation in the EV VP1 may disrupt the attachment process and alter the capsid's conformation. Moreover, the deletion of the 5'UTR region of EV during acute lytic infection may decrease replication rate and non-cytopathic effect (Chapman et al., 2008; Tracy et al., 2008).

Persistent EV infections are associated with chronic diseases such as type 1 diabetes (T1D), dilated cardiomyopathy, post-polio syndrome, and chronic fatigue syndrome, including chronic inflammation in the gut mucosa of the T1D patients (Chia & Chia, 2008; Frisk, 2001; Julien et al., 1999; Oikarinen et al., 2012). For example, an in-vitro study showed that a pancreatic ductal cell line harboring EV infection had disrupted islet-like cell formation because of EV persistence (Yin et al., 2002).

1.2.6 Enteroviruses in a host cell

EV uses the host cell to replicate itself by taking control of the host cell replicating machinery. They shut down the cellular cap-dependent translation to facilitate IRES-driven protein synthesis. The EV's 2A proteinase cleaves eIF4G essential for cap-dependent translation (Cathcart et al., 2015). Also, 2A acts as a scaffold protein to the eIF4F cap-binding complex comprising eIF4E cap-binding protein and eIF4A as helicase (**Figure 4**). Also, eIF4G interacts with poly (A) binding protein (PABP), which binds to the 3'poly (A) tail of cellular mRNAs, enabling multiple translation initiations. The cleavage of eIF4G by EV during the early stage of infection does not permit the eIF4G fragment to aid cap-dependent translation. On the other hand, the component of eIF4G C-terminal binds to eIF3 and engages

the 40s ribosomal subunit to start the viral IRES-driven translation (Aminev et al., 2003; Chase & Semler, 2012; Ohlmann et al., 1997). Additionally, EV affects host transcription and promotes intracellular membrane reordering. 3C proteinase cleaves TATA box-binding protein (TBP) and inhibits RNA polymerase II transcription (Cathcart et al., 2015; Chase & Semler, 2012). Furthermore, the protease of EVs breaks down essential cellular proteins and modulates critical factors that modulate host innate and adaptive immune responses (Liu et al., 2014).

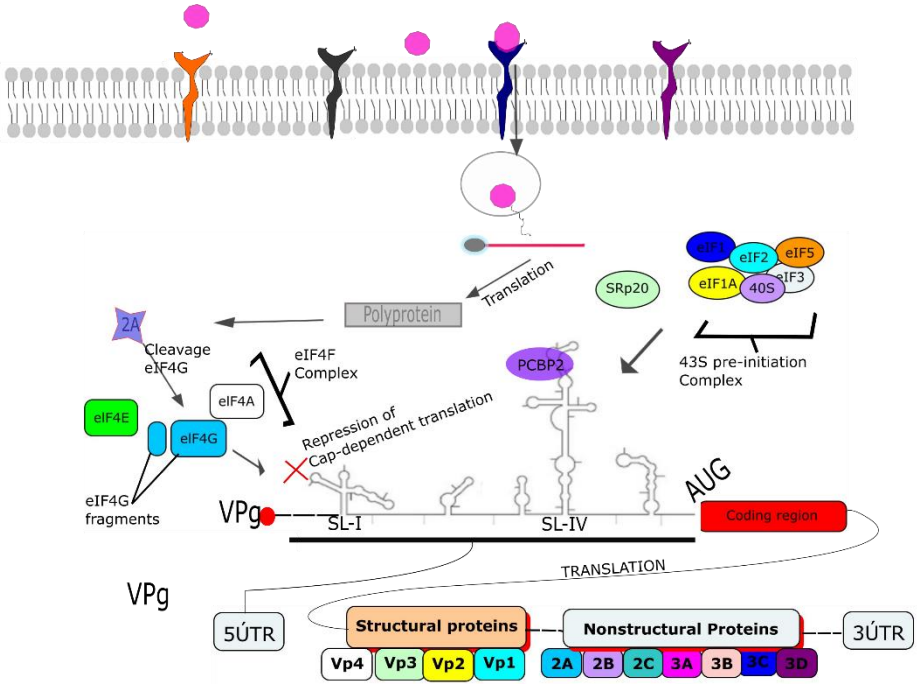

Figure 4. *Enterovirus cap-independent translation. Viral protease 2A cleaves eIF4G and interferes with the eIF4F binding complex to interact with 5'end. The absence of the eIF4F complex (cap) inhibits ribosome scanning, and no cap-dependent translation is allowed. Adopted from (Chase & Semler, 2012).*

1.2.7 Enteroviruses pathogenesis

The exposure routes through which EVs get transmitted are the fecal-oral route and respiratory tract. Most EV infections are asymptomatic, but there could be mild symptoms such as fever, diarrhea, vomiting, and rash during EV replication in the gastrointestinal and respiratory tract. The replication of EV in the lymph node allows the virus to enter the blood circulation in which they are transported to critical organs such as the brain, heart, and muscle (Cathcart et al., 2015; Chapman et al., 2008; Pallansch et al., 2013; Pelletier et al., 1991).

The incubation period of EV infection ranges from 2 to 10 days before the onset of symptoms (Pallansch et al., 2013). The EV's primary target organs are intestinal mucosa and the upper respiratory tract, with a low viral load and mild viremia. In contrast, the EV secondary target organs include the CNS, the heart, and the muscle, which have high viral loads. The spread of the EV infection in the secondary organs is fast and causes myocarditis, paralytic poliomyelitis, aseptic meningitis, acute hemorrhagic conjunctivitis, and flaccid paralysis, depending on the target organ (Howley & Knipe, 2020; Pallansch et al., 2013).

1.3 Innate and adaptive immunity

The immune system's complexity provides sufficient protection against viruses, bacteria, and fungus, including other foreign pathogens invading the body. Moreover, the adaptive immune system comprises immune cells such as B and T lymphocytes responsible for the specific humoral and cell-mediated responses. Innate immunity includes cytokines and cells such as macrophages, neutrophils, and natural killer cells that crosstalk with adaptive immunity in fighting against pathogens (Abbas et al., 2017).

1.3.1 Innate immunity

The innate immune system is the first line of defense against microbial infections. It comprises cellular and biochemical defenses that are ready to respond to any foreign invasion. The innate immune response targets specific structures common to groups of related microbes, and it is nonspecific. Furthermore, innate immunity comprises physical and chemical barriers such as antimicrobial chemicals secreted at epithelial surfaces and epithelia, phagocytic cells such as neutrophils, macrophages, dendritic cells, and innate lymphoid cells (**Figure 5**)(Hansson et al., 2002). Also, natural killer cells, blood proteins that contain the complement system, and other inflammatory mediators are part of innate immunity. The primary goal of innate immunity is to prevent the spread of the infection and crosstalk with the adaptive immune system through antigen-presenting cells (APC) such as dendritic cells and macrophages (**Figure 5**) (Abbas et al., 2015).

The innate immune system can recognize viral pathogen-associated molecular patterns (PAMPs) via the pattern recognition receptors (PRR). The PRRs include Toll-like receptors (TLR), RIG-I-like receptors (RLR), and nucleotide-binding oligomerization domain (NOD) like receptors (NLR). The TLR and RLR detect viral PAMPs and activate adaptor proteins MYD88, TRIF, and IPS-1, thereby switching on multiple kinases (Acheson, 2011; Honda & Taniguchi, 2006; Platanias, 2005). The activated kinases phosphorylate the transcription factor (TF) NF-kB, IRF7, and IRF3. The phosphorylated TF enters the cell nucleus, interacts with the interferon-stimulated response element (ISRE), and then induces the production and release of type 1 IFN proinflammatory chemokines (Von Herrath, 2009).

The innate immune response to the EV infection involves releasing local and systemic inflammatory mediators such as cytokines and chemokines. The function of chemokines is to facilitate leukocyte migration and trafficking. The cytokines produced at an early stage of infection activate the antiviral mediators (Abbas et al., 2015; Chen & Ling, 2019; Raj et al., 2019). In systemic viral infections, cytokine and chemokine levels are high and associated with clinical symptoms and illness severity (Wang et al., 2012; Wang & Liu, 2014). For example, an in-vivo study of the mice deficient in type 1 IFN was more vulnerable to EV infection than wild-type mice (Wang et al., 2010; Wessely et al., 2001).

The TLR3, 7, and 8 have been shown to recognize CVB infection in human cardiac cells (Triantafilou et al., 2005; Triantafilou & Triantafilou, 2004). However, Detecting CVB by both TLR7/8 induces an inflammatory response that may cause myocardial tissue damage (Triantafilou et al., 2005). In vitro, the TLR4 recognized EV infection in pancreatic cells, while TR3 was critical in EV infection prevention (Triantafilou & Triantafilou, 2004; Wessely et al., 2001). Moreover, treating the infected cells with type I and II IFNs can block EVS replication (Hultcrantz et al., 2007). However, EV can invade the innate immunity by disrupting PRR responsible for EV recognition, blocking the IFN activation and release, thus inhibiting the antiviral activity (Chen & Ling, 2019; Liu et al., 2014; Negishi et al., 2008).

1.3.2 Adaptive immunity

Acquired immunity plays a significant role in identifying and responding to many nonmicrobial and microbial-related substances. The main characteristic of adaptive immunity is recognizing foreign antigens and responding more vigorously to repeated exposures of the same antigen. Therefore, adaptive immunity is specific and has memory, and it comprises special cells like lymphocytes and their secreted antibodies (**Figure 5**). Antigens are foreign substances that induce a specific immune response and are recognized by lymphocytes and antibodies (Abbas et al., 2017)

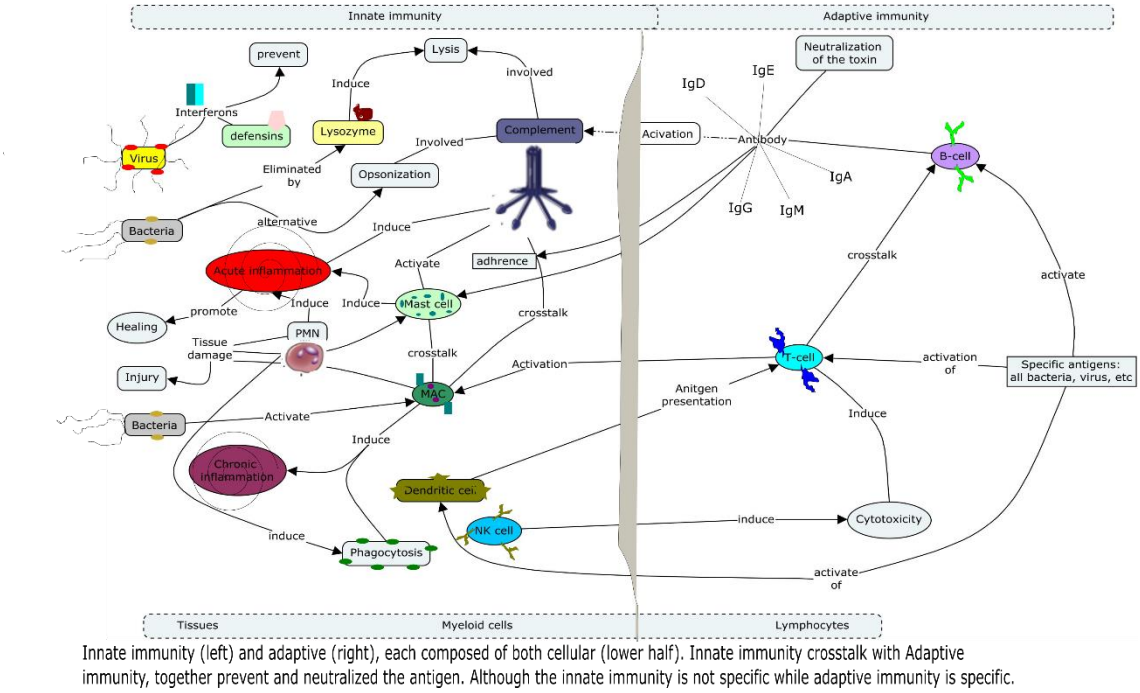

Innate immunity (left) and adaptive (right), each composed of both cellular (lower half). Innate immunity crosstalk with Adaptive immunity, together prevent and neutralized the antigen. Although the innate immunity is not specific while adaptive immunity is specific.

Figure 5. *The interplay between Innate and Adaptive Immunity. Innate immunity (left) is nonspecific and performs a limited function to clear out the toxins or antigen. Adaptive immunity (right) is specific and plays multiple roles in eliminating the foreign antigen, and the cellular components of both innate and adaptive immunity crosstalk to each other. The antigen-presenting cells (APCs) such as dendritic and macrophage cells present the antigen to T-helper cells and B cells. Adopted from creative-diagnostics.com.*

Host immune system, tissue tropism, genetic factors from both host and virus, and the virus virulence play a crucial role in modulating the EV infection. The initial response to EV infection begins with the innate immune system and is followed by the adaptive immune response (Dunn et al., 2003; Pallansch et al., 2013; Tracy et al., 2008). The T and B cells facilitate the elimination of the EVs.

The T cells facilitate cell-mediated immune response, whereas B cells secrete the antibodies, which play a crucial role in the humoral immune response. The antibody's primary function is to prevent viral capsid binding to uninfected cells and recruit macrophages and neutrophils via a complement system (Newton et al., 2016). The secreted antibodies are initially of IgM class and are typically present for seven to ten days. Then, the IgG class antibodies that are smaller, more specific, and have a longer half-life are present for a more extended period (Abbas et al., 2015; Dotzauer, 2012; Gauntt, 1997). In this thesis, the focus is on adaptive immunity B cells' secreted antibodies.

1.4 Antibody structure and function

The immune system's antigen-recognizing molecules, such as T cell receptor (TCR), immunoglobulins (Ig), and major histocompatibility complex (MHC) molecules, recognize the foreign antigen and facilitate its elimination (Forthal, 2014). Here we focus on immunoglobulin G (IgG) and its purification from rat hybridoma cells.

B lymphocytes produce Igs and secrete them into the bloodstream and lymphatic system. The Igs facilitate the neutralization and elimination of the antigen out of the body. Ig's antigen-binding site comprises three complementary determining regions (CDRs) in heavy and light chains (Chiu et al., 2019; Vandyk & Meek, 1992). Antigen molecules such as proteins, lipids, polysaccharides, and small chemicals interact with Ig. The antigen-binding affinity of Ig ranges from KD 10^{-7} – 10^{-11} M, and the average affinity of Igs increases during an immune response. Ig antibodies comprise a family of structurally related glycoproteins produced as membrane-bound or secreted by B lymphocytes. The antibody structure consists of the antibody binding site (Fab), the constant region (Fc), and complement binding sites on the Fc region (**Figure 6**) (Abbas et al., 2015; Forthal, 2014).

The membrane-anchored Ig function as the antigen receptor recognition in immature B cells. In contrast, the secreted antibodies serve as mediators of specific humoral immunity by facilitating different effector mechanisms to eliminate the bound antigens. Furthermore, the antigen-binding regions of antibody molecules

are highly variable. Changes in the Fab region can generate up to millions of different antibodies, each with distinct antigen specificity (Abbas et al., 2015).

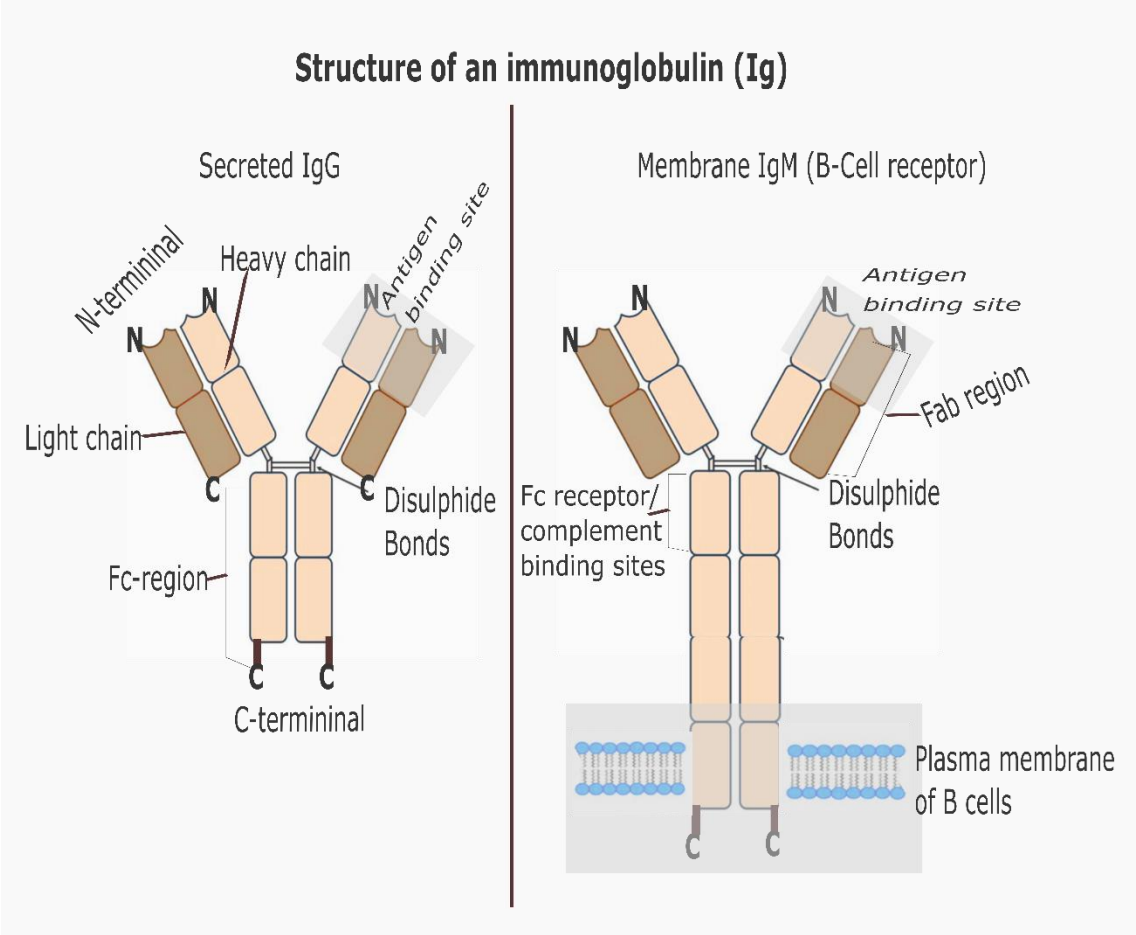

Figure 6. *Schematic diagram of secreted IgG (left) and membrane-bound IgM: The antigen sites are produced by the juxtaposition of variable (V) region of heavy (H)and light (L) chain domains. IgM molecule on the surface of B-cell has more Fc region domain than IgG. The membrane antibody contains C-terminal transmembrane and cytoplasmic portions of the B-cell plasma membrane. Figure adapted from* (Abbas et al., 2015).

All antibodies have a typical symmetric core structure of two identical covalently linked heavy chains and two similar light chains, each bonded to the heavy chains (**Figure 6**). Each chain comprises two or more independently folded Ig domains of several amino acids consisting of conserved sequences and intra-chain disulfide bonds (Chiu et al., 2019). Additionally, the N–terminal domain of the heavy and light chain creates the variable (V) region of antibody molecules, which is different among antibodies of different specificities. The V regions of heavy and light chains contain separate hypervariable regions of about 10 amino acids spatially assembled to form the antibody molecule's antigen-recognizing site (Abbas

et al., 2015). B cells initially produce only the membrane-bound Ig. However, activated B cells (plasma cells) secret the Ig, which have the same antigen-binding specificity as the original membrane-bound Ig receptor (Abbas et al., 2017).

Humans have five Ig classes/subtypes, IgA, IgD, IgE, IgG, and IgM. Each of them has different but overlapping tasks. Some antibody classes have different subtypes that perform various duties. The human antibody isotype IgA has 2 subtypes (subtypes 1 and 2), subtype 2 being the most abundant IgA form and secreted as IgA dimer. IgA plays a critical role in mucosal immunity. IgD is a naïve B-cell receptor with no subtypes and is not secreted. IgE is an essential antibody in immediate hypersensitivity (allergy), and it is secreted as a monomer with no subtype. As **Figure 6** (left) shows, IgG has a molecular weight of about 150 kDa and are the most abundant Ig in mammalian, and their production rate is higher than the rest of the Igs. IgG is a classical antibody that plays a crucial role in opsonization, complement activation, cell-mediated cytotoxicity, neonatal immunity, and B-cells feedback inhibition. The IgG subtypes include IgG1, IgG2, IgG3, and IgG4, secreted as monomers (Vidarsson et al., 2014). IgM is a membrane antibody (**Figure 6**, right) with low antigen-binding affinity but high avidity and secreted as a pentamer with no subtype. IgM is essential in Naïve B cell antigen receptor recognition and complement activation (Abbas et al., 2017; Vandyk & Meek, 1992).

1.5 Monoclonal antibodies

The IgGs are the most abundant antibody found in all human body fluid types, and they have a long half-life. They are also easy to isolate and purify. IgGs, including other antibodies, share a relatively uniform and well-defined protein structure that allows them to be purified, labeled, detected predictably, and reproducible using similar protocols and techniques. For decades antibodies have been used for diagnostics and, more recently, for therapeutic purposes. Antibodies are essential tools for detecting antigens in immunoblotting, immunohistochemistry, and immunoaffinity chromatography (Saarinen et al., 2018; Trier et al., 2012).

Monoclonal antibodies are generated by immunizing rats (**Figure 7**), mice, or other appropriate animals, with an antigen and an adjuvant to stimulate B cells to produce antibodies. Immunizing an animal with very pure antigens results in the production of specific antibodies. At the end of immunization, the animal is sacrificed. The spleen cells containing B cells are extracted and electro-fused with carcinoma cells, resulting in several hybridoma cell lines, each producing a single monoclonal antibody indefinitely, as **Figure 8** illustrates. Poly-specific polyclonal antibodies are present in the immunized animal's serum (Scheringer et al., 2014). Polyclonal antibodies (pAb) are broader in detecting the antigens due to the composition of several kinds of antibodies with different target epitopes, rendering the pAb less specific to antigens than mAb (Trier et al., 2012).

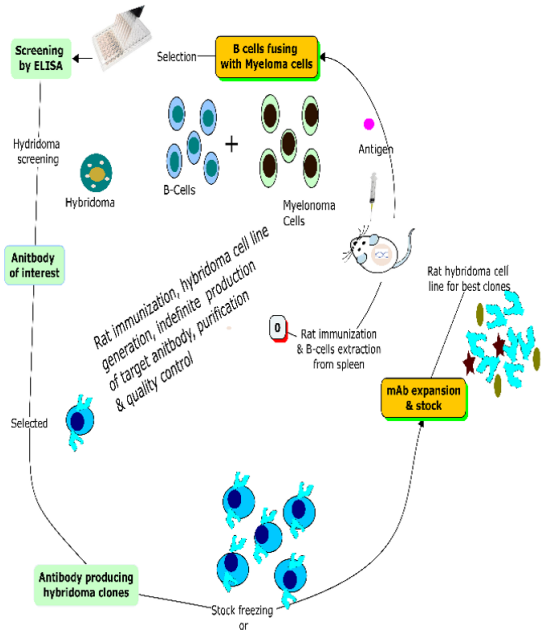

***Figure 7**. Generation of hybridoma cells: 0) rat immunization by a specific antigen. The fusion of innate functions of both immune and cancer cells generates hybridoma cells, which produce mAbs of interest indefinitely.*

Generally, pAbs are more robust and essential in detecting native proteins, although there can be variations between batches in binding, making regular use difficult. On the contrary, mAb produced from cloned cell lines targets the specific epitope of an antigen of interest and with little or no variation between batches in binding affinity (Trier et al., 2012). The hybridoma cell lines are cultured using a

synthetic medium comprising nutrients and additives to promote cell growth and mAb production.

Several monoclonal antibodies have been developed against EVs for the past decades. Some are specific to a single species or serotype, and others are group-specific. For example, Cox mAB 31A2 detects CVB1 and CVB3 by binding to CVB VP1, Dako (5D8/1), and 9D5 act more widely, and 3A6 recognizes EV-B subtypes and poliovirus-3, except EV-A (Saarinen et al., 2018). Many of these antibodies interact with the N-terminal part of VP1, and only a few bind to other parts of the VP1 region (Saarinen et al., 2018; Shin et al., 2003). The 3A6 and Dako monoclonal antibodies recognize an epitope in the N-terminal region of VP1 (Saarinen et al., 2018a). Specific amino acids involved in antibody recognition are present in a highly conserved enteroviral serotypes region, which explains the possible cross-reactivity of antibodies observed within the EVs family (Samuelson et al., 1994; Shin et al., 2003).

1.6 Binding parameters

The interaction between proteins is described as binding affinity comprising a receptor and its respective ligand, for example, antibody-antigen interaction. An antigen binds to the antibody's epitope by using different types of noncovalent bonds such as hydrogen bonds, ionic bonds, Van der Waals, and electrostatic forces. Biomolecular interactions are based on affinity and avidity. Avidity represents a binding strength of more than one binding site. In contrast, affinity indicates the binding strength of one binding site between a protein and a ligand, that is, one epitope (Bongrand, 2014; Božič et al., 2013). The affinity of a molecule to its binding partner is described as the strength of the non-covalent interaction between one ligand-binding site with one analyte binding site. On the other hand, a molecule's avidity is defined by the total strength of all possible binding interactions between the two molecules (Tobias & Kumaraswamy, 2013).

1.6.1 Affinity

Affinity is a measure of binding strength between two interacting partners. When considering the antibody-antigen interactions, the binding strength or affinity represents the interaction between a single antibody binding site and the antigen's epitope. Thermodynamically, affinity is the sum of all forces that leads to increased binding strength subtracted from all forces that lead to decreased binding strength. Binding affinity comprises noncovalent interactions that increase the interacting molecules' affinity (Bongrand, 2014; Božič et al., 2013).

Binding affinity measures the dynamic equilibrium of the ratio of k_{on}, which is the rate at which complex forms, and k_{off}, a rate at which a complex dissociates. For the antibody-antigen interactions, the dynamic equilibrium can be described as follows in equation 1.

$$[Ab] + [Ag] \leftrightarrow [AbAg] \qquad [1]$$

In this equation, Ab represents antibody, and Ag represents antigen.

According to Equation 1, k_{on} is the rate at which antigen binds to the antibody, and k_{off} is the rate at which the antibody-antigen complex dissociates. Therefore, the antibody-antigen complex can be quantified at equilibrium by calculating the association constant Ka using equation 2.

$$K_{off} = K_{on/}K_a \qquad [2]$$

Inversely dissociation constant K_D of the interaction can be calculated by using equation 3.

$$K_D = \frac{K_{off}}{K_{on}} = \frac{[Ab][Ag]}{[AbAg]} \qquad [3]$$

1.6.2 Avidity

Structurally, antibodies are multivalent biomolecules that contain more than one binding site. For example, IgG antibodies are bivalent molecules that can interact with more than one antigen epitope. The sum of the binding strength of an anti-

body at every binding site is referred to as avidity. Therefore, avidity is well defined by the binding affinity describing the interactions' strength at a singular binding site, the valency, and the total number of participating binding sites. The avidity determination also includes the structural arrangement, the participating antibody structure, and an antigen (Bongrand, 2014; Božič et al., 2013). Avidity plays a critical role in kinetics experiments because it can affect the overall generated affinity (Tobias & Kumaraswamy, 2013).

The binding assay enables approximating the binding affinity of the antigen-antibody complex based on the principles of ligand-receptor interaction. In the equilibrium studies, the association and reversibility of the ligand binding to the receptor can be quantified. The equilibrium is achieved through the association and dissociation of the ligand. The ligand-protein complex consists of noncovalent interactions, and this phenomenon allows the study of antibody-antigen interaction based on Equations 1 and 2 (Hein et al., 1982; Lambert, 2004; Motulsky & Neubig, 2010).

The K_D value represents the affinity of the ligand binding to the protein, and at which half the protein's concentration in the sample forms a complex with the ligand. When the K_D is small, the ligand affinity to the protein is high or strong, and when the K_D is large, the ligand affinity to the protein is low or weak. Also, k_{off}/k_{on} is equal to K_D. The K_D of protein-ligand interactions may differ based on association and dissociation constant rate. Equation 4 can generate the saturation binding curves showing the antibody-antigen interaction's binding profile based on a 1:1 binding ratio (**Figure 8**) (Hein et al., 1982; Lambert, 2004; Motulsky & Neubig, 2010).

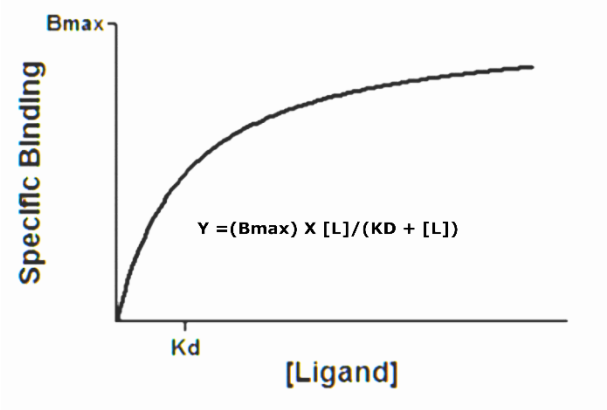

Figure 8. *The binding response of ligand-protein interaction*

$$Y=(B_{max})X[L]/ (K_D + [L]) \qquad [4]$$

Where is X= ligand concentration; Y= binding response.

B_{max} is the maximum specific binding in the same units as Y. It is the specific binding extrapolated to very high concentrations of binding response. Its value is always higher than any specific binding measured in the real-time experiment. K_D is the equilibrium dissociation constant in the same units as X. It is the ligand concentration needed to achieve a half-maximum binding at equilibrium. X is the ligand concentration.

1.7 Antibody and viral protein purification methods

For the purification of antibody and viral protein from cell supernatant or mixtures, different techniques are used. Biological interactions between ligand/antigen and target protein can result from electrostatic or hydrophobic interactions, van der Waals' forces, or hydrogen bonding. Using different pH or high salt concentration buffer or competing ligand, the target molecule can be purified successfully (Block et al., 2009; Bornhorst & Falke, 2000).

1.7.1 Chromatography techniques

The chromatography technique, such as liquid chromatography, allows the separation of molecules dissolved in a liquid mobile phase bypassing the liquid over

an immobilized phase or resin. These molecules have different degrees of interaction and can be separated based on charge, hydrophobicity, size, and affinity using various methods, as seen in (**Figure 9**).

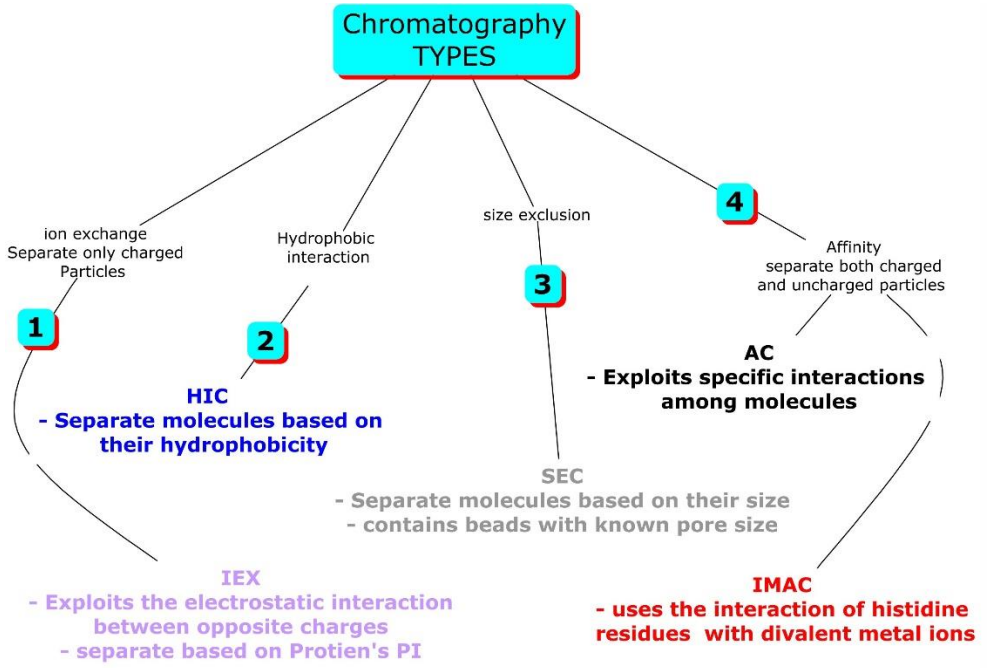

Figure 9. *Commonly used mode of separation based on charge (IEX), hydrophobicity (HIC), particle size (SEC), and affinity (AC/IMAC).*

Ion exchange chromatography (IEX) is a liquid-based chromatography in which ionic substances are analyzed or purified, and the separation is based on charge. IEX allows the separation of the target molecules such as inorganic anions, cations, and proteins, having an opposite charge of the immobilized phase. In IEX, molecules are separated according to the strength of their overall ionic interaction with solid-phase support. Hydrophobic interaction chromatography (HIC) is another method in which molecules are separated based on their hydrophobicity. HIC exploits Van der Waals interactions and uses a reversible interaction between the protein and the hydrophobic ligand of a HIC resin (Grodzki & Berenstein, 2010; Heinevetter, 1997).

Affinity chromatography (AC) enables the separation of the target molecule based on their molecule-specific interaction with a stationary phase. The target molecule has a high affinity to the stationary phase. It can separate charged and uncharged molecules such as antigens, antibodies, and proteins using specific

interactions among molecules in the mobile and immobilized phase. For example, protein G is a recombinant protein produced in expression systems such as *E. coli* and insect cells, immobilized and functionalized to the affinity matrix. When the mobile phase containing mixtures of protein is passed over functionalized protein, the target protein is captured. After that, the bound protein can be released from the stationary phase using a buffer with a low pH or high salt concentration or competing ligand (Ayyar et al., 2012; Darcy et al., 2017; Heinevetter, 1997). On the other hand, glutathione S- transferase (GST) tagged protein can be purified by first binding to glutathione contained stationary phase and subsequently eluted using a high concentration of glutathione. GST interacts with glutathione making protein purification easier (Harper & Speicher, 2011; Walls & Loughran, 2011).

The size exclusion chromatography (SEC) can also isolate a molecule of interest from the mixture based on size and molecular weight. SEC uses resins that comprise beads with known pore sizes, and when a complex mixture is passed over these resins, small molecules go through the bead's pores, and large molecules go around the beads, passing through the beads void space, and elute first. Contrary to AC and IEX, molecules in SEC are not supposed to bind to the chromatography resin, and the buffer composition does not directly affect resolution or degree of separation (Block et al., 2009; Grodzki & Berenstein, 2010). However, in practice, interactions between analytes and the SEC matrix occur.

Immobilized metal affinity chromatography (IMAC) is a valuable method for purifying biological samples such as proteins. The principle of IMAC is that metal ions are immobilized to chromatographic support such as Sepharose containing chelating ligands. The immobilized metal ions interact with amino acid side chains on the surface, such as histidine. Factors such as a chelating ligand, metal ion, absorption, and elution conditions play a role in purifying a protein of interest. The protein adsorption in IMAC is due to the interaction between electron donor groups from the protein surface and an immobilized metal ion. The most used transition metal ions as electron-pair acceptors or electrophiles are Cu2+, Ni2+, Zn2+, Co2+, and Fe3+ (Cheung et al., 2012). Meanwhile, electron donor atoms (nucleophiles) such as N, S, and O exist in the form of a chelating agent bound

to the chromatographic support. The elution, referred to as the desorption of the target protein, occurs by protonation utilizing elution buffers with low pH or high pH (Andjelković et al., 2017).

His-tag is an amino acid that interacts with Ni2 better than any other amino acid (Andjelković et al., 2017). The presence of electron donor groups on the imidazole ring enables histidine to interact with transition metal immobilized to the chromatographic support. Moreover, many proteins consist of cysteine, phenylamine, tyrosine, and tryptophan on the protein's surface, with a high affinity to selective metal ions. The IMAC technique provides ligand stability, mild elution conditions, high protein loading, low cost, easy column reusability, and the use of poly-his tags makes protein purification easier. Although, the IMAC technique is considered unsuitable for therapeutic protein purification (Andjelković et al., 2017; Block et al., 2009).

The amphoteric amino acids are the building blocks for proteins, and their charge is dependent on buffer pH, which allows for fine-tuning the purification conditions. Therefore, using one or two methods described above, antibodies and viral protein can be purified. In our experiment, we used SEC for supernatant pretreatment and AC for antibody purification. The IMAC technique was utilized to purify the VP1 proteins.

1.7.2 Use of protein G in antibody purification

Purifying antibodies is essential because supernatant or serum consists of mixtures of biomolecules that interfere with the target antibody functions. The standard method of purifying mAb is centrifugation, followed by ion-exchange chromatography (IEX) (Heinevetter, 1997). The IEX technique purifies the antibodies based on their isoelectric point (pI) (Chen et al., 2010; Trier et al., 2012). The pI of antibodies ranges from 7.5 to 8.5. With appropriate binding and elution buffer, the mAb can be successfully purified using IEX. To purify mAb from the rat hybridoma cells, we used AC with functionalized protein G.

Protein G is a bacterial cell wall protein extracted from the group G streptococci, and it binds to most mammalian Ig. Protein G bind to the IgG Fc region and

weakly interacts with the fab region. Based on the DNA sequence, protein G is a single, non-glycosylated protein that contains 200 amino acids having a molecular mass of 21.8 kDa. It has two IgG-binding regions, albumin and cell surface binding region. Protein G is produced as a recombinant protein in Escherichia coli, and it has an isoelectric point (pI) of 4.55. The recombinant form of protein G does not contain albumin and cell surface binding sites. These sites have been removed to reduce the nonspecific binding when purifying the IgGs (Chen et al., 2010; Labrou, 2014). Protein G has an affinity to IgG antibodies and enables easy purification of the mAb (Duhamel et al., 1979; Eliasson et al., 1989). However, protein G has different affinities to different Ig of other animals (Lindmark et al., 1983; Ohlson et al., 1989; Trier et al., 2012). Our mAbs were produced in rat hybridoma cells line.

1.8 SDS-PAGE and Western blotting

Sodium dodecyl sulfate-polyacrylamide denaturing gel electrophoresis (SDS-PAGE) separates the proteins primarily based on their molecular weight. At the same time, intrinsic characteristics of the proteins also influence electrophoretic mobility (Gwozdz & Dorey, 2017). SDS-PAGE is used as quality control in assessing the purity of the purified proteins. The visualization of the target protein process comprises sample treatment by heating and exposing the protein to a Laemmli buffer containing SDS-PAGE and a reducing agent (Definition, 2008). Then the SDS-separated protein is transferred from the gel to the membrane for Western blotting (WB) analysis. The membrane is blocked for nonspecific binding sites using BSA. Subsequently, the immunodetection is performed using primary and secondary antibodies, followed by target protein visualization. WB is essential in characterizing antibody-antigen interactions, quality assessment of the purified proteins, and determining the polypeptide chain's relative molecular weight (Brooks et al., 2003; Gräslund et al., 2008).

The sample treatment enables the protein to solubilize and denature, dissociate polypeptides from each other, and reduce disulfide bonds. Also, sample treatment ensures that secondary and tertiary protein structures are broken up to pre-

vent movement changes through the polyacrylamide matrix. The sample treatment comprises heat, denaturing agent (SDS), and a reducing agent, such as beta-mercaptoethanol. The reducing agent facilitates the breaking up of disulfide bonds, and SDS encapsulates the proteins, thus enabling them to carry a negative charge proportional to their length. It masks the inherent charge of the proteins, and the SDS-coated proteins are separated based mostly on their molecular mass. The protein bands on the gel are transferred to nitrocellulose membrane for Western blotting (AP) (Brooks et al., 2003; Gwozdz & Dorey, 2017; Trier et al., 2012).

1.9 Principle of ELISA

The enzyme-linked immunoassay (ELISA) principle is based on identifying and quantifying protein or antigen of interest in a solution (or mixture of cell lysate) using enzyme-linked antibodies. The enzyme is conjugated to the antibodies; for example, alkaline phosphatase (AP) or horseradish peroxidase (HRP) functions as an amplifier of detection signal by changing a substrate color in the wells. There are four main types of ELISA (**Figure 10**), and they differ from each other by way of antigen capture and signal detection (Aydin, 2015).

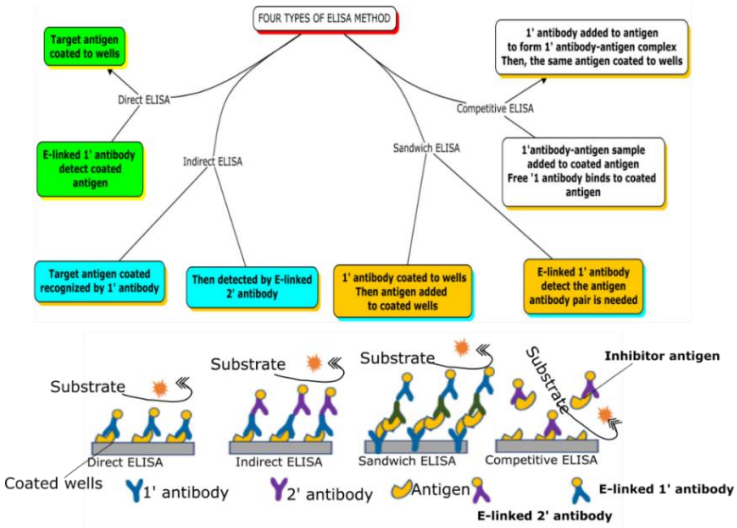

***Figure 10**. Four types of ELISA techniques. 1) direct ELISA, 2) Indirect ELISA, 3) Sandwich ELISA and 4) Competitive ELISA.*

1.9.1 Direct ELISA

Direct ELISA test involves coating the target antigen onto the multi-well plate and uses an enzyme-linked primary antibody to recognize the antigen. Direct ELISA's benefits are that it is quick and straightforward to perform because fewer steps are needed. The disadvantages are that the primary antibody's specificity may be affected by the enzyme-linking, relatively expensive and time-consuming, and less signal amplification. Saturated signals cannot be used for affinity assessment (Masoodi et al., 2021).

1.9.2 Indirect ELISA

In indirect ELISA methods, the antigen of interest is coated first onto the multi-well plate. An unconjugated primary antibody is added to the wells to form a primary antibody-antigen complex. An enzyme-linked secondary antibody recognizes the primary antibody-antigen complex (Tripathi et al., 2021). This technique's advantages are that the primary antibody's specificity is not affected, better signal amplification because many secondary antibodies can bind to the primary antibody. A lot of enzyme-linked secondary antibodies are available and affordable. On the other hand, indirect ELISA's disadvantages are potential cross-reactivity with secondary antibody resulting in the nonspecific signal, and signal saturation makes it challenging to compare two antibody affinities to the target antigen (Sakamoto et al., 2018).

1.9.3 Sandwich ELISA

Sandwich ELISA is usually used in commercially available kits because the technique requires an antibody pair that can target two distinct epitopes on the antigen of interest (Liu et al., 2017). The antibody is coated first to the multi-well plate, followed by a sample containing a target antigen. Then, the addition of an enzyme-linked antibody, detecting the antigen. Thus, the target antigen is sandwiched between the capture and the detection antibodies. This method's benefit includes analysis of the crude sample, the antigen-antibody complex is immobilized to the plate, and everything else can be washed off. Also, Sandwich ELISA is specific because the signal's detection requires the binding of two primary antibodies (Karim, 2018). The disadvantage is that commercially prepared kits may be too expensive (Aydin, 2015).

1.9.4 Competitive ELISA

The basic principle of competitive ELISA is based on competitive binding. The same target antigen is added to a sample containing the primary antibody and coated to the multi-well plate (Li et al., 2021).

At the start, the primary antibody is added to the sample to make antigen-antibody complexes. Subsequently, the sample is added to the wells coated with the antigen of interest. The technique allows the only unbound primary antibody in the sample to interact with the coated antigen in the wells (Engvall, 2010). Therefore, the more antigens in the sample, the less primary antibody binds to the antigen-coated wells leading to a signal reduction. The advantages of competitive ELISA are that it is highly sensitive; by comparing the serial dilution standard curve (SC), the signal can be quantified. Also, a crude sample can be used. The competitive ELISA's downside requires a primary antibody with high specificity to the target antigen (Engvall, 2010; Sakamoto et al., 2018).

1.10 Principle of biolayer interferometry

Biolayer interferometry (BLI) is a label-free method that allows the measurement of protein-protein interactions, interactions between small ligand and proteins, nucleic acid, and lipids in real-time by dip and read technique (Sultana & Lee, 2015). **Figure 11** shows the Octet system detecting the interference of transmitted white light bounced back from an internal reference layer and a stationed biomolecular bait. BLI is based on an analyte's unbound and bound state (Wilson et al., 2010). When the molecules bind to the biosensor tip (surface), the layer gets thicker, and there is a shift in wavelength because of the reflected light from the reference layer (Auer et al., 2015; Weeramange et al., 2020).

BLI measurement is based on two reflections, the first coming from the biocompatible matrix and optical fiber and the second from surface chemistry and solution. The destruction of these two reflected light waves results in the generation of constructive, semi-constructive, and complete destructive interference layouts. Therefore, graphing all wavelengths from three interference profiles generates a

BLI reference set of measurements compared to an analyte-bound sample. Analyzing the reflection patterns at each wavelength shows differences between the analyte-bound and unbound-analyte (Petersen, 2017; Sultana & Lee, 2015; Weeramange et al., 2020)

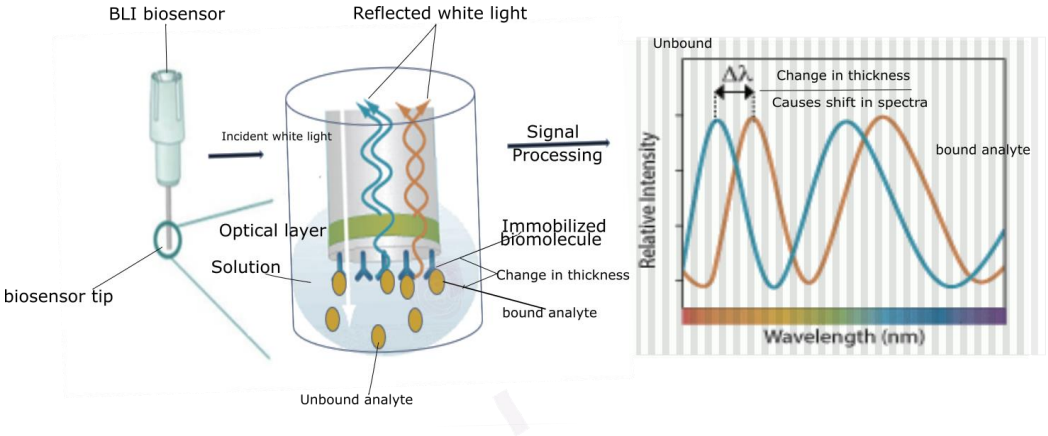

Figure 11. *Principle of the BLI technique. The molecule to be immobilized binds to the biosensor tip, and the analyte binds to the immobilized biomolecule. The binding of an analyte to the immobilized molecule causes a shift in the wavelength (nm) as a sensor tip thickness increase. Adopted after Sultan and Lee 2015.*

.

The interference pattern of the reflected light in the analyte-bound sample generates a right shift of wavelength measured in nm. The BLI profile shift returns to the original location as the analyte dissociates from the probe (Shah & Duncan, 2014). The sensorgram is graphed as binding response measured in wavelength shift on the y-axis versus time in seconds on the x-axis. The association and dissociation of analytes on the biolayer generates changes in the interference pattern because this interference relies on the number of analytes bound to the biolayer (Shah & Duncan, 2014; Sultana & Lee, 2015; Wilson et al., 2010).

Protein may be immobilized to the fiber optic biosensor's tip by utilizing different methods, such as amine-coupling, antibody-anti-Fc, His-tag -Ni-NTA, GST-anti-GST, or FLAG -anti-FLAG interactions. Co-His interaction combined with oxidation may be used to achieve very strong binding(Auer et al., 2017). The biosensor tip coated with bait is immersed in a solution containing an interacting analyte. During the interaction between an analyte and biosensor tip, there is a change in the optical thickness at the biosensor's tip, causing a shift in the reflected interference pattern (Sultana & Lee, 2015; Wilson et al., 2010).

BLI is convenient for analyzing proteins that are difficult to produce and at low concentration (nM). Also, BLI is an essential tool in investigating many samples because it is time-efficient, and experiments are run in parallel. Furthermore, BLI can measure antibody-antigen affinity, screen supernatant from the hybridoma cell line and libraries, and distinguish antibody clones based on their affinities (Frenzel & Willbold, 2014; Petersen, 2017).

There are two BLI systems; the first one is BLItz, a single channel operated manually, and it uses a droplet of only 4 to 5 µl of analyte per kinetic measurement. A complete set of BLI kinetics data can be achieved with five concentration points of 25 µl of the sample. In the case of the limited analyte, BLItz is best utilized than Octet. However, BLItz is inadequate in analyzing micromolar to nanomolar range concentrations, thus limited in generating the association and dissociation rate constant data. Additionally, the BLItz system works well only at room temperature, restricting its use to proteins and other samples unsuitable for RT conditions (Sultana & Lee, 2015).

The second one is the Octet instrument/system. A multichannel and predesigned BLI system that works automatically to measure samples in 96 or 384 well plates. Octet device can analyze interactions involving analyte with molecular weight (Mw) of 150 kDa, and excellent for investigating protein-ligand interactions and peptides with low Mw (Wallner et al., 2013). Furthermore, Octet can measure affinities in concentrations from mM to pM. The temperature plate in the Octet system can be adjusted to the required sample temperature (Li et al., 2011; Shah & Duncan, 2014).

This thesis presents experimental results of five monoclonal antibodies' reactivity to eight Viral protein antigens using western blot, ELISA, and Biolayer interferometry measurement. The preliminary results allowed us to select 3A6 mAb for further analysis as it was a better clone antibody than the other four clones.

2. MATERIALS AND METHODS

Before studying the antigen-antibody affinities, both antigens and antibodies needed to be produced, and some of them were not readily available and purified. Antigens were produced in *E. coli* cultures, and antibodies were produced in rat hybridoma cell cultures. Antibody-antigen interactions were studied using BLI as well as Western blotting and ELISA to investigate the novel antibodies (3A6, 12A4, 9B9, 7C1, and 12A4) and their response to viral antigens (CVA4, CVB1, PV1((Polio1)), EV-D68, RV-A89, RV-B14, and RV-C3). The novel antibodies were screened earlier (Saarinen et al., 2018) and were named based on their hybridoma cell line.

Here we describe how the monoclonal antibodies and viral proteins were produced and purified and how antibody-antigen were studied. **Table 1** shows the material and reagents utilized to produce and purify target monoclonal antibodies and viral proteins.

Table 1. *Material and reagents used in the VP1 and mAb purification*

VP1 production and purification	
BL21 (DE3) *E. coli*	Tris+NaCl buffer
Glutathione resin	Glutathione (reduced)
Histrap resin	Imidazole & 30% glycerol
Monoclonal antibody purification	
PD-10 125 ml	Sodium phosphate buffer
Protein-G column 2 ml	Glycine, Tris-HCl buffer

2.1 VP1 protein production and purification

The VP1 sequence for CVA4, CVB1, E30 (Echo30), PV1(Polio1), EV-D68, RVA-89, RVB-14, and RV-C3 were extracted from online databases. The expression vector's construction comprising the VP1 gene sequence and the cloning and plasmid extraction in *E. coli* was done previously (Saarinen et al., 2020). The expression vectors were fused with GST at N and His-tag at the C-terminus of the VP1 sequence to aid the purification process and make the proteins more

soluble. The constructed recombinant plasmids were transformed in Invitrogen™ One Shot™ TOP10 Chemically Competent E. coli (ThermoFisher) to produce small quantities of plasmid DNA, purified using a QIAprep Spin Miniprep Kit (QIAGEN). The concentrations of the minipreps were measured by Nanodrop, after which good quality and sequence-verified plasmids were selected for protein expression in *E. coli* (**Figure 12**).

The plasmids were transformed by heat shock to chemically competent *E. coli* strain Star BL21 (DE3) (Life Technologies). The bacteria were placed on ice and incubated with the plasmid for 30 min. A heat shock was induced by dipping the bacteria containing microcentrifuge tubes on a water bath at 42°C for 30 seconds. 500µl SOC media was added to the reactions, and they were pregrown at 37°C with agitation for an hour. The transformed cells were plated on an agar plate containing penicillin and incubated at 37°C overnight. The following day, 1-3 single colonies were isolated and seeded in LB medium supplemented with 100 µg/ml ampicillin and 5mM glucose overnight on shaking at + 37°C. The following day, the cultures were scaled up.

When the culture had reached an optical density (OD) of OD600 0.6-0.8 at 37°C, isopropyl-β-D-thiogalactopyranoside (IPTG) was added to a 100µM concentration to induce VP1 production. Post IPTG induction, the culture temperature was lowered to 25°C, and the following day the cells were harvested using centrifugation for 20 min at 4,000 rcf. The cell pellets were resuspended in 50 mM Tris+500Mm NaCl buffer at pH 8 and then lysed by sonication. The lysate was clarified by 20 min centrifugation at 25,000 rcf, the pellets were stored, and supernatants were collected for VP1 purification.

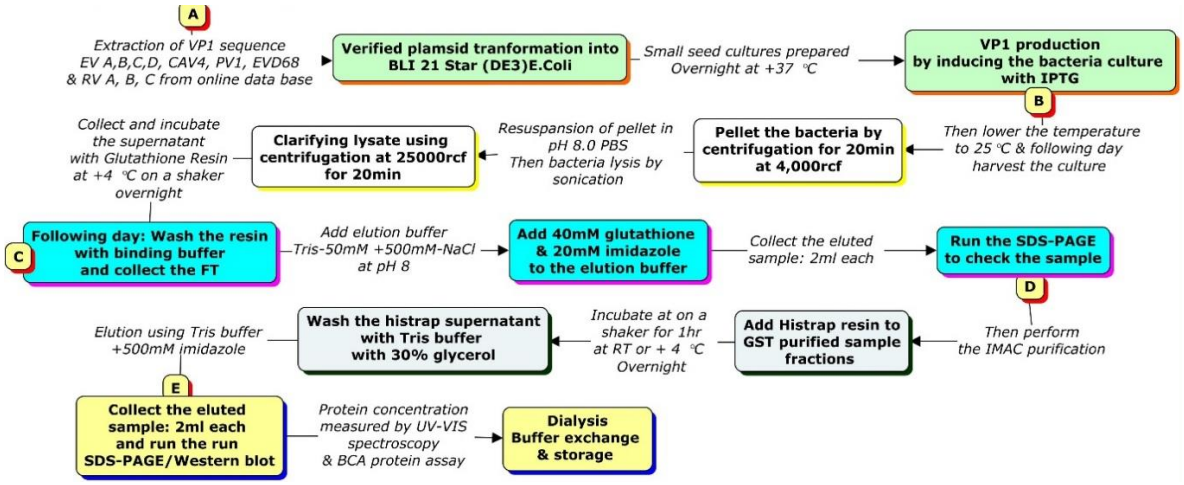

Figure 12. *Overview of VP1 production and purification workflow*

Stepwise purification processes were employed to extract VP1 from supernatants based on their fused affinity tag. The recombinant VP1 proteins were tagged with an N-terminal GST and a C-terminal His-tag. These tags were used in VP1 purification and enabled us to perform two rounds of purification using affinity chromatography. First Protino® Glutathione Agarose 4B (Biocompare), and second HisTrap FF crude immobilized metal affinity chromatography (IMAC) columns (GE Healthcare). The first step involved incubating the supernatants with glutathione resin at +4 °C overnight on a shaker. The following day, the resins were washed with the binding buffer (50 mM Tris + 500 mM NaCl at pH 8), and the VP1 bound to the resins were eluted with 40 mM glutathione diluted in binding buffer. The glutathione eluted fractions were run on SDS-PAGE for quality assessment. If the eluted fractons' quality were not good enough, the second purification round was employed. The second step of the VP1 purification involved incubation of glutathione eluted fractions from the first step with histrap resin at +4 °C overnight or 4 h at room temperature. The following day or after 4 h, the incubated samples were washed with a binding buffer complemented with 30% (v/v) glycerol and eluted with 500 mM imidazole complemented binding buffer. After that, the eluted fractions were once again run on SDS-PAGE to check their quality.

Before running the sample on SDS-PAGE, Laemmli buffer containing a reducing agent, beta-mercaptoethanol, was added to the samples collected from eluted

fraction, supernatant, lysate pellet, and wash, to reduce disulfide bonds. The samples were then incubated for 10 minutes at 100°C to denature the protein and accelerate breaking the disulfide bonds. The treated protein unfolds to migrate properly based solely on its molecular weight on the SDS-PAGE gel. After heat treatment, the samples were loaded onto a ready-made TGX Stain-Free Precast Gels (Bio-Rad) and imaged using ChemiDoc XRS+ System (Bio-Rad). Using Trans-Blot Turbo Transfer System (Bio-Rad), the protein bands were transferred to the nitrocellulose membrane for Western blotting. The membrane was blocked with a blocking buffer containing 1% BSA. After washing, the membrane was incubated with primary antibody overnight at +4°C, then incubated with conjugated secondary antibody. 3A6mAb and anti-his were used as primary antibodies and HR-conjugated goat anti-rat IgG as a secondary antibody. Between each step, the membrane was washed thrice by placing it in TBS-Tween for 5 min.

Based on the WB, the VP1 containing fractions were pooled and dialyzed to remove the imidazole. The first dialysis was in 50 mM Tris-HCl at pH 8 and 500 mM NaCl with an imidazole concentration of 50 mM overnight. The second one contained 10 mM imidazole at RT for 4 h and finally, 0 mM imidazole in Tris buffer overnight at +4 °C and further dialyzed in phosphate-buffered saline (PBS) for biotinylation. The VP1 samples were biotinylated with 20X molar excess of EZ-link biotin reagent (Thermo Scientific) overnight at +4 °C. Unbound biotins were removed by dialysis for 4 h at RT. After dialysis, sample concentrations were measured using a nanoDrop™ One (ThermoFisher).

Equimolar amounts of the dialyzed and concentrated CVA4, CVB1, E30, PV1, EV-D68, RVA-89, RVB-14, RV-C3 VP1 proteins were run on SDS-PAGE gels. WB was used to determine the binding of VP1 antigens to 4D12, 7C1, 12A4, 9B9, and 3A6mAb by using the monoclonals as primary antibodies HRP-conjugated Goat anti-rat IgG as a secondary antibody. Pure GST was used as a negative control. Advansta ECL substrate (Thermofisher) and the Biorad ChemiDoc XRS+ System were used for visualization and imaging, respectively, all western blot samples.

2.2 Production and purification of monoclonal antibodies

2.2.1 mAb production

Table 2 shows the media composition and materials used in the production of mAb from the rat hybridoma cell lines.

Table 2. *Media composition of the mAb production and materials*

Media	Media additives	Plasticware/ equipments	Antibody	Cell line
DMEM	10% fetal calf serum (FCS)	Flask (T25, T75) ml 12 well plate Falcon tubes (15-50) ml	9B9 & 4D12	Rat hybridoma cell line
	1% Penicillin/Streptomycin	Water bath, Hemacytometer slide Centrifuge		

The rat hybridoma cells were collected from liquid nitrogen (-196°), quickly thawed in a water bath at 37˚C, and prewarmed in a freshly prepared DMEM (Sigma) containing 10% FCS and 1% penicillin. Then the cells were pelleted and resuspended in the DMEM. The cells were transferred from Falcon tube to T25 flask and 24 well-plates at day 0, incubated overnight at 37˚C with 5% CO_2. On day 1, the medium was changed, and the cells were incubated with the same condition for day 0. On day 3, the cell culture supernatant was collected, and the cells were subcultured. Before re-seeding, the cells were trypsinized with 0.05% Trypsin-EDTA (ThermoFisher, #12604013), then incubated at 37˚C with 5% CO_2 for 2 minutes. The medium was added to stop trypsinization, and the cell suspension was centrifuged. After that, the supernatant was discarded, and the cells were resuspended in a fresh medium for counting and re-seeding. On days 7 and 11, the supernatant was collected for desalting and purification using SEC and AC chromatography. **Figure 13** illustrates the work overview of rat hybridoma cell culture, purification, and quality assessment of the produced mAb.

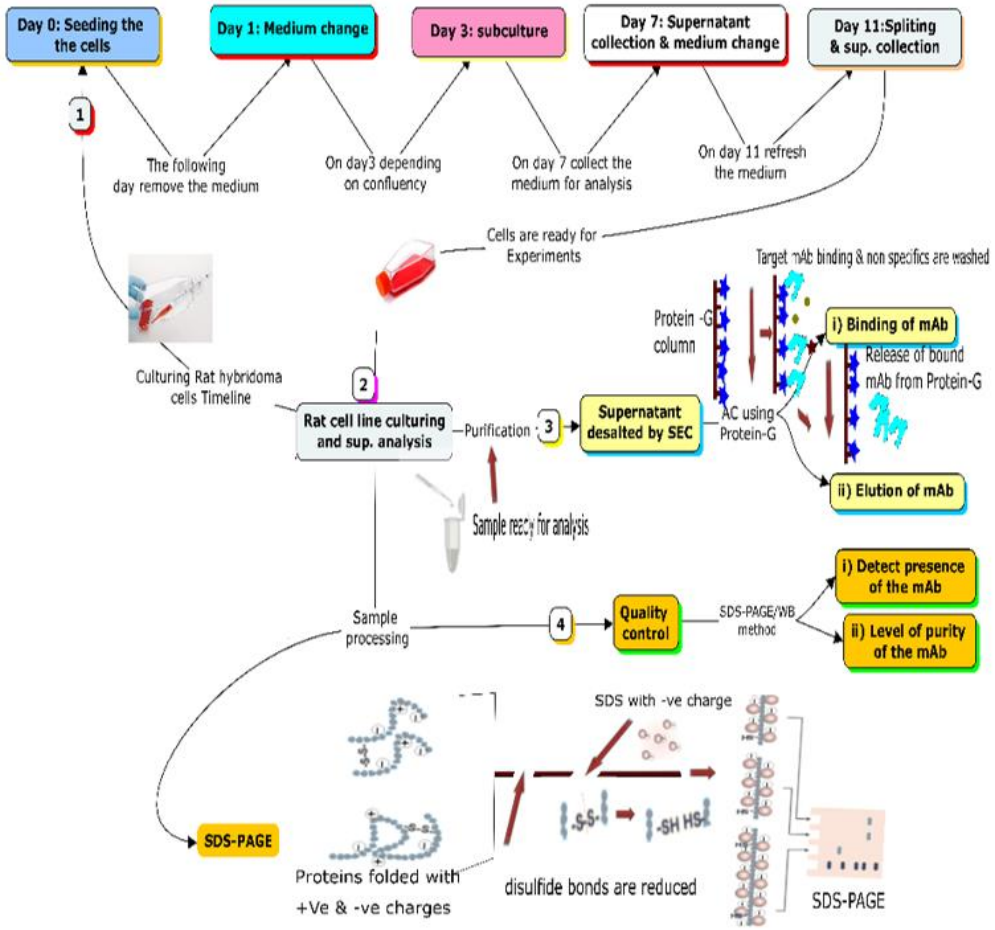

Figure 13. *Monoclonal antibody production and purification overview. 1) The rat hybridoma cells producing the target antibody are cultured in vitro. 2) Collection of supernatants from cultured rat hybridoma cells. 3) Purification of the supernatant using SEC+AC. 4) Quality control of purified target mAb using SDS-PAGE.*

2.2.2 mAb purification

The cell culture supernatant samples containing target mAbs were first desalted by SEC; after that, they were purified by AC using protein G. PD-10 column with a capacity of 125 ml and hitrap-protein-g-hp-prepacked-column 2 ml (GE Healthcare). 20 mM sodium phosphate buffer at pH 7.0 as a loading/binding buffer and 0.1 M glycine–HCl at pH 2.5 as an elution buffer and neutralization buffer (1 M Tris–HCl) at pH 9.0 were used during purification.

PD-10 Desalting Columns (GE Healthcare) were used to exchange buffer and remove high ionic concentrations from the supernatant of the cell culture. HiTrap® Protein G (Sigma, GE17-0404-03) was used to bind the target mAb and elution. Both PD-10 and protein G columns are stored in 20% ethanol to prevent

contamination and maintain the column's quality. During mAb purification, the adjusted parameters included the flow rate for sample loading at 1.5 ml/min (PD10), binding, and elution at 1 ml/min (Protein G). There were two main steps involved in the purification process. The first one involved the buffer exchange and desalting of the cell culture supernatant using PD-10, from which the supernatant was collected as a PD-10 flow throw (FT). The second step was to load the supernatant collected from the first step (PD-10 FT) onto the protein G column for binding and subsequently elution. The collected samples from this second step were named protein G FT (unbound protein during binding phase), wash (after binding the wash away molecules), and eluted samples (containing the target mAb).

Before starting the buffer exchange and desalting, alcohol was removed by loading MilliQ water into the tubing and PD-10 column. Subsequently, the binding buffer (pH ~7.0) was loaded onto a PD-10 column followed by a cell culture supernatant and more binding buffer. UV absorbance and conductance were observed to collect the proteins in a buffer with lower ionic strength. The collected (PD-10) FT was reloaded onto the protein G column. Before sample loading, the protein G column was balanced by washing it with elution buffer (0.1 M glycine at pH 2.5) and binding buffer once more. The monoclonal antibody was eluted with the elution buffer and fractionated. Samples were collected during the purification for quality control. The collected samples included eluted fractions 1-10, cell culture supernatant, Protein-G FT, wash, and PD-10 FT. At the end of the purification process, both PD-10 and protein G column was washed with Milli-Q water followed by alcohol to prevent any precipitation and possible bacterial contamination and stored in 20% ethanol for subsequent reuse.

The binding buffer conditions were optimized to ensure that the 4D12 and 9B9mAb interact effectively with the protein G. After washing through the protein G column, 9B9mAb remained bound while other molecules were washed away. The switching to elution buffer with pH 2.5 altered the ionization of charged groups on the protein G and the bound mAb, thereby reducing the affinity by weakening or reversing the interactions resulting in the release of mAb from the column. Glycine-containing elution buffer effectively dissociated mAb from protein G without permanently affecting the mAb structure. However, the exposure

of mAb to a low pH can damage the protein, and to avoid that, eluted mAb fractions were neutralized immediately with 1/10th volume of alkaline buffer 1 M Tris•HCl, pH 8.5 (Andjelković et al., 2017; Bergmann-Leitner et al., 2008).

The collected 9B9 and 4D12 mAb were run on the SDS-PAGE and transferred to the nitrocellulose membrane for western blot analysis as described in the VP1 purification section.

2.3 ELISA: Mapping of mAb-VP1 antigen interactions

The purified Antibody and VP1 were used in ELISA to determine the antigen-antibody reactivity. Purified VP1 was used as an antigen to coat Maxisorp (Nunc) wells, and each well had a total of 250 ng of the antigen in 50 µl volume. 50 mM carbonate buffer at pH 9.4 was used to dilute the VP1 antigen, and the coated Maxisorp plate was incubated overnight at +4 °C. The following day, the wells containing VP1 antigen were washed in PBS-Tween buffer (PBST) and blocked with 0.1% BSA in PBS buffer for 0.5 h. The primary and secondary antibodies were diluted in an EIA buffer containing 0.05% Tween 20, 1xPBS, 8.5% NaCl, and 1% BSA. For the primary antibody 3A6, 12A4, Dako, 4D12, 7C1, and 9B9mAb, 50 µl was added to the antigen-coated wells in 1:100-1:256000 dilution series and incubated for an hour at +37°C. Subsequently, the antigen wells were washed by PBST, and HRP-conjugated goat anti-rat IgG and HRP-conjugated anti-mouse IgG secondary antibody for 3A6, 12A4, 4D12, 7C1, and 9B9mAb, and DakomAb respectively, 50 µl were added to the wells in 1:1000 ratio and incubated for a one h at +37°C.

O-nitrophenyl diamine (OPD) (Sigma) and hydrogen peroxide were diluted in citrate buffer at pH 5 and used as a substrate buffer. 100ul of freshly prepared substrate buffer was added to each coated well and incubated for 0.5 h at +37°C. The color change was observed during the substrate antigen incubation, and the reaction was stopped using 0.5 M sulfuric acid. The plates with stopped reaction were measured at the absorbance of 590 nm using a Victor Wallac 1420 (Perking Elmer, Turku, Finland) microplate reader.

2.4 Biolayer interferometry (BLI)

Biolayer interferometry was carried out for antibody-antigen pairs to map their interactions. Sensor loading and regeneration conditions were tested with 3A6mAb interaction with CVB1 before carrying out the bulk of the pairwise measurements. The reagents and materials, including the kinetic assay setting used for BLI measurements, are listed (**Table 3**).

Table 3. *Materials and reagents used for BLI measurements*

Sensor type	Plasticware/ tips	Buffers and reagents	Biotinylated VP1 Antigens	Antibodies
streptavidin	Black 96 well plates	Biocytin 20 µg/ml	CVA4, CVB1, E30, PV1, EV-D68, RVA-89, RVB-14 and RV-C3	3A6,12A4, 4D12,7C1, 9B9, and Dako mAb
	384 TW microplate well plates	Kinetic buffer (1XPBS, 0.1% BSA, 0.02% Tween20, 0.05% sodium azide, pH 7.4)		

Table 4. *Settings used for kinetic assay*

Step#	Step name	Time (s)	Flow (RPM)	Sample plate column
1	Equilibration	30	1,000	1
2	Loading	600	1,000	2
3	Baseline	300	1,000	3
4	Quenching	300	1,000	4
5	Association	900	1,000	5
6	Dissociation	1800	1,000	3

During BLI measurements, 80 µl diluted kinetic buffer in sample plate column 1 was used for equilibration, 80 µl diluted VP1(A-G rows concentration: 20, 10, 5, 2.5, 1.25, 0.625, 0.313, and 0 µg/ml) onto column 2 as loading. Column 3 contained 80 µl of biocytin 10 µg/ml as quenching buffer, and column 4 contained diluted kinetic buffer as a baseline. Column 5 contained antibody as a sample with concentration range of 250, 125, 62.5, 31.25, 15.625, 7.813, 3.91, and 0 nM

for kinetic measurements. Step 6 involved the dissociation phase completed in column 3.

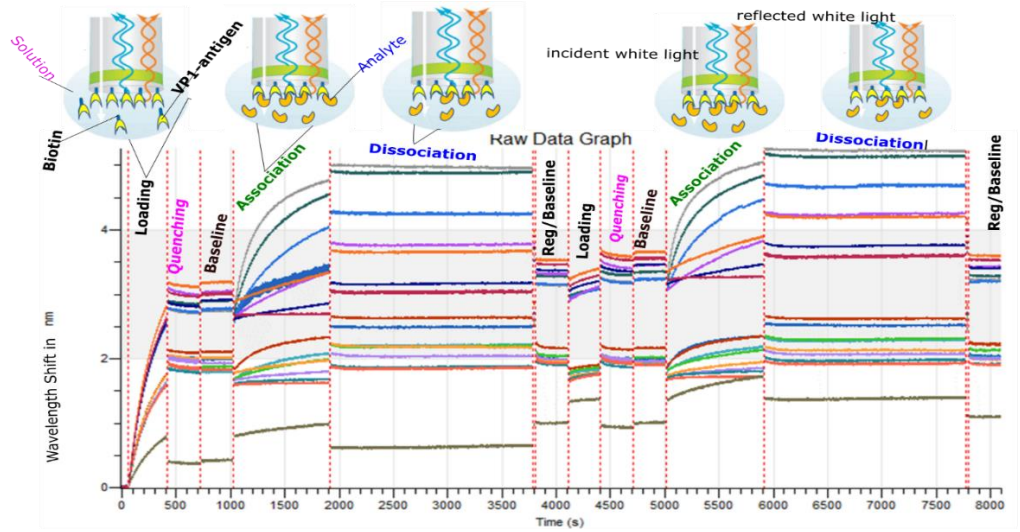

Figure 14. *Shows practical steps in Octet sensorgram. Starting with custom (KB), loading of VP1-antigen to streptavidin sensor, quenching (biocytin), baseline (KB), and binding/association analyte to Biotinylated VP1 (mAb), and dissociation of the interactions (KB). All reagents were diluted in kinetic buffer (KB).*

Biolayer interferometry measurements were performed on the ForteBio Octet Red 384 instrument (Fortebio, Pall Life Sciences, Menlo Park, USA). Before use, streptavidin biosensors (Streptavidin (SA) Dip and Read® Biosensors, ForteBio, CA, USA) were soaked in the kinetic buffer for at least 10 min. BLI assay protocol consisted of five steps (**Figure 14**), first, measuring baseline in kinetic buffer (30 s), second, VP1 antigen loading (600 s), third, quenching and baseline (300 s each), fourth association (900 s), and fifth, dissociation (1800 s). VP1 antigens were immobilized onto streptavidin biosensors. The control values were measured by using a biosensor with no antigen loaded. The background response contained a sensor with no antibody (0 nM).

Three types of experiments were performed, first was a loading scout to select the best loading concentration for the kinetic measurements using a series of VP1 antigen dilutions as described above. The second was performed to determine the best regeneration condition to use for the kinetic measurements. The third was the kinetic measurement using the single best possible concentration from the loading scout and different antibody dilutions.

Initial experiments showed that non-loaded reference sensors and sensors loaded with VP1 and dipped into the kinetic buffer only (0 nM mAb) generated the same results. So nonspecific binding was not observed (**Figure 15**). Sensorgrams were fit both globally and individually to a 1:1 binding model. Unless specified, streptavidin biosensors were regenerated. The Octet software calculated K_D and K_a was not used in this study because they were unreliable based on the antibody's binding profile. However, to estimate the dissociation constant (K_D), we used the Prism GraphPad nonlinear model (one site saturation model) to generate K_D for each fitted curve.

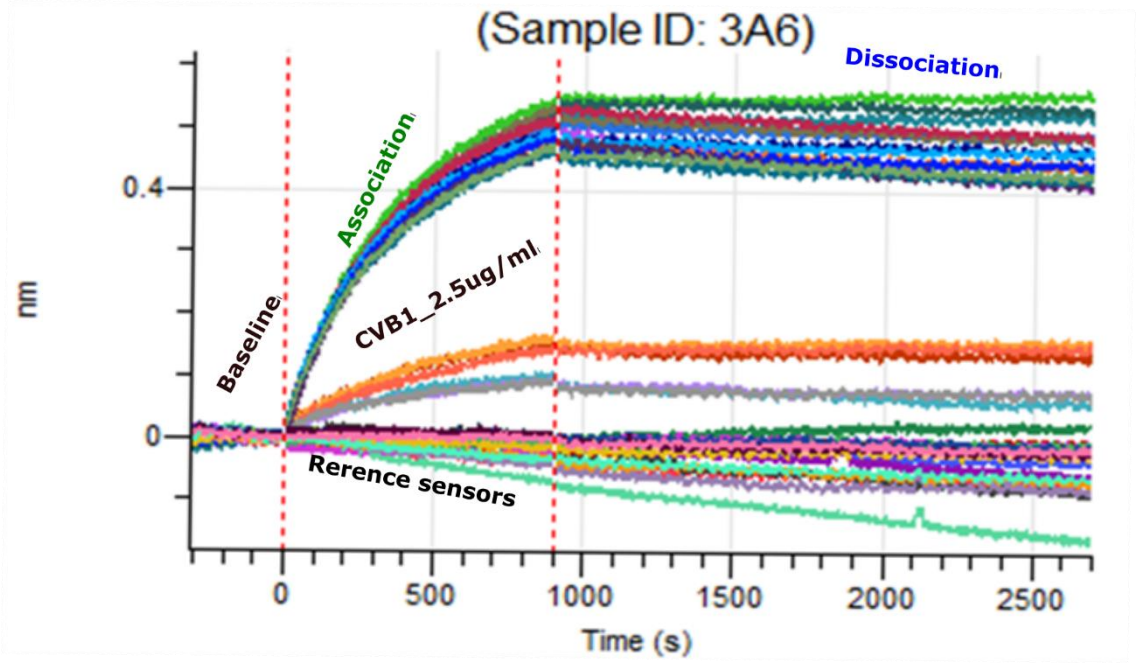

Figure 15. *No unspecific binding was observed with reference sensors: Reference sensors dipped and measured in 0ug/ml of CVBI VP1 and 0 nM 3A6mAb. Control sensors loaded with 0 µg/ml of CVBI dipped in 0 nM 3A6mAb were comparable to reference sensors. In contrast, other sensors loaded with 2.5 µg/ml of CVB1 VP1 and dipped into different 3A6mAb concentrations showed a binding response.*

3. THE MAIN SCOPE OF THE THESIS

Monoclonal antibodies (mAbs) are essential in studying and diagnosing enterovirus infection and in neutralization. Therefore, this thesis's main goal was to produce and characterize novel mAbs against produced recombinant viral protein 1 (VP1). Also, we were interested in studying the binding profile of each mAb to the VP1 antigens using different techniques. The project consisted of the following objectives:

1. Production and purification of recombinant VP1 proteins, including quality assessment
2. Purification of monoclonal antibodies, including quality control
3. Using different techniques to characterize antibody-VP1 antigen affinity

4. RESULTS

This study aimed to produce VP1 antigens and monoclonal antibodies and characterize their interactions. The study also evaluated the diagnostic potential of the novel mAbs against 8 different VP1 antigens by utilizing Western blot, enzyme-linked immunoassay, and biolayer interferometry. In this section, we present results for VP1 and mAb quality assessment and mAbs reactivity to VP1 antigens based on SDS-PAGE (**Figure 16**), WB (**Figure 17 & Figure 18**), ELISA, and BLI (**Figure 19, Figure 20, Figure 21** *)*, and BLI (**Figure 23, Figure 24).**

4.1 Quality assessment of purified proteins

VP1 antigens were produced in *E. coli*, and mAb was generated from rat hybridoma cell line and purified according to the method section's protocol. The quality control was carried out on all produced VP1 and mAb to determine their purity and quality. Purified VP1 and mAb were run on SDS-PAGE (**Figure 16**).

For VP1, double bands around 60 kDa were observed for the target protein except for RVA-his and RVB-his. RVA and RVB were subjected to two rounds of purification based on their purity. The first round of purification used glutathione resins, and RVA/B pure fractions were labeled RVA/B-gst. The second round of purification used IMAC with selected RVA/B fractions impure from the first round of purification and was labeled RVA/B-his. **Figure 16a** illustrates protein bands for CVB1-S&E and CVB1-S, representing sonication (S) and Avastin Emulsiflex C3 (E) methods used to homogenize the bacteria cell culture. The preliminary results (not shown) proved that sonication was a better lysis method than emulsification. Samples that were sonicated had less VP1 in the pellet than after emulsification. Therefore, all the bacteria cell lysates were carried out by sonication.

4.2 VP1 antigens detected in SDS-PAGE and Western blotting

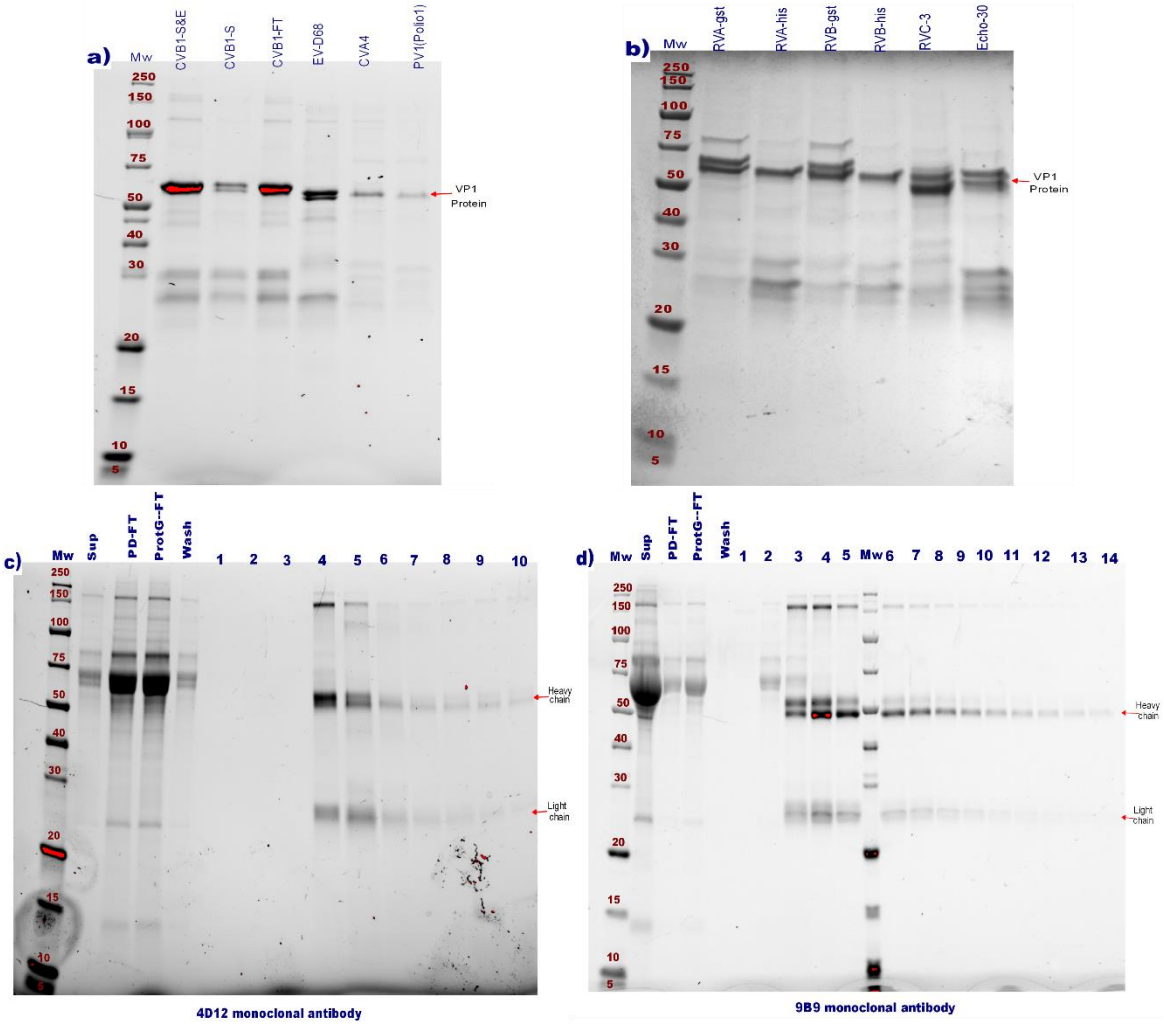

Figure 16. *Detection of VP1 antigens and mAb in SDS-PAGE.VP1 and mAb quality assessment after purification phase. a) RV-A89-GST, RV-A89-his, RV-B14-GST, RV-B14-his, and RV-C3 and E30 (Echo30), respectively. b) CVB1, EV-D68, CVA4, and PV1(Polio1), respectively. c) 4D12 and eluted fractions 1-10. d) 9B9 and eluted fractions 1-14.*

According to the observation in **Figure 16a & b**, CVA4, CVB1, E30, PV1, EV-D68, RV-A89, RV-B14, and RV-C3 VP1 all showed double band possibly due to partial proteolysis of C-terminal part of the protein or because breaking up of proteins into fragments due to exposure to the heat and reducing agents during sample preparation for SDS-PAGE. **Figure 16c** shows eluted fractions from 4 to 10 containing 4D12mAb as the target antibody. **Figure 16d** illustrates 9B9mAb eluted fractions 3-14 at 150, 50, and 25 kDa because of breaking down the disulfide bond by a reducing agent during sample preparation. Samples collected from the supernatants, PD-10 FT, and protein G FT of 9B9 and 4D12 showed traces of

target protein, whereas the wash sample had none. The bands at 50 and 25 kDa in 4D12 and 9B9mAb (**Figure 16c**, **d**) represent heavy and light chains, respectively.

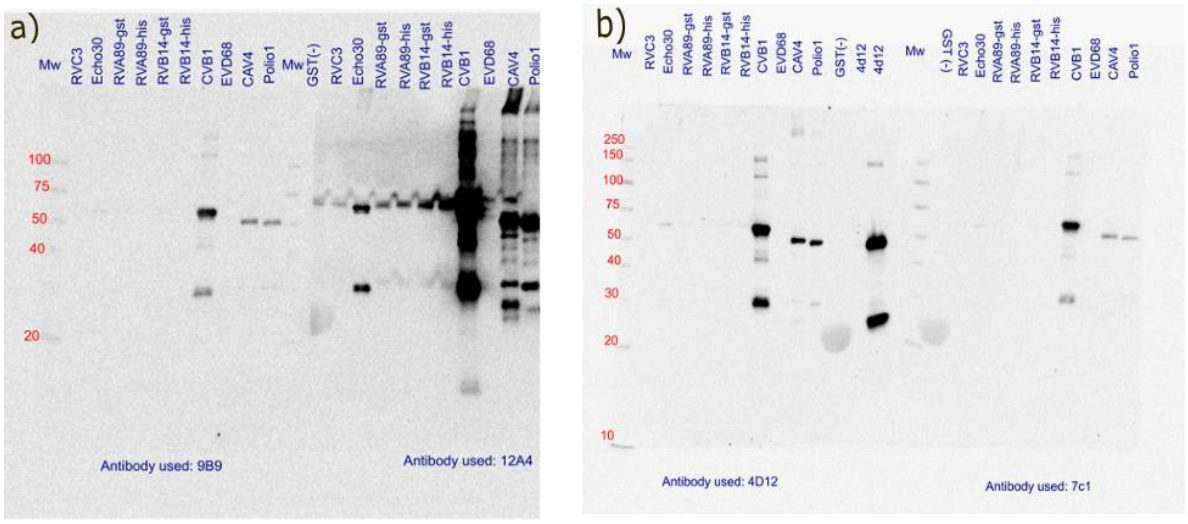

Figure 17. *Determination of antigenicity of novel mAbs to VP1 antigen in WB. The purified mAbs were used as primary antibodies to detect VP1. a) 9B9 and 12A4 recognizes VP1 antigen. b) 4D12 and 7C1 recognizes few VP1 antigens.*

The binding of VP1 (CVA4, CVB1, E30, PV1, EV-D68, RV-A89, RV-B14, and RV-C3) to anti-VP1 antibodies were tested using purified 9B9, 4D12, 7C1, and 12A4mAb as primary antibodies in Western blot (WB). **Figure 17a** shows that 9B9mAb detected CVA4, CVB1, and PV1 VP1 antigens compared to 12A4mAb, which detected almost all VP1 antigens, excluding RV-C3 and EV-D68. 4D12mAb recognized E30, CVB1, CVA4, and PV1 compared to 7C1mAb, which detected PV1, CVA4, and CVB1 (**Figure 17b)**. GST was used as the negative control, and it did not react with 9B9, 12A4, 4D12, or 7C1mAb.

4.2.1 All viral protein antigens were successfully purified

Equal amounts of VP1 proteins were run on SDS-PAGE to determine their quality. Briefly, equal amounts of (5 µg/well) of all purified VP1 antigens were prepared and run on SDS-PAGE. **Figure 18** shows that CVA4, CVB1, E30, RV-A89, RV-B14, EV-D68, PV1, and RV-C3 were successfully visualized with SDS-PAGE.

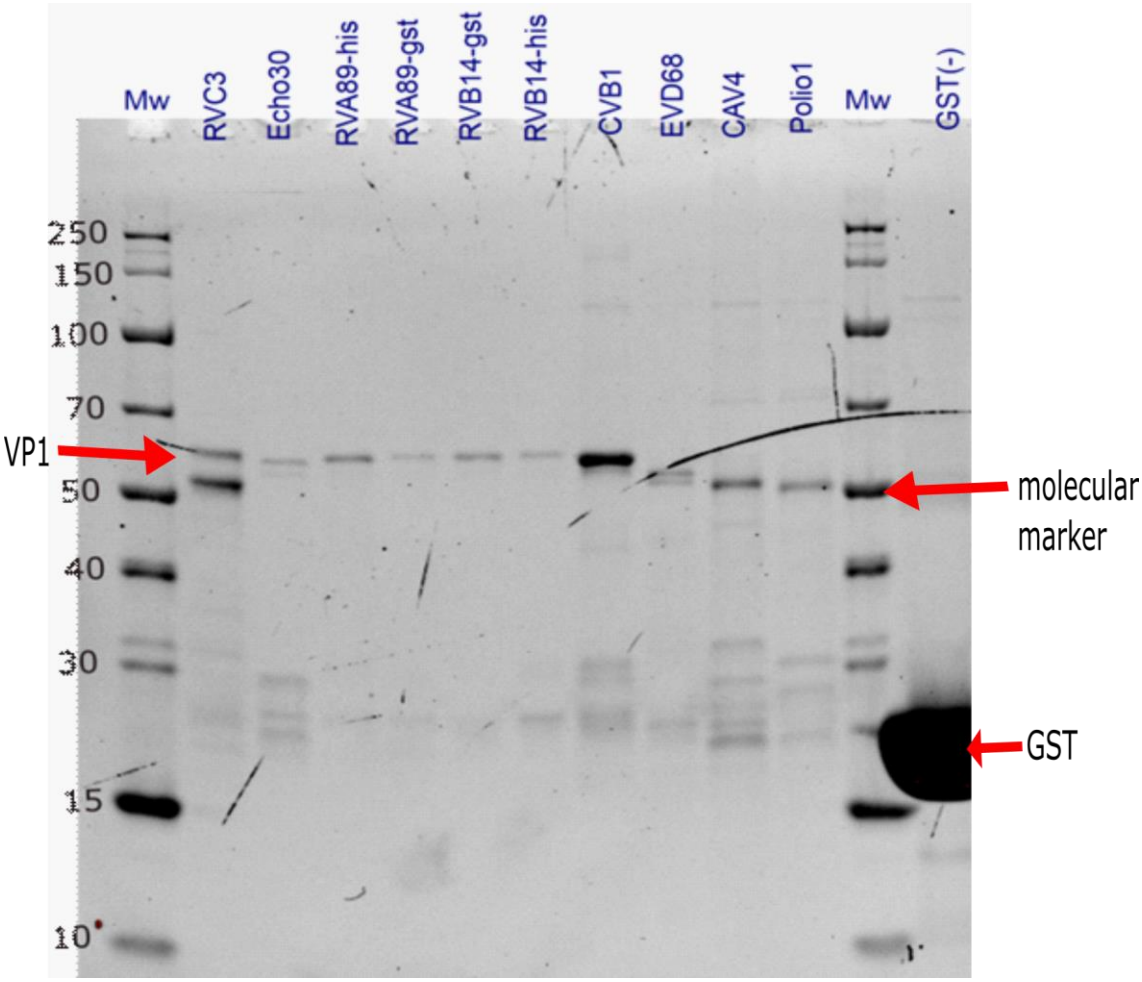

Figure 18. *SDS-PAGE analysis for the VP1 purified proteins. The proteins were detected using the stain-free method. 5µL was loaded onto the first and 12th well as a molecular mass marker. 5 µg/well of VP1 antigens (RV-C3, E30, RV-A89-his, RV-A89-gst, RV-B14-gst, RV-B14-his, CVB1, EV-D68, CVA4, and Polio1) were loaded onto wells 2 to 11, and 5 µL GST was loaded onto 13th well as a control. Based on a ladder, the purified VP1 antigens were observed between 70 kDa and 50 kDa, and GST was observed at about 28 kDa*

4.3 Determination of Antibody-Antigen interaction by ELISA

An ELISA was carried out with Dako, 12A4, 3A6, 4D12, 7C1, and 9B9 mAb to determine their reactivity to CVA4, CVB1, E30, PV1, EV-D68, RV-A89, RV-B14, and RV-C3 VP1 antigens. **Figure 19a** shows Dako recognizing CVA4, CVB1, PV1 at 300 nM-18.75 nM, whereas EV-D68, RV-A89, RV-B14, and RV-C3 were poorly recognized. 9B9mAb only recognized CVB1 and CVA4 and PV1 at 18.75 nM with absorbance less or equal to 1 (**Figure 19b)**.

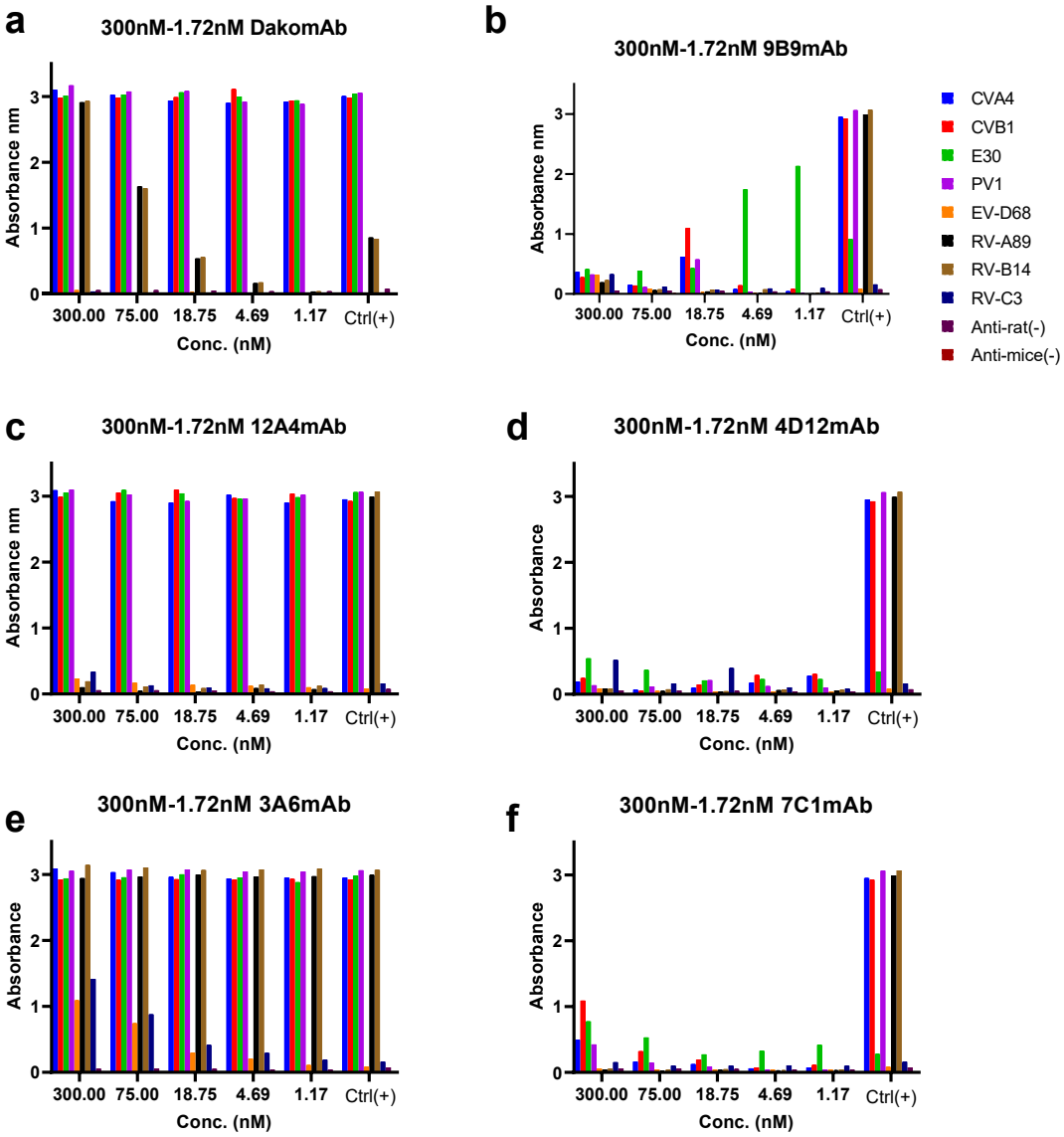

Figure 19. *Characterization of the binding response of six different mAb clones against eight different VP1 antigens using ELISA. The response of a) Dako mAb, b) 9B9 mAb, c) 12A4 mAb, and d) 4D12 e) 3A6 mAb and f) 7C1 mAb to CVA4, CVB1, E30, PV1, EV-D68, RV-A89, RV-B14, and RV-C3 VP1 antigens. 3A6 mAb was used as a positive control ctrl (+), and Anti-rat (-) and Anti-mice (-) were used as negative controls.*

12A4mAb recognized CVA4, CVB1, and PV1 VP1 antigens except RV-A89, RV-B14, EV-D68 and RV-C3 at concentration range 300 nM-18.75 nM (**Figure 19c)** whereas, 3A6 mAb detected all 8 VP1 antigens at 300 nM-75 nM (**Figure 19d**). 4D12 mAb recognized RV-C3 at 300 nM with low absorbance, and 7C1 mAb detected only CVB1 at an appreciable signal of 300 nM concentration **Figure 19d & f**). According to **Figure 19**, E30 VP1 interacted strongly with 3A6, 12A4, and Dako mAb compared to the rest of the mAb. The negative control samples were

Anti-rat for 3A6, 12A4, 7C1, 9B9, and 4D12 mAbs and Anti-mice for DakomAb. Anti-rat and anti-mice secondary antibodies were added to wells containing only VP1 antigens with no primary antibodies, and no positive responses were detected, as observed in **Figure 19**. 3A6 mAb was used as a positive control. The BSA wells were used as the background signal and subtracted from all the VP1 signals.

Since higher mAb concentration generated saturated signal, ELISA assay was redone using a lower concentration of mAb and to map the mAb's affinities to VP1 antigen. The 75 nM to 0.29 nM range concentration (**Figure 20a, d, & g)** did not differ from the previous results (**Figure 19).** However, using the concentration range of 8 pM-0.03 pM **Figure 20b, e, & h**) showed concentration-dependent reactivity of mAb to VP1 antigen.

Dako mAb detected better CVA4, CVB1, E30, PV1 than RV-A89, RV-B14 at 75 nM-1.17 nM and showed no binding response to EV-D68 and RV-C3 (**Figure 20a**). 12A4 recognized all VP1 antigens except RV-A89, RV-B14, ED68, and RV-C3 (**Figure 20d**). In contrast, **Figure 20g** shows that 3A6 mAb yielded a response to all the VP1 antigens except EV-D68 and RV-C3. However, at 0.5 pM - 0.03 pM concentration, Dako mAb only recognized CVA4, CVB1, E30, and PV1 whereas, 12A4 mAb detected CVA4, CVB1, E30 and PV1 better at 0.5pM than 0.13 pM-0.03 pM (**Figure 20c & e**). 3A6mAb yielded a higher binding response at 0.8 pM-0.5 pM than at 0.1 3 pM-0.03 pM to all VP1 antigens except ED68 and RV-C3 (**Figure 20h**). The binding graphs represent the binding response of Dako, 12A4, and 3A6 mAb to all 8 VP1 antigens are illustrated in **Figure 20c, f & i**.

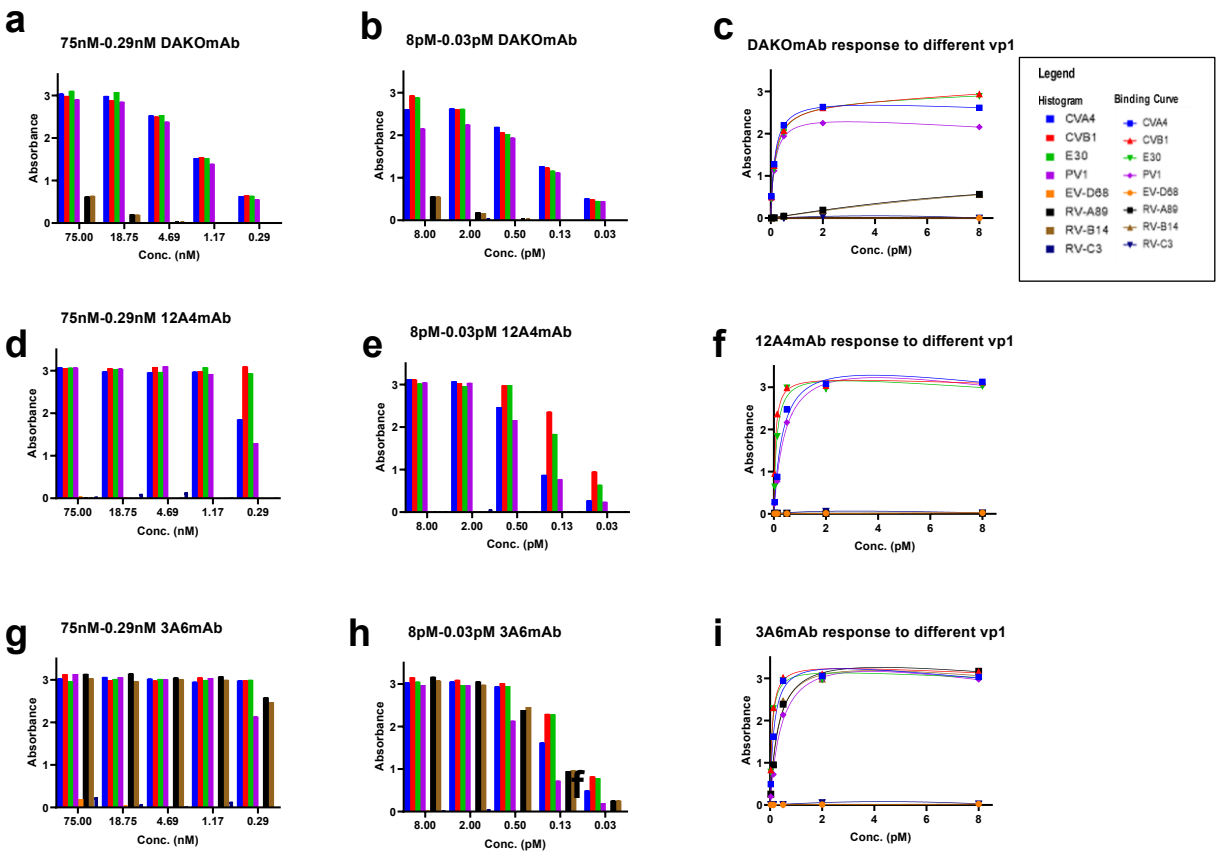

Figure 20. *Determination of binding response of Dako, 12A4, and 3A6mAb to eight different VP1 antigens using ELISA. The reactivity of mAbs against VP1 antigens at a concentration range of 75 nM-0.29 nM representing a) Dako mAb, d) 12A4 mAb, g, and at 8 pM-0.03 pM range representing b) Dako, f) 12A4, and h) 3A6 mAb. The c) Dako, f) 12A4, and i) 3A6mAb show the graphed binding response of all 8 VP1 antigens.*

4.4 Determination of 3A6mAb Dako and 12A4mAb affinity

Dissociation constant (K_D) values were calculated for each mAb response to a specific VP1 antigen from the ELISA assay's data using nonlinear regression in Prism GraphPad. **Figure 21** shows the generated K_D values, and column 1 shows K_D values for Dako mAb in picomolar with R^2 value between 1 - 0.99 except for RV-A89 and RV-B14. Column 2 K_D values for 12A4mAb with similar results to DakomAb. Column 3 shows K_D values for 3A6mAb in picomolar for selected six VP1 antigens with R^2 ranging from 1.0 - 0.99. Based on the measured K_D, it was observed that 3A6 mAb recognized all 6 VP1 antigens chosen for the test in ELISA with relatively high apparent affinity. CVB1, E30, RVA30, RVA-89, and

RV-B14 interacted better with 3A6 mAb than Dako and 12A4 mAb. In contrast, Dako mAb showed a higher binding affinity to PV1 than 12A4 and 3A6 mAb.

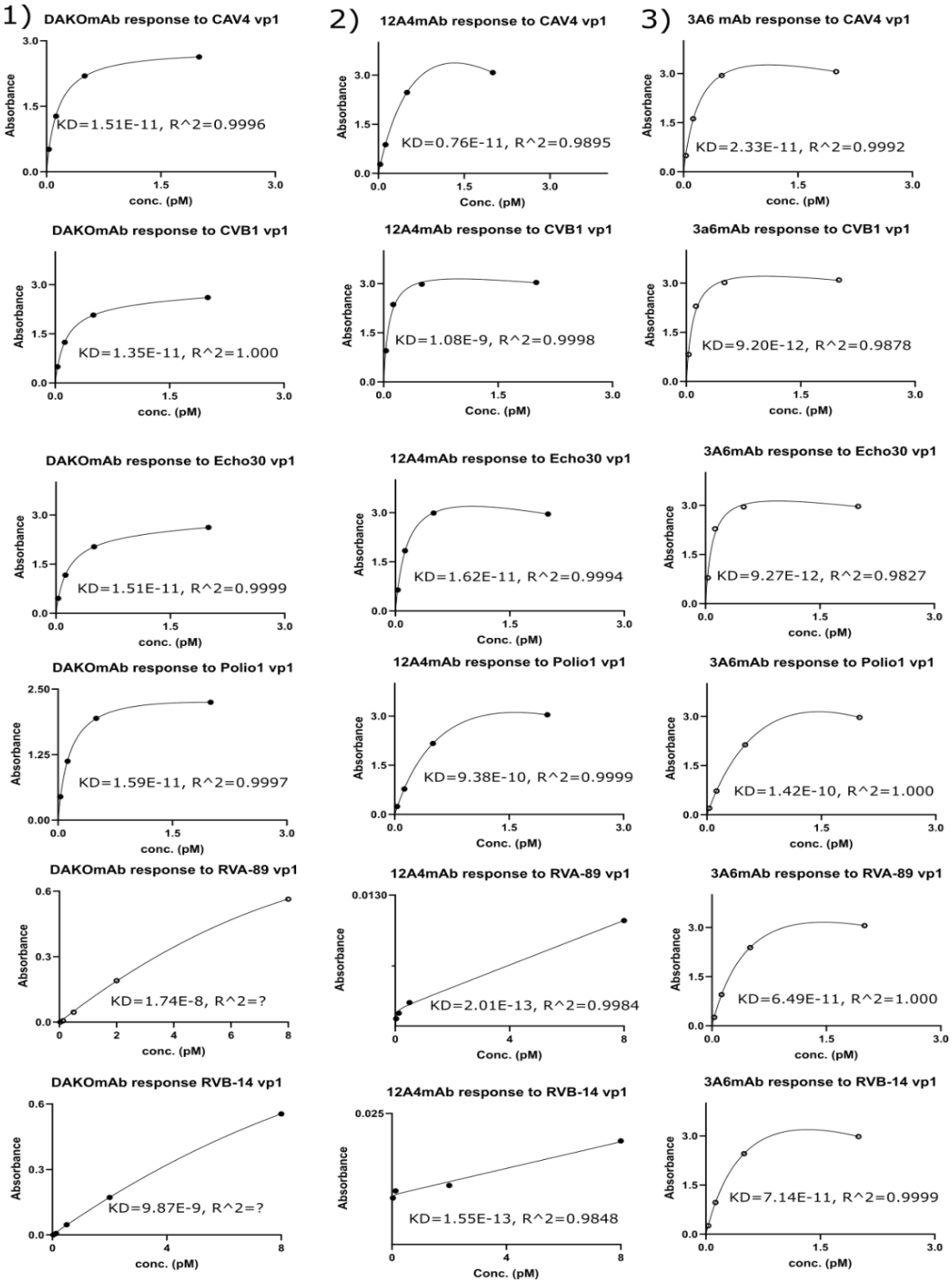

Figure 21. *Determination of binding affinities of 12A4, 3A6, and Dako mAb-based on the ELISA data. The measured absorbance is plotted as a function of the Ab concentration. Column 1 represents Dako mAb and related K_D determination for six VP1 proteins. Column 2 represents 12A4 and K_D determination for six VP1 proteins. Finally, column 3 shows 3A6 mAb binding to sixVP1 proteins. The saturation binding curve was fitted into the data using the Prism™ software with a nonlinear regression method using one-site binding mode [Y=Bmax*X/ K_D +X)].*

4.5 Biolayer interferometry BLI

Antibody-antigen interactions were investigated further using a label-free optical BLI equipped with streptavidin-functionalized sensors. Before carrying out, the actual analysis of antibody-antigen interaction, loading scout, and regeneration conditions were tested. The optimal concentration from loading scout and best regeneration condition were selected for the bulk analysis.

4.5.1 Regeneration condition

In the beginning, the aim was to determine the optimal condition that could allow the regeneration of the streptavidin biosensor. Successful regeneration saves resources and may improve data quality. The best regeneration condition was assessed by determining the level of mAbs binding for streptavidin biosensor across all the binding cycles. The 1st round was without regeneration. The 2nd and the 3rd round were regenerated biosensors. The Biosensors dipped onto acetic acid (HAC) + sodium chloride (NaCl) buffer were effectively regenerated, as illustrated in **Figure 22,** and best matched the 1st binding response level compared to other regeneration conditions. Therefore, based on the result (**Figure 22),** 0.5 M HAC + 0.5 M NaCl showed good reproducibility of mAbs binding across all binding cycles; thus, it was selected as the best regeneration condition.

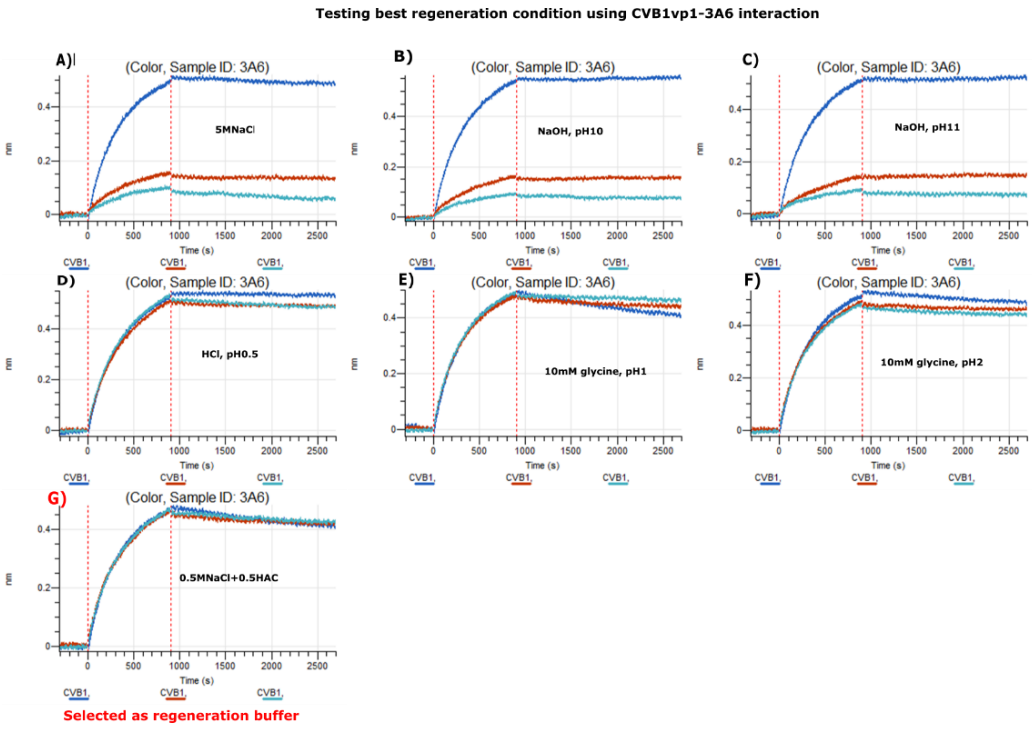

Figure 22. *BLI determination of the best regeneration buffer. Biosensor regeneration conditions were tested using 7 different conditions, A) 5 M NaCl, B) NaOH pH 10, C) NaOH pH 11, D) HCl pH 0.5, E) 10 mM glycine pH 1, F) 10 mM glycine pH 2, and G) 0.5 M HAC + 0.5 M NaCl.*

4.5.2 3A6mAb reacts broadly with enterovirus antigens

3A6 mAb recognized CVA4, CVB1, PV1, E30, RV-A89, and RV-B14 in BLI measurements (**Figure 23 a, c, e, g, i, & k**). As illustrated in **Figure 23 c & d,** the binding response of 3A6 mAb to CVB1 was four times higher than the rest of the 3A6 mAb-VP1 antigen interactions. Using GraphPad Prism software, nonlinear curves were plotted (**Figure 23 b, d, f, h, j, & l**), and their respective dissociation constant (K_D) was calculated. The estimated K_D for 3A6 mAb was based on the assumption of the 1:1 binding model. The antigen was immobilized to the sensor and dipped into a solution containing mAb; the reverse was not performed.

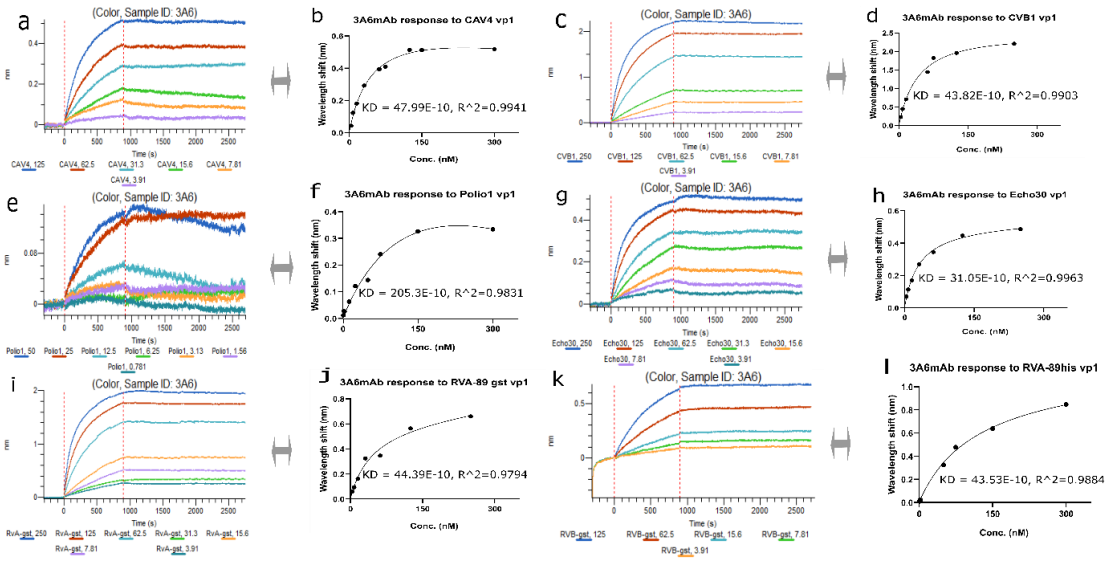

Figure 23. *Characterization of 3A6 mAb binding profile to 6 different VP1 antigens using BLI. The measurements of the binding response of 3A6 mAb to VP1 antigens at varying concentrations: a and b) 3A6mAb response to CVA4, c, and d) 3A6 mAb response to CVB1, e, and f) 3A6 mAb response to PV1, g, and h) 3A6 mAb response to E30 VP1, and i and j) 3A6 mAb response to RV-A89 and k and l) 3A6 mAb response to RV-B14. The binding response curves (Figure 1, b, d, f, h, j, and i) were generated using the Prism™ software and the equation for one-site binding mode [Y=Bmax*X/ K_D +X)].*

4.5.3 12A4, 9B9, 4D12, and 7C1 did not recognize VP1 in BLI

The binding response of 9B9, 4D12, and 7C1 to all 8 VP1 antigens in BLI was weak. Thus, there were no appreciable observable interactions based on the wavelength shift (nm) between mAb and the VP1 antigen, and the binding response was less than 0.1 nm (**Figure 24, a-d)**. In contrast, 12A4 mAb showed a better binding response to CVA4 than the other 7 VP1 antigens (**Figure 24a**).

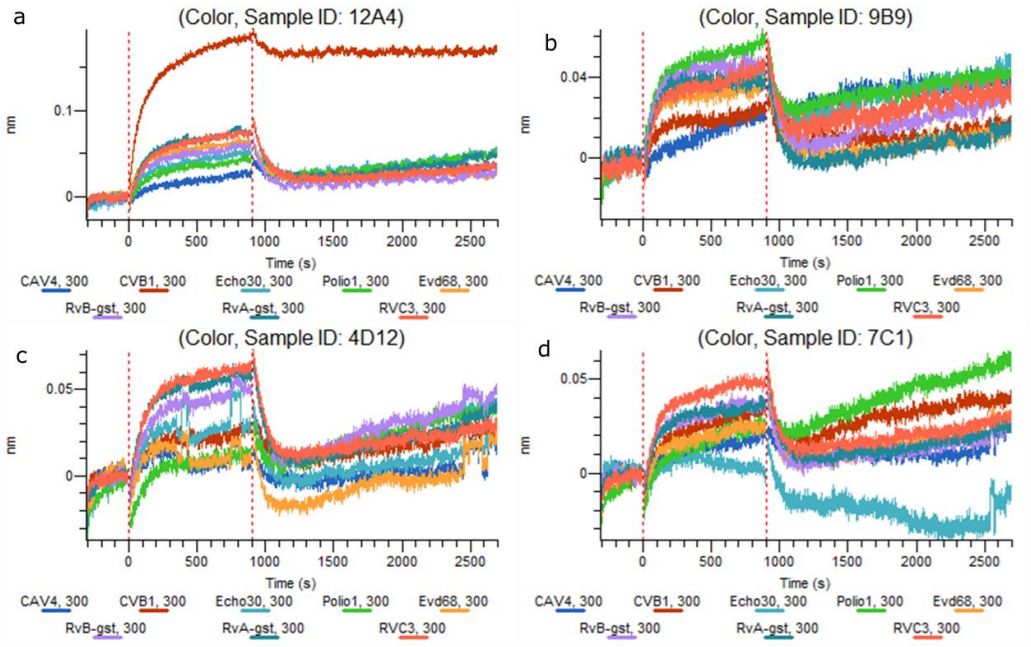

Figure 24. *Characterization of the binding response of 12A4, 9B9, 4D12, 7C 1mAb to various VP1 antigens using BLI. The binding response for 12A4, 9B9, 4D12, 7C1mAb to CVA4, CVB1, E30, PV1, EV-D68, RV-A89, RV-B14, and RV-C3VP1 antigens using a) 12A4mAb, b) 9B9mAb, c) 4D12mAb, and d) 7C1 mAb as a probe.*

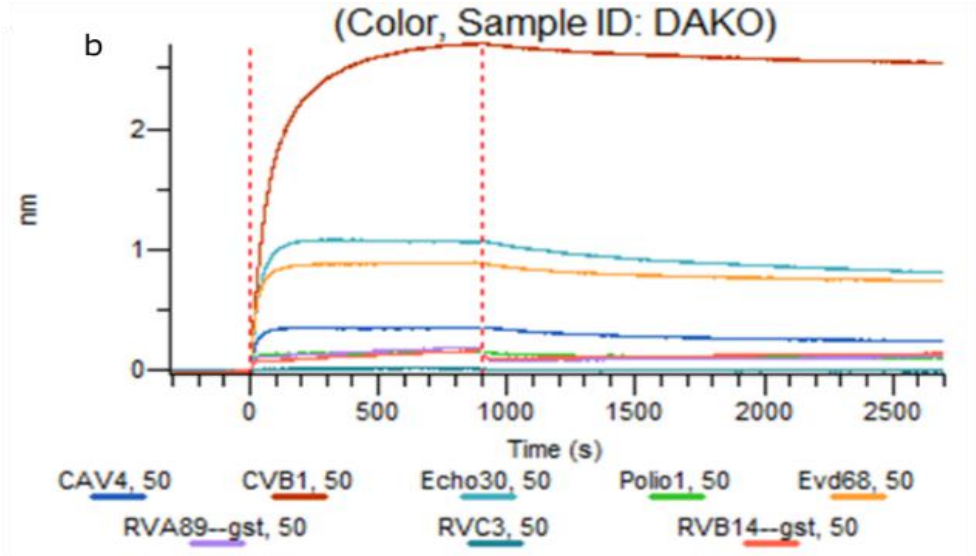

Figure 25. *Determination of Dako mAb binding responses to 8 VP1 proteins in BLI. Dako mAb reactivity to CVA4, E30, PV1, EDV68, RV-A89, RV-B14, RV-C3. In this assay, Dako mAb-CVB1 generated the highest binding response of almost 2.5 nm.*

The binding profile of each mAb (3A6, 12A4, 9B9, 4D12, and 7C1 mAb), including Dako mAb (**Figure 25**), to 8 VP1 antigens (CVA4, CVB1, E30, PV1, EV-D68, RV-A89, RV-B14, and RV-C3) were mapped and compared. Based on the affinities of all mAb, the 3A6 mAb binding profile was superior to the rest of the mAb

(**Figure 23, Figure 26**). Although there was existing knowledge about 3A6 mAb (Saarinen et al., 2018), in the current study, we further showed that 3A6 mAb could bind to E30, RVA-89, and RVB-14 VP1 antigens better than the other mAb clones.

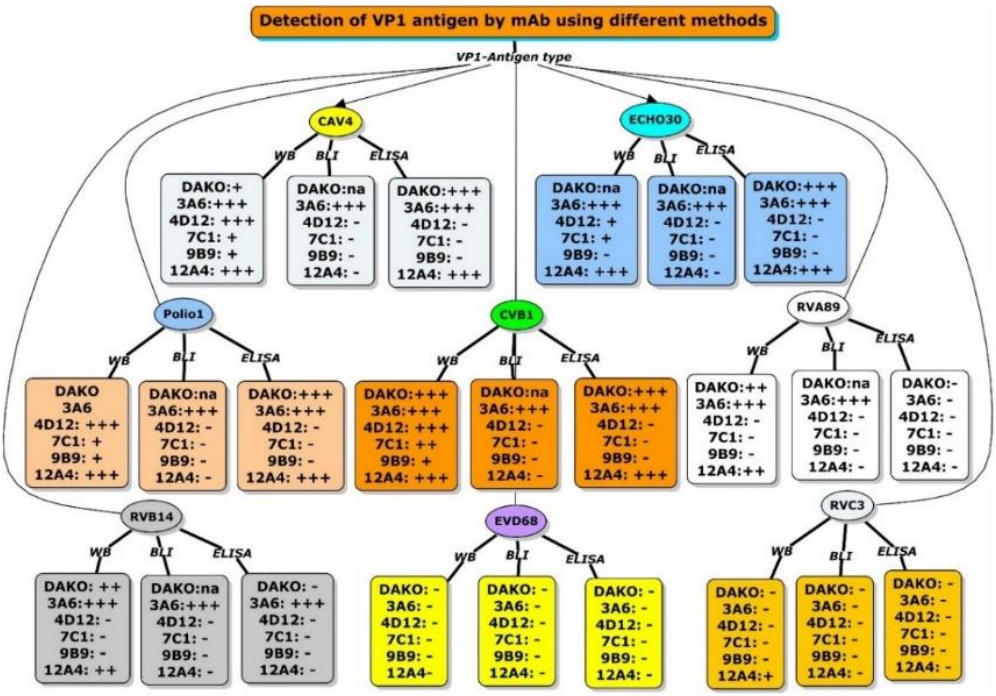

Figure 26. *The intensity of interaction: Dako, 3A6, 4D12, 7C1, 9B9, and 12A4 interaction with CVA4, CVB1, E30, PV1, EV-D68, RV-A89, RV-B14, and RV-C3.*

5. DISCUSSION

Several antibodies have been developed to target EVs for diagnostic purposes for the past decades. These include, at least, Cox mAB 31A2, Dako mAb, 9D5 mAb, and 3A6 mAb, which detects CVB1 and CVB3 and a wide range of enteroviruses (Saarinen et al., 2018). Dako and 3A6 mAb interact with the N-terminal part of VP1 (Saarinen et al., 2018; Shin et al., 2003). Specific amino acids that interact with the antibody are present in a highly conserved enteroviral serotypes region. This information suggests possible cross-reactivity of antibodies observed within the EVs family.

An EVs subtype not containing a conserved region does not have a common epitope (Samuelson et al., 1994; Shin et al., 2003) where antibodies such as 3A6 mAb and Dako mAb could bind. For example, some echoviruses do not have a common epitope in the N-terminal region as the rest of the EVs family have. But in ELISA 3A6, 12A4, and DakomAb reacted to E30 because E30 has a **PALTA**C ETRHTSQV epitope with conserved amino acids to other EVs' common epitopes such as SESI**PALTA**VETGA (Saarinen et al., 2018; Shin et al., 2003). Additionally, Saarinen et al. concluded that 3A6 recognizes EV-B subtypes and poliovirus-3, except EV-A (Saarinen et al., 2018). However, based on the BLI and ELISA results (**Figure 19, Figure 20, Figure 23**), 12A4, Dako, and 3A6 mAb detected CVA4. Thus, EV-A detection is possible, although it might be serotype-dependent.

Monoclonal antibodies are used for serological diagnosis of EV infections. However, most EV antibodies that bind to the N terminal segment do not neutralize the virus. Still, they provide information on the presence of an ongoing or past EV infection. Furthermore, antibody binding to this epitope by a single antibody does not necessarily tell you anything about which EV is the infecting agent because of the highly conserved region across multiple enterovirus species (Samuelson et al., 1994)

The current PCR-based technique for diagnosing HEV and HRV infection cannot distinguish between infecting EV species because they comprise identical 5' noncoding sequence, a universal primer used in qPCR amplification (Österback, 2015). Moreover, the PCR-based tests are laborious, and the results take time, whereas antibody-based tests are quick to perform and enable rapid assays. Also, the use of antibody tests can help reduce the wrong diagnosis and unnecessary use of antibiotics. Therefore, new mAbs against EV are needed, and using multiple antibodies to test a single sample could provide information about infecting EV species. This study addressed the binding response of 3A6, 12A4, 9B9, 4D12, and 7C1 monoclonal antibody clones to CVA4, CVB1, E30, PV1, EV-D68, RVA-89, RVB-14, and RV-C3 VP1 antigens. Mapping the binding profile of each mAb to VP1 antigen enabled us to determine the cross-reactivity of these novel mAbs to the VP1 antigens. Presently, there is a need to develop a new approach to diagnose EV-related infection (Harvala et al., 2018; Kiselev et al., 2020).

At the time of this study, we had prior knowledge about the binding profile of 3A6 mAb, 12A4, and Dako mAb (commercial product) (Saarinen et al., 2018). But some information was still lacking on 3A6 mAb 12A4 mAb, 4D12, 9B9, and 7C1 mAb clones. Based on the antibody screening results (Saarinen et al., 2018), 4D12, 9B9, and 7C1 clones bind to the other VP1 region rather than N-terminal. All five mAb clones were thoroughly characterized for their antigenicity to eight VP1 antigens using WB, ELISA, and BLI assay.

5.1 Good quality purified VP1 antigens and mAb

All the VP1 antigens and mAb were successfully purified and used in BLI, ELISA, and WB. According to the observation made in **Figure 15a & b**, CVA4, CVB1, E30, PV1, EV-D68, RV-A89, RV-B14, and RV-C3 VP1, all purified proteins appeared as double-band in SDS-PAGE analysis. The previous study also observed the VP1 double band in SDS-PAGE (Saarinen et al., 2018, 2020). The bands observed in 20 and 30 kDa of the VP1 antigens (**Figure 16a & b**) are GST-

tag fusion breaking down from VP1 protein during sample preparation or via proteolysis.

For antibodies, 4D12 and 9B9 mAb molecular weight are around 150 kDa in solution. The antibody sample can be denatured in the presence of a denaturing agent, which facilitates the breakage of disulfide bridges between the light and heavy chains, as illustrated in (**Figure 16c & d**) in two protein bands in SDS-PAGE. The breaking of disulfide bonds generates 50 kDa for the heavy chain (2 copies per Ab) and 25kDa for the light chain (2 copies per Ab). As expected, both the light chain and the heavy chain were present in our purified mAb samples. However, the presence of double bands at Mw 50 kDa and 25 kDa could result from different glycosylation degrees because, in mammalian cells, carbohydrates are added to proteins (Amand et al., 2016).

All the purified VP1 antigens and mAb were used in BLI, WB, and ELISA. In BLI, the VP1 antigens used were biotinylated, and in ELISA and WB, the VP1 antigens used were non-biotinylated. Although all VP1 were biotinylated in BLI, PV1 and RVA-89 VP1 were unstable as observed by the formation of white precipitation, possibly due to protein aggregation and solubility problems, which led to an inaccurate binding response curve.

5.2 Binding profile of 3A6 mAb, Dako mAb, and 12A4 mAb in ELISA

The use of ELISA in mapping the binding profile of all mAb showed that the binding responses could be used to detect and distinguish the VP1 antigens. For example, based on ELISA results data, 3A6 mAb, 12A4 mAb, and Dako mAb can distinguish between EVs such as CVA4, CVB1, E30, and PV1 and Rhinoviruses such as RVA and RVB when used together (**Table 5).** These ELISA results can provide information if the RV infection is present or absent. Rhinovirus infections cause the common cold, which frequently affects everyone globally (Österback, 2015). Common colds are among the most reported illness of the worker's absence from work (Jacobs et al., 2013; Leotte et al., 2017).

Also, RV-related Infections have been shown to worsen respiratory diseases such as asthma, cystic fibrosis, and chronic obstructive pulmonary disease. Moreover, there is no protection against RV serotypes each season (Kennedy et al., 2012). Therefore, having 3A6 mAb detecting HRV species can help better manage EV-related infections and treatment options. **Table 5** shows one possible way to distinguish between EV and RV infections using the combination of 3A6, 12A4, and Dako mAb. However, the ELISA assay we used was optimized to detect antibodies in serum and not for detecting antibody recombinant VP1 antigen interaction. Thus, optimization of the ELISA is required for optimal detection of the interaction between antibodies and recombinant VP1 antigens.

Table 5. *Possible reactivity of 3A6 and 12A4 mAb to HEVs and HRVs in patient serum*

Antibody	Antigen	Response	HEVs	HRVs
3A6/12A4/Dako	CVA4	+/-	+	+/-
3A6/12A4/Dako	CVB1	+/-	+	+/-
3A6/12A4/Dako	PV1(Polio1)	+/-	+	+/-
3A6/12A4/Dako	E30 (Echo30)	+/-	+	+/-
Dako	RVA/RVB	-	+/-	
12A4	RVA/RVB	-	+/-	-
3A6	RVA/RVB	+	+/-	+

5.3 3A6mAb had a better binding profile to VP1 than other mAbs in BLI

BLI provides the possibility to have a single incubation step, fast and easy detection of low-affinity analytes, even analytes hardly detected in ELISA, including the use of non-labeled reagents, and possible coupling of regeneration of used biosensors. Biosensors can be regenerated by removing the bound analyte under conditions that do not permanently disrupt the ligand's binding capacity. After

each round of dissociation in our BLI assay, we coupled the streptavidin biosensor regeneration to the analytical protocol. The regenerated streptavidin biosensors were reused to measure the next mAb-VP1 interaction. Each biosensor was used twice.

Based on the BLI results, 12A4, 9B9, 4D12, and 7C1 did not recognize VP1 proteins from CVA4, CVB1, PV1, E30, RV-A89, RV-B14, RV-C3, and EV-D68 with a significant signal. However, there was weak interaction between 12A4mAb and CVB1 VP1. On the contrary, 3A6 mAb reacted to all VP1 antigens except EV-D68 and RV-C3. For this reason, 3A6 mAb was selected for further analysis. Dako mAb was used as a reference point, although its binding profile was limited to one round of BLI measurements due to insufficient quantity.

3A6 mAb had a strong affinity for CVA4, CVB1, PV1, E30, RV-A89, and RV-B14, while Dako mAb response to CVB1 was stronger than E30, EV-D68, and CVA4 VP1 (**Figure 26).** The high affinity of Dako mAb to CVB1 VP1 was expected because Dako mAb was produced against the CVB5 virus and is commonly used as a standard gold antibody for EV detection. Moreover, there was a difference between Dako and 3A6 mAb responses to different VP1 proteins. Dako mAb response to VP1 was quicker, and this can be verified by the association curve being sharp at the start of the binding phase. Also, Dako mAb seemed to dissociate quicker from the VP1 antigen, as evidenced by the high CVB1 and E30 VP1 dissociation rate (**Figure 25**). Therefore, Dako mAb may generate a robust early signal if the CVB1 and E30 VP1 are present in the testing sample. However, the signal may become weaker or fade away faster due to the loss of interaction between the mAb and VP1 antigen in immunoassay, such as immunofluorescence, during extensive washing steps.

The association of 3A6 mAb to VP1 antigen was slow, and the dissociation step took time to occur. Consequently, at an early stage, the response of 3A6 mAb to the VP1 antigen signal may not be as strong as Dako mAb's response. But when the binding saturation is reached, 3A6 mAb dissociate slowly from the VP1 antigen. Therefore, depending on the application, 3A6 mAb may be the preferred mAb because of a slower dissociation and prolonged detection signal. Dako mAb

may be preferred because of generating quick response and a strong signal with fewer minutes than 3A6 mAb. Both fast association and slow dissociation of antigen from the mAb enhance binding affinity (Meyerkord & Fu, 2015; Schreiber et al., 2009).

The binding kinetics of Dako and 3A6 mAb could also identify the virus species causing EV infection. For example, some EVs may bind to Dako or 3A6 mAb faster than others and dissociate quicker than others, distinguishing them from a slow EV binder and a slow dissociation rate. On the other hand, Dako mAb appears to have weaker reactivity with CVA4, PV1, RV-A89, RV-B14, and RV-C3 than 3A6 mAb. Surprisingly, Dako mAb recognized EV-D68 (see **Figure 25**) contrary to ELISA data, and none of the produced mAb detected EV-D68 in WB and ELISA. Thus, Dako mAb may be critical in detecting EV-D68 in BLI. However, BLI assay optimization is needed to determine if binding kinetics and time factors can distinguish elements between EV infecting species.

In our BLI assay design, the streptavidin-VP1 biosensor was dipped onto a solution containing mAb. This assay setup was intended to prevent T-T dimerization caused by the GST fused in the recombinant VP1 antigens for easy VP1 purification (Costa et al., 2014). Thus, with stationed VP1 and mobile bivalent mAb, there is a possibility of mAb interacting with more than one exposed antigen epitope. Our BLI setup did not address the avidity effect of the bivalent nature of mAbs. Therefore, BLI measurements may have generated false affinity values which are not comparable to ELISA. Avidity effects have been attributed to cause non-ideal binding profiles and to generate artificially high-affinity measurement (Tobias & Kumaraswamy, 2013). The immobilization of antibody to the biosensor helps prevent the avidity effect and restrict the interaction to a 1:1 ratio (Dennison et al., 2018). But, based on our experimental setup, the generated K_D values (**Table 6**) were considered apparent K_D and calculated by GraphPad Prism using the 1:1 binding model.

The GST-tag at the N terminal of VP1 in ELISA and Octet did not influence the mAb binding response. The study (Sun et al., 2010) showed that GST fused protein did not affect optical density or bind response curve. However, the GST

dimer formation can affect the antibody-VP1 antigen interaction. Thus, immobilizing the GST VP1 protein in ELISA and BLI measurements helped limit any artifact from the GST-GST dimerization (Bell et al., 2013)

5.4 Generated KD values from ELISA and BLI experiment

Based on **Figure 24**, Dako mAb K_D values were in picomolar with R^2 value between 1-0.99 except for RV-A89 and RV-B14. 12A4 mAb K_D values were like those measured for Dako mAb. 3A6 mAb K_D values were also in picomolar for CVA4, CVB1, PV1, E30, RV-A89, and RV-B14 with the best fit value of 1 to 0.99. The ELISA and BLI results showed that 3A6 mAb recognized more VP1 antigens than Dako or 12A4 mAb. Using Prism GraphPad, one site-specific binding model generated the best fit and K_D values using nonlinear regression (see **Table 4**). For example, 3A6 mAb binding affinity to CVB1 and E30 (Echo30) VP1 were higher than Dako or 12A4 mAb. However, Dako mAb responded better to PV1(Polio1) VP1 than 3A6 mAb or 12A4 mAb in ELISA. Antibody affinity varies greatly (Bizzarri & Cannistraro, 2012), and our purified 12A4 and 3A6 mAb, including Dako mAb affinity constant, were approximated to be in the range of picomolar.

As shown in **Table 6,** the BLI and ELISA K_D values are different, for example 3A6 mAb affinity to CVB1 VP1 was calculated to be $K_D =$ 4 nM in BLI measurements compared to $K_D =$ 9 e-13 nM in ELISA test, signifying a big difference in generated apparent affinities, which should not be the case because affinity should stay within the same range across all bioassay platforms. Also, the results from **Table 6** show that ELISA gave a higher estimate for mAb affinity than BLI in contrast to (Sanders et al., 2016), who compared BLI and ELISA results and found out that BLI gave a higher antibody affinity than ELISA using a similar setup like ours. However, their condition varies from ours in buffer selection and instrumentation. Therefore, based on our BLI and ELISA set up, factors such as availability of exposed epitope, orientation, and immobilizing molecule of the VP1 to the biosensor or 96 well plate contributed to the determined K_D values to vary.

Table 6. *Determination of K_D and best-fit values for Dako, 12A4, and 3A6 mAb*

		Biolayerinterferometry (BLI)			**Enzyme-linked-Immunosorbent Assay**		
VP1-Antigen	mAb	KD (M)	Bmax Response	R^2	KD (M)	Bmax Response	R^2
CVA4	Dako	na	na	na	1.54e-13	2.86	0.999
	12A4	-	-	-	1.29e-12	13.29	1.000
	3A6	4.89e-8	0.76	0.994	2.42e-13	4.84	1.000
CVB1	Dako	na	na	na	1.36e-13	2.56	0.999
	12A4	-	-	-	7.45e-14	3.62	0.994
	3A6	4.38e-8	2.73	0.990	9.13e-14	3.79	0.992
E30	Dako	na	na	na	1.54e-13	2.57	0.999
	12A4	-	-	-	1.65e-13	4.32	1.000
	3A6	3.11e-8	0.53	0.996	9.22e-14	3.76	0.988
PV1	Dako	na	na	na	1.63e-13	2.62	0.999
	12A4	-	-	-	1.10e-12	9.317	1.000
	3A6	2.03e-7	1.23	0.983	1.76e-12	16.05	1.000
RVA-89	Dako	na	na	na	-	-	-
	12A4	-	-	-	-	-	-
	3A6	4.44e-8	0.637	0.979	7.24e-13	7.214	1.000
RVB-14	Dako	na	na	na	-	-	-
	12A4	-	-	-	-	-	-
	3A6	4.35e-8	0.79	0.988	8.02e-13	8.331	1.000

The use of biotinylated VP1 in BLI and non-biotinylated VP1 antigens in ELISA may have resulted in limited epitope availability in BLI than in ELISA. In both BLI and ELISA, the orientation of the immobilized VP1 could have masked the epitope from interacting with mAb. The VP1 in BLI was immobilized to streptavidin, whereas in ELISA, VP1 was stationed to a resin. The difference in experimental design between BLI and ELISA played a significant role in generating different affinities, as represented in **Table 6** with K_D values. Moreover, our experimental design did not address the avidity effect. Thus, our essay should be redesign to address the avidity effects, for example, immobilizing mAb to the biosensor and dipping onto a solution containing VP1 antigen. Alternatively, lowering the antigen density can help increase the distance between VP1 antigens on the biosensor surface and possibly restrict the interaction to 1:1 with mAb. However,

reducing antigen density may also decrease the assay sensitivity (Hadzhieva et al., 2017; Tobias & Kumaraswamy, 2013).

In Octet measurements, 250 nM - 3.9 nM generated 3A6 mAb quantifiable binding response to CVA4, CVB1, E30, PV1, RV-A89, and RV-B14 comparable to ELISA with dilution series of 8 pM to 0.03 pM. Both Octet and ELISA-generated K_D values were equivalent to micro-picomolar range concentration. Interestingly, the response of 12A4 mAb to all 8 VP1 proteins at 300 nM in Octet assay was insignificant. However, in ELISA at 8 pM-0.03 pM concentration range, 12A4 mAb detected CVA4, CVB1, E30, and PV1 with K_D values of 1e-3 nM, 7e-5 nM, 2e-4 nM, and 1e-3 nM respectively. The condition in which VP1-mAb interaction occurred in ELISA and BLI differed greatly. The number of exposed epitopes and orientation of the VP1 could somehow explain why 12A4mAb detected CVA4, CVB1 E30, and PV1 in ELISA than in BLI. The 12A4mAb pattern of recognition of VP1 could be attributed to our experimental setup. However, to overcome this challenge, all the VP1 should be biotinylated and immobilized to streptavidin biosensor in BLI and coated to 96 well plates in ELISA for true comparison and reference.

Overall, our BLI and ELISA setup required a series of optimization such as optimal antigen density, biotinylation of all VP1 antigens, utilization of streptavidin for VP1 immobilization, and a series of lower mAb concentrations in both ELISA and BLI to determine the mAb limit of detection. Also, customizing the ELISA to measure recombinant VP1 interaction with mAb can help generate reliable mAb affinity comparable to other bioassays.

5.5 Future studies

5.5.1 Recommended optimization steps

Optimization is required for WB, BLI, and ELISA to achieve a more reliable mAb-VP1 antigen interaction and to compare different mAb affinities across bioassays. For the BLI measurements, optimization is needed by immobilizing (loading) a mAb on the biosensor's surface. Then antibody-loaded biosensor can be dipped

into a solution containing the VP1 antigen during the association step and subsequently dipping the antibody-antigen complex into a kinetic buffer to monitor the dissociation phase. The results can be compared to the current results presented here. Also, quality assessment of the biotinylated antigen/antibody needs to be carried out before starting real-time measurements and optimizing the antibody concentration to generate its own BLI affinity constant. For the instrumentation, optimize the loading of antigen/antibody to the biosensor by modifying the current protocol. For example, an increase in the antibody's loading density will increase the mAb-VP1 antigen association phase.

As for the ELISA, future studies should consider optimizing substrate dilution, incubation time, primary and secondary antibody concentration. Also, consider using a streptavidin-coated plate to maximize the number of antigens to coat onto ELISA wells. In WB, a further test should exclude a reducing agent during sample (VP1) preparation to test mAb antigenicity. A native PAGE, 2D-PAGE, and mass spectrometry or SEC can be helpful to identify possible contaminants in the produced recombinant proteins. The native PAGE technique can detect mAb-VP1 complex based on their net charge, size, and shape (Valentijn et al., 2008). At the same time, affinity mass spectrometry can probe antigen-antibody interactions as an alternative to WB (Zhao & Chait, 1996).

5.5.2 Challenges in diagnosing HEV and RV infection

EV infections are often underdiagnosed. Although, proper and early detection of EV and human rhinoviruses (HRVs) is essential at the individual and global level to reduce antibiotic usage and avoid or limit the unnecessary costly clinical investigation. Additionally, proper EV and HRVs can help minimize the risk of complications in susceptible individuals and shorten the length of hospitalization (Harvala et al., 2018). EV infection may have similar symptoms to bacterial infections. Thus, early detection of EV infecting species can help health providers respond on time, evaluate the appropriate treatment options, and avoid antibiotic overuse (Harvala et al., 2018; Kiselev et al., 2020).

Currently, the diagnostic of EV infections is done through serological examination. The virus is identified by immunoassays such as ELISA. Reverse transcription-Polymerase Chain reaction (RT-PCR) is a highly sensitive and golden standard for diagnosing EV infections. RT-PCR reveals the infecting EV species in serological samples because it is specific. However, it is not considered liable for chronic EV infections since viruses are cleared quickly from the bloodstream. Thus, the chance of finding the viral RNA in the blood by PCR is low (Genoni et al., 2017). Other tests include immunohistochemistry (IHC) using biopsies or autopsy sections. However, biopsies are not likely to be obtained from the brain, heart, and muscles, limiting the IHC application (Harvala et al., 2018; Saarinen et al., 2020; Xu et al., 2010).

5.5.3 Application of 3A6 and 12A4mAb

Based on our results, both 12A4 and 3A6 mAb can detect EV species (CVA4, CVB1, E30, and PV1, but 3A6 mAb can also recognize HRV species (RV-A89 and RV-B14). The use of 3A6 and 12A4 mAb together to detect EV infection can be fast and relatively reliable. Since both 12A4 and 3A6 mAbs bind to the N-terminal segment of VP1 (Saarinen et al., 2018), sandwich ELISA cannot be performed. Still, they could be utilized in WB, BLI, indirect and competitive ELISA. ELISA and BLI assay can detect EV species based on their antigenic structure; these assays are sensitive, specific, low price, require only simple sample processing, and allow easy data analysis. Additionally, as broadly reactive and serotype-specific EV antibodies such as 3A6, 12A4, and Dako, 9D5 mAb become more and more available. They can be paneled together to identify specific EV groups or serotypes based on their binding kinetics and profile.

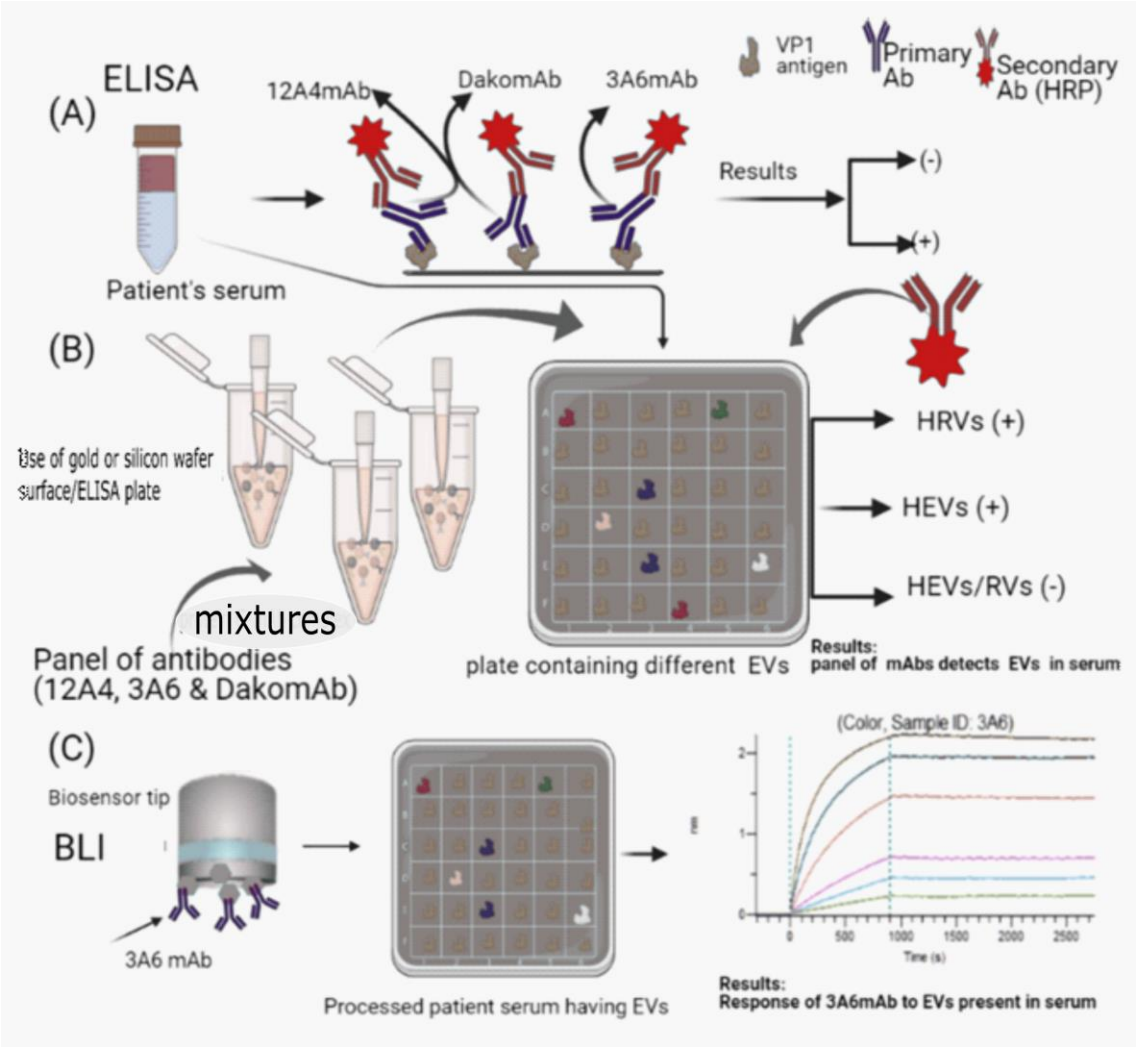

Figure 27. *Possible techniques to determine mAb response to VP1 antigens. The purified antibody can be used to detect the HEVs and HRVs, A) ELISA assay, B) Antibody-protein Immobilization, and C) BLI assay.*

For example, as illustrated in **Figure 27**, 3A6, 12A4, and Dako mAb's can be used to recognize the presence of HEV/RV's infection in a patient's sample, such as serum or stools suspected to have a viral infection. **Figure 27A**, in indirect ELISA, we can first process the patient's serum suspected to have EV infection and coat it onto an ELISA plate. Second, add 3A6 or 12A6 mAb to the coated wells. Third, add HRP conjugated secondary antibody to the coated wells containing 12A4/3A6 mAb-(serum) VP1 antigen complex to amplify the detection signal and quantify. The ELISA test will provide information about the presence and absence of HEV/RV infection. However, it cannot distinguish between HEV and HRV infecting agents. Carrying out ELISA in parallel with some wells containing only 3A6 mAb and other wells with only 12A4 mAb can distinguish HEV and HRV

infecting agents. Method optimization may be needed to achieve reliable results (Atmar, 2014; Harvala et al., 2018).

In **Figure 27B**, we could also design an assay that combines 12A4, 3A6, and Dako mAb to detect HEV/RV infection based on the idea of (Einavid & Bloomid, 2020; Koefoed et al., 2011; Laursen et al., 2018). Briefly, coat the processed patient's sample onto an ELISA plate or other surface, then add a mixture of 3A6/12A4/DakomAb. After that, add the secondary antibody for detection and quantification. Note that the in-between step is needed based on the methods section. The paneling of mAb together enables mAb to compete for the binding site. Furthermore, the mixture composition, relative concentration of each mAb can affect each other's affinity (Einavid & Bloomid, 2020). Therefore, it is crucial to understand the behavior of each mAb participating in a mixture.

As **Figure 27C** shows, the BLI technique described in the method section can be modified to the desired assay. Start by immobilizing biotinylated 3A6 mAb and DakomAb to a biosensor. Then dip the biosensor onto a well-plate containing processed serum samples suspected to have HEV/RV infection. Measure and monitor the signal based on the shift in wavelength (nm). Alternatively, we can perform a BLI-immunosorbent assay (BLI-ISA) (**Figure 27**). In BLI-ISA, the secondary HRP antibody can be used to detect the primary antibody (3A6 and 12A4mAb)-Viral protein complex in serum or stool, a modification protocol from (Dzimianski et al., 2020). **Table 7** shows a recommended stepwise approach for BLI-ISA. Optimization may be needed for the 3A6 or DakomAb loading, assay buffer, serum dilution, or stool procession for good results.

Table 7. *Recommended steps that can be used to perform BLI-immunosorbent assay*

Step#	Step name	Time (s)	Flow (RPM)	Sample plate column
1	Baseline	30	1,000	1: Equilibration
2	Loading	600	1,000	2: Plasma protein
3	Baseline1	300	1,000	3: Baseline
4	Quenching	300	1,000	4: Blocking
5	Association	900	1,000	5: 1st Ab(3A6) binding
6	Baseline2	60	1,000	6: Wash
7	Assocition 1	900	1,000	7: 2nd Ab binding

Western blotting can also detect viral infections in serum samples, as demonstrated by (Yang et al., 2016). 12A4, 3A6, including Dako mAb, can be used to recognize the HEV/RV infection in the Western Blot. When the patient sample is run out on the gel, the 12A4, 3A6, or Dako mAb will bind to the VP1 antigen. After adding the secondary antibody, the presence of viral antigen is detected (Atmar, 2014). Based on the described method above, we can first process the sample to remove the albumin and other non-targeted proteins using commercial resin, PHEMA beads, or AC (Raoufinia et al., 2016) to reduce unspecific binding. Then perform immunodetection, pull down the antibody-antigen complex in the sample, and run the 3A6/12A4mAb-antigen complex on the SDS-PAGE. Perform WB using HRP as a secondary antibody and visualize the mAb-VP1 antigen complex (**Figure 28**).

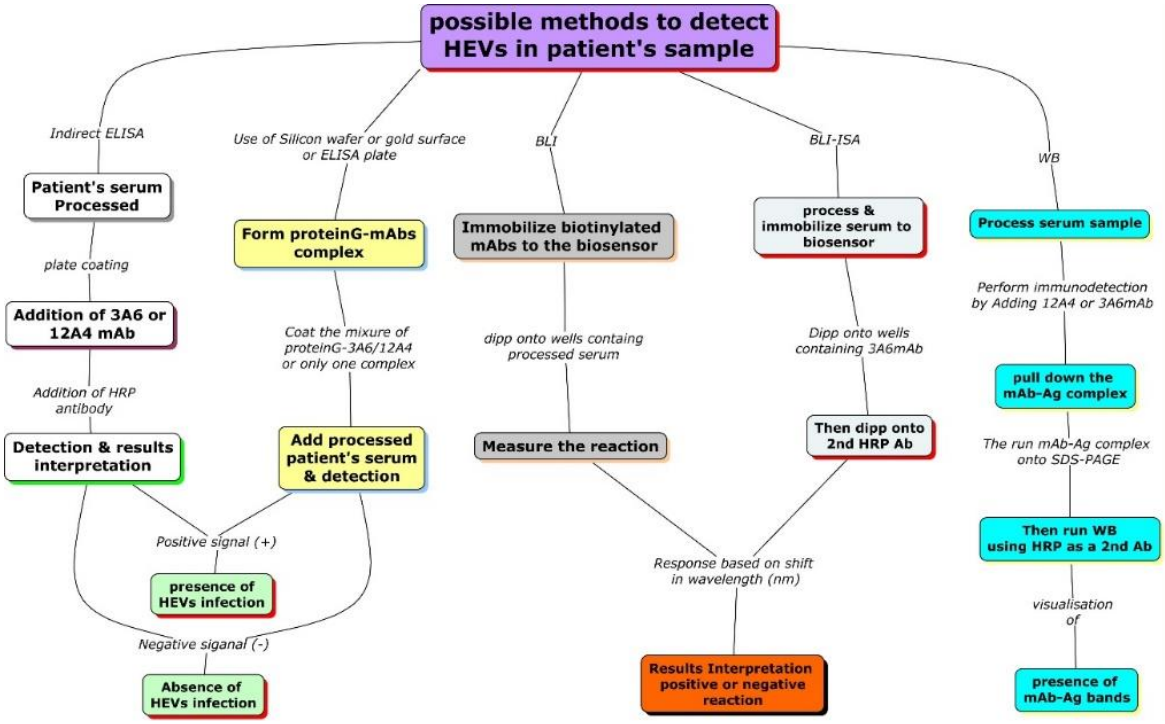

Figure 28. *Possible methods to detect EVs in the human patient's sample using Indirect ELISA, proteinG-mAb complex, BLI, and BLI-ISA including WB.*

6. CONCLUSIONS

In summary, the binding response of five in-house rat mAbs (9B9, 4D12, 7C1, 12A4, and 3A6) to eight VP1 antigens (CV-A4, CV-B1, PV1, EV-D68, E30, RVA-89, RVB-14, and RV-C3), and the commercial mouse mab Dako 5D8/1 were mapped. In ELISA and BLI measurements, 3A6 mAb had broad specificity and strong affinity to CVB1 and E30. In contrast, Dako mAb showed specificity and a strong affinity to CVB1 in BLI and PV1 in ELISA. 3A6 mAb was found to be a better clone in detecting broadly VP1 antigens than 12A4 and Dako mAb's. Clones 9B9, 4D12, and 7C1 had low binding affinity or no reactivity to the VP1 antigens. Therefore, 3A6, 12A4, and Dako mAb's could be investigated further to assess the possibility of using them as an alternative to each other or as a coupled array of antibodies to study and distinguish EV infecting agents based on the binding response and specificity.

7. REFERENCES

Abbas, A. K., Lichtman, A. H., & Pillai, S. (2015). *Cellular and molecular immunology* (Eighth). Elsevier Saunders.

Abbas, A. K., Litchtman, A. H., & Pillai, S. (2017). *Cellular and Molecular Immunology* (Ninth). Elsevier Saunders.

Acheson, N. H. (2011). *Fundamentals of Molecular Virology* (Vol. 2007, Issue 36). https://doi.org/10.1002/pauz.200790112

Amand, M. M., Hayes, J., Radhakrishnan, D., Fernandez, J., Meyer, B., Robinson, A. S., & Ogunnaike, B. A. (2016). Identifying a robust design space for glycosylation during monoclonal antibody production. *Biotechnology Progress*, *32*(5). https://doi.org/10.1002/btpr.2316

Aminev, A. G., Amineva, S. P., & Palmenberg, A. C. (2003). Encephalomyocarditis viral protein 2A localizes to nucleoli and inhibits cap-dependent mRNA translation. *Virus Research*, *95*(1–2), 45–57. https://doi.org/10.1016/S0168-1702(03)00162-X

Andjelković, U., Giacometti, J., & Josić, D. (2017). Protein and peptide separations. In *Liquid Chromatography: Applications: Second Edition* (Vol. 2). https://doi.org/10.1016/B978-0-12-805392-8.00005-0

Atmar, R. L. (2014). Immunological detection and characterization. In *Viral Infections of Humans: Epidemiology and Control*. https://doi.org/10.1007/978-1-4899-7448-8_3

Auer, S., Azizi, L., Faschinger, F., Blazevic, V., Vesikari, T., Gruber, H. J., & Hytönen, V. P. (2017). Stable immobilization of His-tagged proteins on BLI biosensor surface using cobalt. *Sensors and Actuators B: Chemical*, *243*, 104–113. https://doi.org/10.1016/J.SNB.2016.11.090

Auer, S., Koho, T., Uusi-Kerttula, H., Vesikari, T., Blazevic, V., & Hytönen, V. P. (2015). Rapid and sensitive detection of norovirus antibodies in human serum with a biolayer interferometry biosensor. *Sensors and Actuators, B: Chemical*, *221*. https://doi.org/10.1016/j.snb.2015.06.088

Aydin, S. (2015). A short history, principles, and types of ELISA, and our laboratory experience with peptide/protein analyses using ELISA. *Peptides*, *72*, 4–15. https://doi.org/10.1016/j.peptides.2015.04.012

Ayyar, B. V., Arora, S., Murphy, C., & O'Kennedy, R. (2012). Affinity chromatography as a tool for antibody purification. In *Methods*. https://doi.org/10.1016/j.ymeth.2011.10.007

Baggen, J., Thibaut, H. J., Strating, J. R. P. M., & Van Kuppeveld, F. J. M. (2018). The life cycle of non-polio enteroviruses and how to target it. *Nature Reviews Microbiology*. https://doi.org/10.1038/s41579-018-0005-4

Bell, M. R., Engleka, M. J., Malik, A., & Strickler, J. E. (2013). To fuse or not to fuse: What is your purpose? In *Protein Science* (Vol. 22, Issue 11). https://doi.org/10.1002/pro.2356

Bergmann-Leitner, E. S., Mease, R. M., Duncan, E. H., Khan, F., Waitumbi, J., & Angov, E. (2008). Evaluation of immunoglobulin purification methods and their impact on quality and yield of antigen-specific antibodies. *Malaria Journal*, *7*, 1–10.

https://doi.org/10.1186/1475-2875-7-129

Bizzarri, A. R., & Cannistraro, S. (2012). Dynamic force spectroscopy and biomolecular recognition. In *Dynamic Force Spectroscopy and Biomolecular Recognition*. https://doi.org/10.1201/b11637

Block, H., Maertens, B., Spriestersbach, A., Brinker, N., Kubicek, J., Fabis, R., Labahn, J., & Schäfer, F. (2009). Chapter 27 Immobilized-Metal Affinity Chromatography (IMAC). A Review. In *Methods in Enzymology* (Vol. 463, Issue C). https://doi.org/10.1016/S0076-6879(09)63027-5

Bongrand, P. (2014). *Biomolecular Recognition : The Current Challenge Biomolecular Recognition : The Current Challenge*. 1–49.

Bornhorst, J. A., & Falke, J. J. (2000). Purification of proteins using polyhistidine affinity tags. In *Methods in Enzymology*. https://doi.org/10.1016/s0076-6879(00)26058-8

Božič, B., Čučnik, S., Kveder, T., & Rozman, B. (2013). Affinity and Avidity of Autoantibodies. In *Autoantibodies: Third Edition*. https://doi.org/10.1016/B978-0-444-56378-1.00005-8

Brooks, S. A., Schumacher, U., Blancher, C., & Jones, A. (2003). SDS-PAGE and Western Blotting Techniques. *Metastasis Research Protocols*, *57*, 145–162. https://doi.org/10.1385/1-59259-136-1:145

Cathcart, A. L., Baggs, E. L., & Semler, B. L. (2015). Picornaviruses: Pathogenesis and Molecular Biology. *Reference Module in Biomedical Sciences*, 0–11. https://doi.org/10.1016/b978-0-12-801238-3.00272-5

Chapman, N. M., Kim, K. S., Drescher, K. M., Oka, K., & Tracy, S. (2008). 5′ terminal deletions in the genome of a coxsackievirus B2 strain occurred naturally in human heart. *Virology*, *375*(2), 480–491. https://doi.org/10.1016/j.virol.2008.02.030

Chase, A. J., & Semler, B. L. (2012). *Viral subversion of host functions for picornavirus translation and RNA replication*.

Chen, K. R., & Ling, P. (2019). Interplays between Enterovirus A71 and the innate immune system. *Journal of Biomedical Science*, *26*(1), 1–11. https://doi.org/10.1186/s12929-019-0596-8

Chen, S., Lau, H., Brodsky, Y., Kleemann, G. R., & Latypov, R. F. (2010). The use of native cation-exchange chromatography to study aggregation and phase separation of monoclonal antibodies. *Protein Science*, *19*(6), 1191–1204. https://doi.org/10.1002/pro.396

Cheung, R. C. F., Wong, J. H., & Ng, T. B. (2012). Immobilized metal ion affinity chromatography: A review on its applications. In *Applied Microbiology and Biotechnology* (Vol. 96, Issue 6). https://doi.org/10.1007/s00253-012-4507-0

Chia, J. K. S., & Chia, A. Y. (2008). Chronic fatigue syndrome is associated with chronic enterovirus infection of the stomach. *Journal of Clinical Pathology*, *61*(1), 43–48. https://doi.org/10.1136/jcp.2007.050054

Chiu, M. L., Goulet, D. R., Teplyakov, A., & Gilliland, G. L. (2019). *Antibody Structure and Function: The Basis for Engineering Therapeutics*. https://doi.org/10.3390/antib8040055

Costa, S., Almeida, A., Castro, A., Domingues, L., & Rosano, G. L. (2014). *Fusion tags for protein solubility, purification, and immunogenicity in Escherichia coli: the novel Fh8 system*. https://doi.org/10.3389/fmicb.2014.00063

Coyne, C. B., & Bergelson, J. M. (2006). Virus-induced Abl and Fyn kinase signals permit coxsackievirus entry through epithelial tight junctions. *Cell*, *124*(1), 119–131. https://doi.org/10.1016/j.cell.2005.10.035

Darcy, E., Leonard, P., Fitzgerald, J., Danaher, M., Ma, H., & O'Kennedy, R. (2017). Purification of antibodies using affinity chromatography. In *Methods in Molecular Biology* (Vol. 1485). https://doi.org/10.1007/978-1-4939-6412-3_15

Definition, W. B. (2008). The Popular Technology SDS PAGE & Western blotting : Principle and Application. *Molecular Biology*, *July*.

Dennison, S. M., Reichartz, M., Seaton, K. E., Dutta, S., Wille-Reece, U., Hill, A. V. S., Ewer, K. J., Rountree, W., Sarzotti-Kelsoe, M., Ozaki, D. A., Alam, S. M., & Tomaras, G. D. (2018). Qualified Biolayer Interferometry Avidity Measurements Distinguish the Heterogeneity of Antibody Interactions with Plasmodium falciparum Circumsporozoite Protein Antigens. *The Journal of Immunology*, *201*(4). https://doi.org/10.4049/jimmunol.1800323

Dotzauer, A. (2012). Innate and adaptive immune responses against picornaviruses and their counteractions: An overview. *World Journal of Virology*, *1*(3), 91. https://doi.org/10.5501/wjv.v1.i3.91

Duhamel, R. C., Schur, P. H., Brendel, K., & Meezan, E. (1979). pH gradient elution of human IgG1, IgG2, and IgG4 from protein A-Sepharose. *Journal of Immunological Methods*, *31*(3–4), 211–217. https://doi.org/10.1016/0022-1759(79)90133-9

Duncan, G., & Colbère-Garapin, F. (1999). Two determinants in the capsid of a persistent type 3 poliovirus exert different effects on mutant virus uncoating. *Journal of General Virology*, *80*(10), 2601–2605. https://doi.org/10.1099/0022-1317-80-10-2601

Dunn, J. J., Bradrick, S. S., Chapman, N. M., Tracy, S. M., & Romero, J. R. (2003). The stem loop II within the 5′ nontranslated region of clinical coxsackievirus B3 genomes determines cardiovirulence phenotype in a murine model. *Journal of Infectious Diseases*, *187*(10), 1552–1561. https://doi.org/10.1086/374877

Dzimianski, J. V, Lorig-Roach, N., O'rourke, S. M., Alexander, D. L., Kimmey, J. M., & Dubois, R. M. (2020). *Rapid and sensitive detection of SARS-CoV-2 antibodies by biolayer interferometry*. https://doi.org/10.1038/s41598-020-78895-x

Einavid, T., & Bloomid, J. D. (2020). *When two are better than one: Modeling the mechanisms of antibody mixtures*. https://doi.org/10.1371/journal.pcbi.1007830

Eliasson, M., Andersson, R., Olsson, A., Wigzell, H., & Uhlen, M. (1989). Differential IgG-binding characteristics of staphylococcal protein A, streptococcal protein G, and a chimeric protein AG. *Journal of Immunology (Baltimore, Md. : 1950)*, *142*(2), 575–57581.

Engvall, E. (2010). The ELISA, enzyme-linked immunosorbent assay. In *Clinical Chemistry* (Vol. 56, Issue 2). https://doi.org/10.1373/clinchem.2009.127803

Fan, P., Li, X., Sun, S., Su, W., An, D., Gao, F., Kong, W., & Jiang, C. (2015). Identification of a common epitope between enterovirus 71 and human MED25 proteins which may explain virus-associated neurological disease. *Viruses*, *7*(4), 1558–1577. https://doi.org/10.3390/v7041558

Feuer, R., Mena, I., Pagarigan, R., Slifka, M. K., & Whitton, J. L. (2002). Cell Cycle Status Affects Coxsackievirus Replication, Persistence, and Reactivation In Vitro. *Journal of Virology*, *76*(9), 4430–4440. https://doi.org/10.1128/jvi.76.9.4430-4440.2002

Forthal, N. D. (2014). Functions of Antibodies. *Antibodies for Infectious Diseases*, *2*(4), 25–48. https://doi.org/10.1128/microbiolspec.aid-0019-2014

Frenzel, D., & Willbold, D. (2014). Kinetic titration series with biolayer interferometry. *PLoS ONE*, *9*(9). https://doi.org/10.1371/journal.pone.0106882

Frisk, G. (2001). Mechanisms of chronic enteroviral persistence in tissue. *Current Opinion in Infectious Diseases*, *14*(3), 251–256. https://doi.org/10.1097/00001432-200106000-00002

Gauntt, C. J. (1997). Roles of the humoral response in coxsackievirus B-induced disease. *Current Topics in Microbiology and Immunology*, *223*(1), 259–282. https://doi.org/10.1007/978-3-642-60687-8_12

Genoni, A., Canducci, F., Rossi, A., Broccolo, F., Chumakov, K., Bono, G., Salerno-Uriarte, J., Salvatoni, A., Pugliese, A., & Toniolo, A. (2017). Revealing enterovirus infection in chronic human disorders: An integrated diagnostic approach. *Scientific Reports*, *7*(1). https://doi.org/10.1038/S41598-017-04993-Y

Gräslund, S., Nordlund, P., Weigelt, J., Hallberg, B. M., Bray, J., Gileadi, O., Knapp, S., Oppermann, U., Arrowsmith, C., Hui, R., Ming, J., dhe-Paganon, S., Park, H. W., Savchenko, A., Yee, A., Edwards, A., Vincentelli, R., Cambillau, C., Kim, R., … Gunsalus, K. C. (2008). Protein production and purification. In *Nature Methods* (Vol. 5, Issue 2). https://doi.org/10.1038/nmeth.f.202

Grodzki, A. C., & Berenstein, E. (2010). Antibody purification: ion-exchange chromatography. *Methods in Molecular Biology (Clifton, N.J.)*, *588*, 27–32. https://doi.org/10.1007/978-1-59745-324-0_4

Gwozdz, T., & Dorey, K. (2017). Western Blot. In *Basic Science Methods for Clinical Researchers* (pp. 99–117). Elsevier Inc. https://doi.org/10.1016/B978-0-12-803077-6.00006-0

Hadzhieva, M., Pashov, A. D., Kaveri, S., Lacroix-Desmazes, S., Mouquet, H., & Dimitrov, J. D. (2017). Impact of Antigen Density on the Binding Mechanism of IgG Antibodies OPEN. *Scientific Reports* , 1–11. https://doi.org/10.1038/s41598-017-03942-z

Hansson, G. K., Libby, P., Schönbeck, U., & Yan, Z. Q. (2002). Innate and adaptive immunity in the pathogenesis of atherosclerosis. In *Circulation Research* (Vol. 91, Issue 4). https://doi.org/10.1161/01.RES.0000029784.15893.10

Harper, S., & Speicher, D. W. (2011). Purification of proteins fused to glutathione S-transferase. *Methods in Molecular Biology (Clifton, N.J.)*, *681*. https://doi.org/10.1007/978-1-60761-913-0_14

Harvala, H., Broberg, E., Benschop, K., Berginc, N., Ladhani, S., Susi, P., Christiansen, C., McKenna, J., Allen, D., Makiello, P., McAllister, G., Carmen, M., Zakikhany, K., Dyrdak, R., Nielsen, X., Madsen, T., Paul, J., Moore, C., von Eije, K., … Fischer, T. K. (2018). Recommendations for enterovirus diagnostics and characterization within and beyond Europe. In *Journal of Clinical Virology* (Vol. 101). https://doi.org/10.1016/j.jcv.2018.01.008

Hein, P., Michel, M. C., Leineweber, K., Wieland, T., Wettschureck, N., & Offermanns, S. (1982). *Receptor and Binding Studies Radioligand Binding Studies in Cardiovascular Research (Saturation and Competition Binding Studies)*. 723–783.

Heinevetter, L. (1997). The Protein Protocols Handbook. Edited by J. M. Walker, XVIII and 809 pages, numerous figures and tables. Human Press Inc., Totowa, New Jersey, 1996. Price: 89.50 US $. *Food / Nahrung*, *41*(3). https://doi.org/10.1002/food.19970410327

Honda, K., & Taniguchi, T. (2006). IRFs: Master regulators of signalling by Toll-like receptors and cytosolic pattern-recognition receptors. *Nature Reviews Immunology*, *6*(9), 644–658. https://doi.org/10.1038/nri1900

Howley, P. M., & Knipe, D. M. (2020). Fields Virology: Emerging viruses. In *Fields Virology*.

Hultcrantz, M., Hühn, M. H., Wolf, M., Olsson, A., Jacobson, S., Williams, B. R., Korsgren, O., & Flodström-Tullberg, M. (2007). Interferons induce an antiviral state in human pancreatic islet cells. *Virology*, *367*(1), 92–101. https://doi.org/10.1016/j.virol.2007.05.010

Jacobs, S. E., Lamson, D. M., St George, K., & Walsh, T. J. (2013). *Human Rhinoviruses*. https://doi.org/10.1128/CMR.00077-12

Julien, J., Leparc-Goffart, I., Lina, B., Fuchs, F., Foray, S., Janatova, I., Aymard, M., & Kopecka, H. (1999). Postpolio syndrome: Poliovirus persistence is involved in the pathogenesis. *Journal of Neurology*, *246*(6), 472–476. https://doi.org/10.1007/s004150050386

Karim, M. R. (2018). ELISA: History, Types, and Applications. *Nova Science Publishers, Inc.*

Kennedy, J. L., Turner, R. B., Braciale, T., Heymann, P. W., & Borish, L. (2012). Pathogenesis of rhinovirus infection. In *Current Opinion in Virology* (Vol. 2, Issue 3). https://doi.org/10.1016/j.coviro.2012.03.008

Kiselev, D., Matsvay, A., Abramov, I., Dedkov, V., Shipulin, G., & Khafizov, K. (2020). Current trends in diagnostics of viral infections of unknown etiology. In *Viruses* (Vol. 12, Issue 2). https://doi.org/10.3390/v12020211

Koefoed, K., Steinaa, L., Søderberg, J. N., Kjær, I., Jacobsen, H. J., Meijer, P. J., Haurum, J. S., Jensen, A., Kragh, M., Andersen, P. S., & Pedersen, M. W. (2011). Rational identification of an optimal antibody mixture for targeting the epidermal growth factor receptor. *MAbs*, *3*(6). https://doi.org/10.4161/mabs.3.6.17955

Labrou, N. E. (2014). Protein Downstream Processing, Design, Development, and Application of High and Low-Resolution Methods. In *Methods in molecular biology (Clifton, N.J.)*.

Lambert, D. G. (2004). Drugs and receptors. *Continuing Education in Anaesthesia, Critical Care and Pain*, *4*(6), 181–184. https://doi.org/10.1093/bjaceaccp/mkh049

Laursen, N. S., E Friesen, R. H., Zhu, X., Jongeneelen, M., Blokland, S., Vermond, J., van Eijgen, A., Tang, C., van Diepen, H., Obmolova, G., van der Neut Kolfschoten, M., Zuijdgeest, D., Straetemans, R., B Hoffman, R. M., Nieusma, T., Pallesen, J., Turner, H. L., Bernard, S. M., Ward, A. B., Wilson, I. A. (2018). *Universal protection against influenza infection by a multidomain antibody to influenza hemagglutinin*.

Leotte, J., Trombetta, H., Faggion, H. Z., Almeida, B. M., Nogueira, M. B., Vidal, L. R., & Raboni, S. M. (2017). Impact and seasonality of human rhinovirus infection in hospitalized patients for two consecutive years. *Jornal de Pediatria*, *93*(3). https://doi.org/10.1016/j.jped.2016.07.004

Li, J., Schantz, A., Schwegler, M., & Shankar, G. (2011). Detection of low-affinity anti-drug antibodies and improved drug tolerance in immunogenicity testing by Octet® biolayer interferometry. *Journal of Pharmaceutical and Biomedical Analysis*, *54*(2). https://doi.org/10.1016/j.jpba.2010.08.022

Li, Y., Ye, H., Liu, M., Song, S., Chen, J., Cheng, W., & Yan, L. (2021). Development and evaluation of a monoclonal antibody-based competitive ELISA for the detection of antibodies against H7 avian influenza virus. *BMC Veterinary Research*, *17*(1). https://doi.org/10.1186/s12917-021-02772-6

Lindmark, R., Thorén-Tolling, K., & Sjöquist, J. (1983). Binding of immunoglobulins to protein A and immunoglobulin levels in mammalian sera. *Journal of Immunological Methods*, *62*(1), 1–13. https://doi.org/10.1016/0022-1759(83)90104-7

Liu, A., Xiong, Q., Shen, L., Li, W., Zeng, Z., Li, C., Liu, S., Liu, Y., & Han, G. (2017). A sandwich-type ELISA for the detection of Listeria monocytogenes using the well-oriented single chain Fv antibody fragment. *Food Control*, *79*. https://doi.org/10.1016/j.foodcont.2017.03.042

Liu, Y., Zhang, Z., Zhao, X., Yu, R., Zhang, X., Wu, S., Liu, J., Chi, X., Song, X., Fu, L., Yu, Y., Hou, L., & Chen, W. (2014). Enterovirus 71 inhibits cellular type I interferon signaling by downregulating JAK1 protein expression. *Viral Immunology*, *27*(6), 267–276. https://doi.org/10.1089/vim.2013.0127

Masoodi, K. Z., Lone, S. M., & Rasool, R. S. (2021). ELISA (enzyme-linked immunosorbent assay). In *Advanced Methods in Molecular Biology and Biotechnology*. https://doi.org/10.1016/b978-0-12-824449-4.00022-0

Meyerkord, C. L., & Fu, H. (2015). Protein-protein interactions: Methods and applications: Second edition. *Protein-Protein Interactions: Methods and Applications: Second Edition*, *1278*, 1–613. https://doi.org/10.1007/978-1-4939-2425-7

Motulsky, H. J., & Neubig, R. R. (2010). Analyzing Binding Data. In *Current Protocols in Neuroscience* (Vol. 52, Issue 1). https://doi.org/10.1002/0471142301.ns0705s52

Negishi, H., Osawa, T., Ogami, K., Ouyang, X., Sakaguchi, S., Koshiba, R., Yanai, H., Seko, Y., Shitara, H., Bishop, K., Yonekawa, H., Tamura, T., Kaisho, T., Taya, C., Taniguchi, T., & Honda, K. (2008). *A critical link between Toll-like receptor 3 and type II interferon signaling pathways in antiviral innate immunity*.

Newton, A. H., Cardani, A., & Braciale, T. J. (2016). The host immune response in respiratory virus infection: balancing virus clearance and immunopathology. *Seminars in Immunopathology*, *38*(4), 471–482. https://doi.org/10.1007/s00281-016-0558-0

Ohlmann, T., Pain, V. M., Wood, W., Rau, M., & Morley, S. J. (1997). The proteolytic cleavage of eukaryotic initiation factor (elf) 4G is prevented by eIF4E binding protein (PHAS-I; 4E-BP1) in the reticulocyte lysate. *EMBO Journal*, *16*(4), 844–855. https://doi.org/10.1093/emboj/16.4.844

Ohlson, S., Hansson, L., Glad, M., Mosbach, K., & Larsson, P. O. (1989). High performance liquid affinity chromatography: a new tool in biotechnology. *Trends in Biotechnology*, *7*(7), 179–186. https://doi.org/10.1016/0167-7799(89)90096-6

Oikarinen, M., Tauriainen, S., Oikarinen, S., Honkanen, T., Collin, P., Rantala, I., Mäki, M., Kaukinen, K., & Hyöty, H. (2012). Type 1 diabetes is associated with enterovirus

infection in gut mucosa. *Diabetes*, *61*(3), 687–691. https://doi.org/10.2337/db11-1157

Österback, R. (2015). *Detection , Identification, and Molecular Variation*.

Pallansch, M. A., Oberste, M. S., & Lindsay Whitton, J. (2013). Enteroviruses: Polioviruses, coxsackieviruses, echoviruses, and newer enteroviruses. In *Fields Virology: Sixth Edition* (Vol. 1). https://doi.org/10.1002/0470857285.ch6

Patel, K. P., Coyne, C. B., & Bergelson, J. M. (2009). Dynamin-and Lipid Raft-Dependent Entry of Decay-Accelerating Factor (DAF)-Binding and Non-DAF-Binding Coxsackieviruses into Nonpolarized Cells. *JOURNAL OF VIROLOGY*, *83*(21), 11064–11077. https://doi.org/10.1128/JVI.01016-09

Pavio, N., Couderc, T., Girard, S., Sgro, J. Y., Blondel, B., & Colbere-Garapin, F. (2000). Expression of mutated poliovirus receptors in human neuroblastoma cells persistently infected with poliovirus. *Virology*, *274*(2), 331–342. https://doi.org/10.1006/viro.2000.0462

Pelletier, I., Couderc, T., Borzakian, S., Wyckoff, E., Crainic, R., Ehrenfeld, E., & Colbere-Garapin, F. (1991). Characterization of persistent poliovirus mutants selected in human neuroblastoma cells. *Virology*, *180*(2), 729–737. https://doi.org/10.1016/0042-6822(91)90086-Q

Petersen, R. L. (2017). Strategies using bio-layer interferometry biosensor technology for vaccine research and development. In *Biosensors* (Vol. 7, Issue 4). https://doi.org/10.3390/bios7040049

Platanias, L. C. (2005). Mechanisms of type-I- and type-II-interferon-mediated signalling. *Nature Reviews Immunology*, *5*(5), 375–386. https://doi.org/10.1038/nri1604

Raj Kumar Patro, A., Mohanty, S., Prusty, B. K., Singh, D. K., Gaikwad, S., Saswat, T., Chattopadhyay, S., Das, B. K., Tripathy, R., & Ravindran, B. (2019). Cytokine signature associated with disease severity in dengue. *Viruses*, *11*(1), 1–12. https://doi.org/10.3390/v11010034

Raoufinia, R., Mota, A., Keyhanvar, N., Safari, F., Shamekhi, S., & Abdolalizadeh, J. (2016). Overview of Albumin and Its Purification Methods. *Adv Pharm Bull*, *6*(4), 495–507. https://doi.org/10.15171/apb.2016.063

Saarinen, N. V. V., Laiho, J. E., Richardson, S. J., Zeissler, M., Stone, V. M., Marjomäki, V., Kantoluoto, T., Horwitz, M. S., Sioofy-Khojine, A., Honkimaa, A., Hankaniemi, M. M., Flodström-Tullberg, M., Hyöty, H., Hytönen, V. P., & Laitinen, O. H. (2018). A novel rat CVB1-VP1 monoclonal antibody 3A6 detects a broad range of enteroviruses. *Scientific Reports*, *8*(1), 1–13. https://doi.org/10.1038/s41598-017-18495-4

Saarinen, N. V. V., Lehtonen, J., Veijola, R., Lempainen, J., Knip, M., Hyöty, H., Laitinen, O. H., & Hytönen, V. P. (2020). Multiplexed high-throughput serological assay for human enteroviruses. *Microorganisms*, *8*(6), 1–16. https://doi.org/10.3390/microorganisms8060963

Sakamoto, S., Putalun, W., Sornkanok Vimolmangkang, ·, Phoolcharoen, W., Shoyama, Y., Hiroyuki Tanaka, ·, & Morimoto, · Satoshi. (2018). Enzyme-linked immunosorbent assay for the quantitative/qualitative analysis of plant secondary metabolites. *Journal of Natural Medicines*, *72*, 32–42. https://doi.org/10.1007/s11418-017-1144-z

Samuelson, A., Forsgren, M., Johansson, B. O., & Wahren, B. (1994). *Serological Cross-Reactivity*. *1*(3), 336–341.

Sanders, M., Mcpartlin, D., Moran, K., Guo, Y., Eeckhout, M., O'kennedy, R., De Saeger, S., & Maragos, C. (2016). *Comparison of Enzyme-Linked Immunosorbent Assay, Surface Plasmon Resonance and Biolayer Interferometry for Screening of Deoxynivalenol in Wheat and Wheat Dust*. https://doi.org/10.3390/toxins8040103

Schreiber, G., Haran, G., & Zhou, H.-X. (2009). ChemInform Abstract: Fundamental Aspects of Protein-Protein Association Kinetics. *ChemInform*, *40*(21). https://doi.org/10.1002/chin.200921262

Shah, N. B., & Duncan, T. M. (2014). Bio-layer interferometry for measuring kinetics of protein-protein interactions and allosteric ligand effects. *Journal of Visualized Experiments*, *84*. https://doi.org/10.3791/51383

Shin, S. Y., Kim, K. S., Lee, Y. S., Chung, Y. S., Park, K. S., Cheon, D. S., Na, B. K., Kang, Y., Cheong, H. M., Moon, Y., Choi, J. H., Cho, H. E., Min, N. Y., Son, J. S., Park, Y. H., Jee, Y., Yoon, J. D., Song, C. Y., & Lee, K. H. (2003). Identification of enteroviruses by using monoclonal antibodies against a putative common epitope. *Journal of Clinical Microbiology*, *41*(7), 3028–3034. https://doi.org/10.1128/JCM.41.7.3028-3034.2003

Sultana, A., & Lee, J. E. (2015). Measuring protein-protein and protein-nucleic acid interactions by biolayer interferometry. *Current Protocols in Protein Science*, *2015*, 19.25.1-19.25.26. https://doi.org/10.1002/0471140864.ps1925s79

Sun, S. Q., Guo, H. C., Sun, D. H., Yin, S. H., Shang, Y. J., Cai, X. P., & Liu, X. T. (2010). Development and validation of an ELISA using a protein encoded by ORF2 antigenic domain of porcine circovirus type 2. *Virology Journal*, *7*. https://doi.org/10.1186/1743-422X-7-274

Tobias Renee, & Sriram Kumaraswamy. (2013). *Biomolecular Binding Kinetics Assays on the Octet Platform*.

Tracy, S., Chapman, N. M., & Beck, M. A. (1991). Molecular biology and pathogenesis of coxsackie B viruses. *Reviews in Medical Virology*, *1*(3). https://doi.org/10.1002/rmv.1980010304

Tracy, S., Oberste, M. S., & Drescher, K. M. (2008). *Group B Coxsackieviruses. CURRENT TOPICS IN MICROBIOLOGY AND IMMUNOLOGY*.

Triantafilou, K., Orthopoulos, G., Vakakis, E., Ahmed, M. A. E., Golenbock, D. T., Lepper, P. M., & Triantafilou, M. (2005). Human cardiac inflammatory responses triggered by Coxsackie B viruses are mainly Toll-like receptor (TLR) 8-dependent. *Cellular Microbiology*, *7*(8), 1117–1126. https://doi.org/10.1111/j.1462-5822.2005.00537.x

Triantafilou, K., & Triantafilou, M. (2004). Coxsackievirus B4-Induced Cytokine Production in Pancreatic Cells Is Mediated through Toll-Like Receptor 4. *Journal of Virology*, *78*(20), 11313–11320. https://doi.org/10.1128/jvi.78.20.11313-11320.2004

Trier, N. H., Hansen, P. R., & Houen, G. (2012). Production and characterization of peptide antibodies. *Methods*, *56*(2), 136–144. https://doi.org/10.1016/j.ymeth.2011.12.001

Tripathi, L., Hietanen, E., Merilahti, P., Teixido, L., Sanchez-Alberola, N., Tauriainen, S., & Susi, P. (2021). Monoclonal antibody against VP0 recognizes a broad range of human parechoviruses. *Journal of Virological Methods*, *293*, 114167.

https://doi.org/10.1016/j.jviromet.2021.114167

Valentijn, A. J., Upton, J. P., & Gilmore, A. P. (2008). Analysis of endogenous Bax complexes during apoptosis using blue native PAGE: Implications for Bax activation and oligomerization. *Biochemical Journal*, *412*(2). https://doi.org/10.1042/BJ20071548

Vandyk, L., & Meek, K. (1992). Assembly of igh CDR3: Mechanism, regulation, and influence on antibody diversity. *International Reviews of Immunology*, *8*(2–3), 123–133. https://doi.org/10.3109/08830189209055568

Vidarsson, G., Dekkers, G., Rispens, T., & Klinman, D. (2014). *IgG subclasses and allotypes: from structure to effector functions*. https://doi.org/10.3389/fimmu.2014.00520

Von Herrath, M. (2009). Can we learn from viruses how to prevent type 1 diabetes? the role of viral infections in the pathogenesis of type 1 diabetes and the development of novel combination therapies. *Diabetes*, *58*(1), 2–11. https://doi.org/10.2337/db08-9027

Wallner, J., Lhota, G., Jeschek, D., Mader, A., & Vorauer-Uhl, K. (2013). Application of Bio-Layer Interferometry for the analysis of protein/liposome interactions. *Journal of Pharmaceutical and Biomedical Analysis*, *72*. https://doi.org/10.1016/j.jpba.2012.10.008

Walls, D., & Loughran, S. T. (2011). Purification of proteins fused to glutathione S-tranferase. *Methods in Molecular Biology (Clifton, N.J.)*, *681*(3). https://doi.org/10.1007/978-1-60761-913-0

Wang, J. P., Cerny, A., Asher, D. R., Kurt-Jones, E. A., Bronson, R. T., & Finberg, R. W. (2010). MDA5 and MAVS Mediate Type I Interferon Responses to Coxsackie B Virus. *Journal of Virology*, *84*(1), 254–260. https://doi.org/10.1128/jvi.00631-09

Wang, S. M., Lei, H. Y., & Liu, C. C. (2012). Cytokine immunopathogenesis of enterovirus 71 brain stem encephalitis. In *Clinical and Developmental Immunology* (Vol. 2012). https://doi.org/10.1155/2012/876241

Wang, S. M., & Liu, C. C. (2014). Update of enterovirus 71 infection: Epidemiology, pathogenesis, and vaccine. In *Expert Review of Anti-Infective Therapy* (Vol. 12, Issue 4). https://doi.org/10.1586/14787210.2014.895666

Weeramange, C. J., Fairlamb, M. S., Singh, D., Fenton, A. W., & Swint-Kruse, L. (2020). The strengths and limitations of using biolayer interferometry to monitor equilibrium titrations of biomolecules. *Protein Science*, *29*(4). https://doi.org/10.1002/pro.3827

Wessely, R., Klingel, K., Knowlton, K. U., & Kandolf, R. (2001). Cardioselective infection with coxsackievirus B3 requires intact type I interferon signaling: Implications for mortality and early viral replication. *Circulation*, *103*(5), 756–761. https://doi.org/10.1161/01.CIR.103.5.756

Wilson, J. L., Scott, I. M., & McMurry, J. L. (2010). Optical biosensing: Kinetics of protein A-IGG binding using biolayer interferometry. *Biochemistry and Molecular Biology Education*, *38*(6). https://doi.org/10.1002/bmb.20442

Xu, F., Yan, Q., Wang, H., Niu, J., Li, L., Zhu, F., He, S., Zhang, S., Weng, Z., Cheng, T., Cai, Y., He, D., Chen, Y., Ge, S., Yeo, A. E. T., Zhang, J., Ng, M. H., & Xia, N. (2010). Performance of detecting IgM antibodies against enterovirus 71 for early diagnosis. *PLoS ONE*, *5*(6). https://doi.org/10.1371/journal.pone.0011388

Yang, Z., Lee, J., Ahn, H. J., Chong, C. K., Dias, R. F., & Nam, H. W. (2016). Western blot detection of human anti-Chikungunya virus antibody with recombinant envelope 2 protein. *Korean Journal of Parasitology*, *54*(2). https://doi.org/10.3347/kjp.2016.54.2.239

Yin, H., Berg, A. K., Westman, J., Hellerström, C., & Frisk, G. (2002). Complete nucleotide sequence of a coxsackievirus B-4 strain capable of establishing persistent infection in human pancreatic islet cells: Effects on insulin release, proinsulin synthesis, and cell morphology. *Journal of Medical Virology*, *68*(4), 544–557. https://doi.org/10.1002/jmv.10236

Zhao, Y., & Chait, B. T. (1996). Probing antibody-antigen interactions by mass spectrometry. *Methods in Molecular Biology (Clifton, N.J.)*, *66*. https://doi.org/10.1385/0-89603-375-9:129